PONTIFICIA UNIVERSIDAD CATÓLICA DEL PERÚ

TECHNISCHE UNIVERSITÄT ILMENAU

Pontificia Universidad Católica del Perú

Escuela de Posgrado

Tesis de Maestría

Nonlinear Adaptive Observer Design for a Reverse Osmosis Plant

Para optar el grado académico de
Magíster en Ingeniería de Control y Automatización

Presentado por:
B. Eng. Kristina Korder

Profesor Responsable en TU Ilmenau:	Prof. Dr.-Ing. Johann Reger
Profesor Responsable en PUCP:	Dr.-Ing. Carlos Gustavo Pérez Zuñiga
Supervisor en TU Ilmenau:	M. Sc. Matti Noack

Agosto, 2021

Abstract

This thesis proposes a novel approach for a nonlinear adaptive observer design applied to a reverse osmosis desalination plant. The considered mathematical model of the desalination system includes nonlinearities of the states and the parameters that cannot be handled with previously published estimation methods which are based on the modulating function technique. Therefore, the proposed real-time capable approach uses a decoupled parameter estimator and state observer. These estimates can be utilized for developing a controller or a fault detection system of the desalination plant with the aim of improving the quality and effort of fresh water production.

The parameter estimator is composed of a convolution filter with modulating functions and the common Extended Kalman-Bucy Filter in order to estimate nonlinear parameters of a state-linear input/output relation. To receive a regression form of the nonlinear system for the state observer and to avoid the necessity of time-derivatives of the measured input and output signals, a linearization by means of the Taylor series and the modulating function technique are applied. The estimates can be non-asymptotically obtained by using a sliding window of finite length. This procedure allows a continuous and recursive update of the state estimates and extends the possible applications of the modulating function technique to nonlinear systems.

Comparative simulations are executed with the considered nonlinear system of a reverse osmosis desalination plant. Distinct scenarios with respect to the parameter change and the impact of noise are examined. The parameter and state coupled Extended Kalman-Bucy Filter shows an asymptotic convergence of its estimates, whereas the decoupled proposed adaptive observer confirms its non-asymptotic behavior by fast estimation results.

Contents

Acronyms **iv**

Symbols **vi**

1 Introduction **1**
1.1 Motivation . . . 1
1.2 Objective of Research . . . 1
1.3 Limitations and Structure of the Thesis . . . 2

2 System Modeling of the Reverse Osmosis Plant **4**
2.1 Structure . . . 4
2.1.1 Pre-treatment . . . 5
2.1.2 High Pressure Pump Module . . . 7
2.1.3 Membrane Module . . . 8
2.1.3.1 Reverse Osmosis . . . 8
2.1.3.2 Membrane Fouling and Concentration Polarization . . . 12
2.1.3.3 Membrane Type and Material . . . 13
2.2 Sensor Configuration . . . 15
2.3 State-space Representation . . . 17
2.3.1 Nonlinear Representation . . . 17
2.3.2 Linearized Representation . . . 18

3 Observability of Nonlinear Systems **20**
3.1 Observability Definitions . . . 21
3.2 Observability Analysis of the Reverse Osmosis Plant . . . 25
3.2.1 Symbolic Analysis . . . 25
3.2.2 Numerical Analysis . . . 26

4 Extended Kalman-Bucy Filter **29**
4.1 Definition . . . 30
4.2 Structure . . . 32
4.3 Convergence Analysis . . . 33

5 Adaptive Observer with Modulating Functions **36**
5.1 Definition of Modulating Functions . . . 37
5.2 Modulating Function Method . . . 38
5.3 Parameter Estimation . . . 40
5.3.1 Persistence of Excitation . . . 41
5.3.2 Structure of the Parameter Estimator . . . 41
5.4 Extended Modulation Filter . . . 44
5.4.1 Input-Output Relation . . . 44
5.4.2 State Estimation . . . 46
5.4.3 Mixed Boundary Conditions . . . 47
5.4.4 Structure of the EMF . . . 48
5.4.5 Error Analysis . . . 50
5.4.6 Iterated EMF . . . 51
5.4.7 Numerical Implementation . . . 52
5.5 Joint Parameter and State Estimation . . . 54

6 Comparative Simulations **56**
6.1 Preliminaries . . . 56
6.2 Scenarios . . . 59
6.2.1 Constant Parameter . . . 59
6.2.2 Step Decline in Parameter . . . 63
6.2.3 Gradual Decrease in Parameter . . . 65
6.2.4 Noise Impact . . . 67

7 Conclusion and Outlook **72**

A Determinant of the Observability Matrix **75**

B State-space Representation **77**
B.1 Nonlinear State-space Representation . . . 77
B.2 Linearized State-space Representation . . . 78
B.3 Comparison of the Nonlinear and Linearized State-space Representation 78

C Simulation Plots **80**
C.1 Step Decrease . . . 80
C.2 Noise Impact . . . 82

Bibliography **83**

List of Figures **89**

List of Tables **92**

Statutory Declaration **93**

Acronyms

PUCP	*Pontifical Catholic University of Peru*
CP	Concentration Polarization
DMR	State - **D**ecoupled Parameter Estimation via **M**odulated **R**egression
EKF	Extended Kalman-Bucy Filter
EMF	Extended Modulation Filter
FIR	Finite Impulse Response
GMF	Generalized Modulating Function
H.O.T.	Higher Order Terms
I/O	Input/Output
IEMF	Iterated Extended Modulation Filter
ISS	Input-to-State-Stable
KF	Kalman Filter
LMF	Left Modulating Function
LTI	Linear Time-Invariant
LTV	Linear Time-Variant
LWO	Locally Weakly Observable
MF	Modulating Function
MFM	Modulating Function Method
MSF	Multi-Stage Flash Distillation
NaCl	Sodium Chloride

ODE	Ordinary Differential Equation
PDE	Partial Differential Equation
RDE	Riccati Differential Equation
RO	Reverse Osmosis
SISO	Single-Input Single-Output
TMF	Total Modulating Function
UO	Uniformly Observable
UV	Ultraviolet
w.r.t.	with respect to

Symbols

A_m	Surface area of the membrane
A_m^*	Nominal surface area of the membrane
A_v	Cross sectional area of the valve
α_v	Flow coefficient of the valve
A_v^*	Nominal cross sectional area of the valve
b_f	Constant around operating point of feed stream
b_p	Constant around operating point of permeate stream
C_b	Concentration of the brine stream
C_f	Concentration of the feed stream
C_m	Salt concentration on the membrane surface (low)
C_ms	Salt concentration on the membrane surface (high)
C_p	Salt concentration of the permeate stream
d	Friction coefficient of the pump
ΔP	Pressure difference across the membrane
$\Delta\pi$	Osmotic pressure difference across the membrane
γ_f	Conductivity of the feed stream
γ_p	Conductivity of the permeate stream
J_p	Moment of inertia of the pump
k_m	Solvent permeability of the membrane
k_s	Solute permeability of the membrane
L_s	Inductance of the stator
M	Mutual inductance between stator and rotor
M_m	Molar mass of salt
M_p	Torque generated by the pump

n	Order of the system
p	Number of pole pairs of the motor
Q	Process noise covariance matrix
Q_b	Volumetric flow rate of the brine stream
Q_f	Volumetric flow rate of the feed stream
Q_m	Volumetric flow rate passing through the membrane
Q_p	Volumetric flow rate of the permeate stream
Q_s	Mass flow rate of salt passing through the membrane
$\mathcal{R}$	Ideal Gas constant
R	Measurement noise covariance matrix
ρ_b	Density of the brine stream
R_r	Electrical resistance of the rotor
T	Temperature of the solvent
τ_p	Torque produced by the motor of the pump
τ_v	Mechanical time constant of the valve
U_eff	Effective voltage of the stator
u_p	Weighting factor of the frequency
u_v	Opening factor of the valve
V_b	Control volume on the brine side of the membrane module
V_d	Pump displacement
V_p	Control volume on the permeate side of the membrane module
ω_el	Output frequency of the variable frequency controller
ω_el^*	Nominal value of the supply frequency
ω_p	Rotational speed of the pump

1 Introduction

1.1 Motivation

Water is the most important good in the world: Without it, humanity cannot survive. Although two thirds of the earth is covered with water, almost all of it is saltwater, which is mostly stored in ocean. Of the remaining 2.5% fresh water are only 0.3% accessible to humans because the rest is bonded as glaciers or is located as groundwater deep under the earth. [Bun17]

On the one hand, the global water consumption by humans is rising since the 1930s approximately 1% every year, which is caused due to the steady growth of the world population and economy. On the other hand, the climate change and natural disasters like prolonged heat and the resulting aridity limit the access to drinkable water. Because of the rising demand of accessible fresh water, new methods must be developed or existing ones must be improved to satisfy the demand of fresh water. [Foo17]

One idea is to use a part of the 97.5% saltwater of the earth and transform it into fresh water with a seawater Reverse Osmosis (RO) desalination plant. The aim of a RO process is to diminish the content of salt and other minerals in a brackish or seawater stream, which is done by pressing the water through a semipermeable membrane. As the membrane rejects the salt, the input stream is separated into the permeate stream with a lower salt concentration and the brine stream with a higher salt concentration. The permeate stream is used for the supply of freshwater for the industry or domestic sector. [Bun17; FRL17]

1.2 Objective of Research

This leads to the problem at hand and thus to the research question of how to improve the efficiency of water desalination with a RO plant. Before developing a controller or a scheme for a fault detection of the desalination plant, all process states and parameters of the time-varying nonlinear system have to be known. It is usually not possible to measure all the necessary process states due to costs and physical limitations of the nonlinear system. For instance, the salt concentration of the streams cannot be measured but must be calculated with the conductance and the pH value. Moreover, the parameters of the system change under certain conditions, e.g. the amount of particles

clogging the membrane has to be supervised in order to prevent the destruction of the membrane rack. [Riv+19]

Therefore, an adaptive observer for the dynamic system with time-varying parameters, uncertainties, multivariable coupling and sensor noise must be designed in order to estimate the system states and parameters only by using input and output measurements. The observer approach is based on a mathematical model of the system which describes the behavior of the desalination process and must fulfill a certain accuracy.

The general objective is the development of two different nonlinear observer approaches for the RO seawater desalination plant and setting the boundaries of each observer considering several requirements like the model itself, the sensor placement and noise, nonlinearities or parameter changes. The Extended Kalman-Bucy Filter (EKF) is considered as a common observer already used in industrial solutions. In contrast, the Modulating Function Method (MFM) is a current research interest and is applied with the aim of new results to the investigative contribution of the nonlinear adaptive observer design. This is one of the objectives of the *PURE-WATER* project, namely a real-time capable observer design for membrane systems for water desalination by using an advanced parameter and state estimation technique including the Modulating Function (MF) approach.

1.3 Limitations and Structure of the Thesis

This research is limited to a theoretical framework and the simulation of nonlinear observers for the RO seawater desalination plant. The implementation and test with the real RO plant in the laboratories of the *Pontifical Catholic University of Peru* (*PUCP*) in Lima is not possible due to the COVID-19 pandemic but can be part of further research.

The content of this thesis will cover the application of a common observer and the development of a decoupled adaptive observer for nonlinear systems using the MF technique. The outline of contents is constructed as shown in figure 1.1. In chapter 2, the RO system is modeled with respect to (w.r.t.) the sensor configuration and the model is given in form of a state-space representation. After introducing the necessary nonlinear observability definitions, the observability of this nonlinear system is analyzed in chapter 3. Chapter 4 describes the EKF which will be used as a part of the parameter estimator in section 5.3 and in chapter 6 as a basis for a comparison.

The main focus of this work is built around the MF approach which is outlined in chapter 5. The MFM is applied for both, a parameter and a state estimation. Both

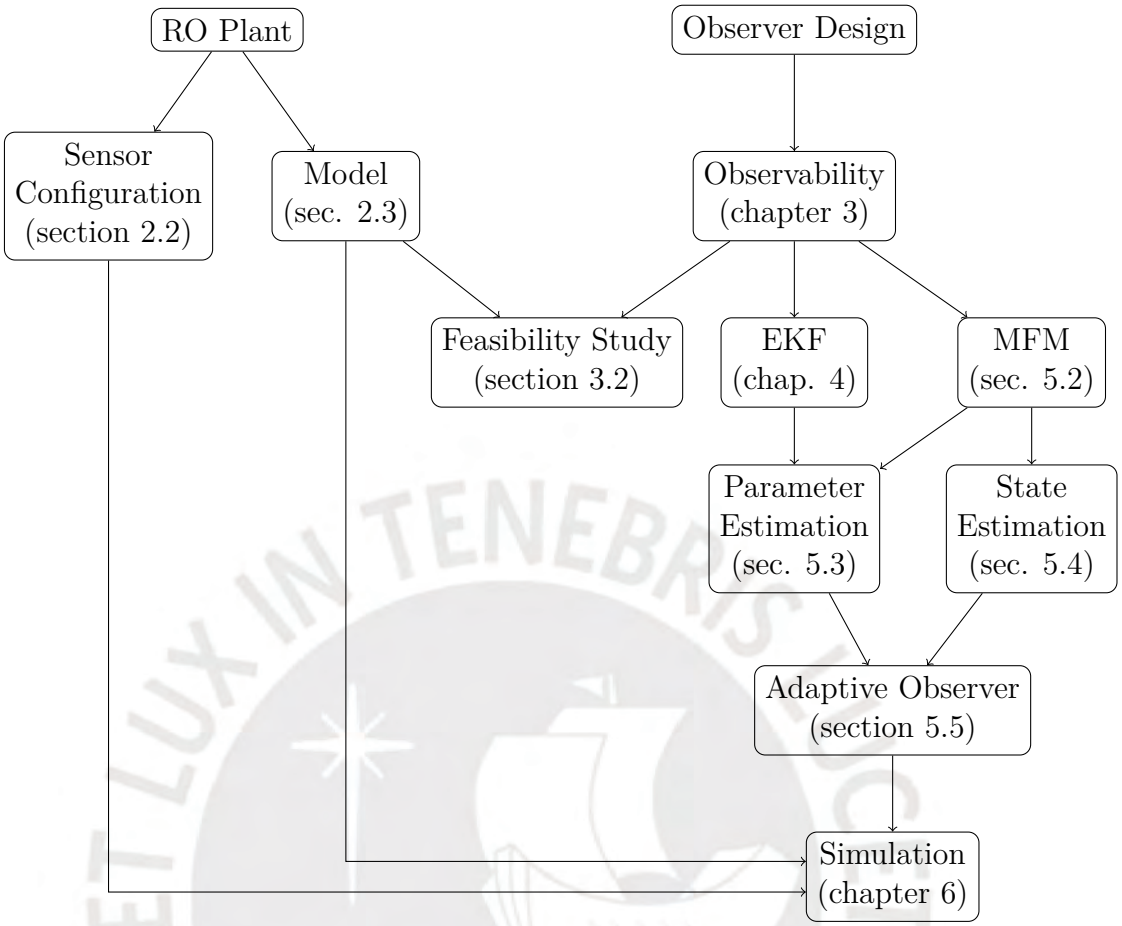

Figure 1.1: Structure of the thesis

estimators can be used as a standalone one or coupled in order to receive an adaptive observer in section 5.5. This observer is applied to the model of the RO desalination system and compared to the EKF in chapter 6.

2 System Modeling of the Reverse Osmosis Plant

The considered system is a pilot-scale RO desalination plant and is set up in the Control and Automation Laboratory of the *PUCP*. This plant is used for training and optimization purposes which can then be applied to commercial desalination plants. Compared to these commercial desalination plants, no post-treatment stage and no energy recovery devices are necessary in the pilot-scale setup since the water stays in a closed-loop system of the plant. [Riv+19]

2.1 Structure

The mathematical modeling of the RO plant is based on a light-gray-box model which is a mixture of theoretical and experimental modeling. This identification method uses physical laws in form of Ordinary Differential Equations (ODEs) if the process is only time-dependent. If the process is time- and space-dependent, Partial Differential Equations (PDEs) are used to describe the process behavior. The parameters of the model are unknown and must therefore be estimated by the measured process signals. In contrast, a white-box model is completely defined by established physical laws and known parameters, whereas a black-box model only assumes the model structure by measured signals of the process. [IM11]

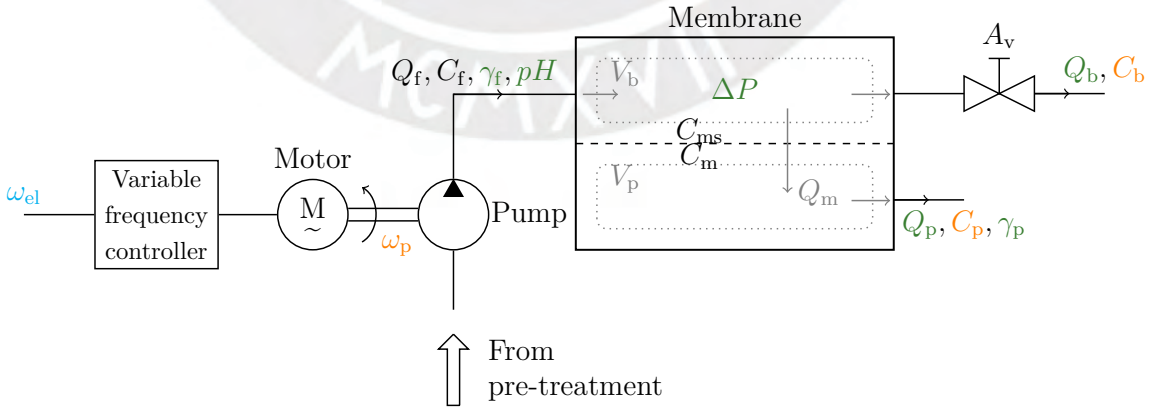

Figure 2.1: Schematic representation of the RO [Göp21]

In [Göp21] a light-gray-box model of the considered RO plant has been developed

which will be further used in this work. The pilot-scale RO plant was divided into three subsystems, namely the pre-treatment, the membrane module and the high pressure pump module which is shown in figure 2.1.

Additionally, [Göp21] proposed a hydraulic circuit to model the interaction between the high pressure pump and the brine valve (see figure 2.3). Since the dynamics of the brine valve is slow, it is not used for the further mathematical model of the considered system. Therefore, the cross sectional area of the valve A_v is assumed to be constant and is measured in $[A_\mathrm{v}] = \mathrm{cm}^2$ in order to minimize numerical errors due to the huge differences of values. Accessorily, the pressure change is calculated in $[\Delta P] = \mathrm{bar}$ and all flows in $[Q] = \dfrac{\mathrm{m}^3}{\mathrm{min}}$.

All static parameters of the model are assumed to be known and are listed in table 2.1. The data of the installed membrane in the considered plant are extracted from [TOR19]. Since the pilot-scale RO desalination plant is set up in Peru, the peruvian utility frequency $f_{el} = 60\,\mathrm{Hz}$ is used in the model. Besides fixed physical parameters like the ideal gas constant $\mathcal{R}$, the rest of the static parameters are an estimation of the real parameters of the plant since the validation of the parameter values has not been possible yet.

$V_\mathrm{p} = 0.576 \times 10^{-3}\,\mathrm{m}^3$	$pH^* = 7.0$	$C_\mathrm{f}^* = 2\,\mathrm{kg\,m^{-3}}$	$p = 1$
$V_\mathrm{b} = 14.9 \times 10^{-3}\,\mathrm{m}^3$	$A_\mathrm{m}^* = 16\,\mathrm{m}^2$	$C_\mathrm{p}^* = 0.5\,\mathrm{kg\,m^{-3}}$	$\rho_\mathrm{b} = 1\,\mathrm{kg\,l^{-1}}$
$V_\mathrm{d} = 13.04 \times 10^{-6}\,\mathrm{m}^3/\mathrm{rev}$	$A_\mathrm{v}^* = 3.67\,\mathrm{cm}^2$	$\gamma_\mathrm{f}^* = 0.108\,\mathrm{S\,m^{-1}}$	$\alpha_\mathrm{v} = 0.04$
$\kappa = 0.2\,\mathrm{kg\,m^2\,s^{-1}\,rad^{-1}}$	$\omega_\mathrm{el}^* = 377\,\mathrm{rad\,s^{-1}}$	$\gamma_\mathrm{p}^* = 0.05\,\mathrm{S\,m^{-1}}$	$\tau_\mathrm{v} = 1.5\,\mathrm{s^{-1}}$
$b_\mathrm{p1} = b_\mathrm{f1} = 0.05\,\mathrm{S\,m^{-1}}$	$J_\mathrm{p} = 0.2\,\mathrm{kg\,m^2}$	$k_\mathrm{s} = 12.0 \times 10^{-6}\,\mathrm{m\,min^{-1}}$	
$b_\mathrm{p0} = b_\mathrm{f0} = 0.1\,\mathrm{S\,m^2\,kg^{-1}}$	$d = 0.002\,\mathrm{N\,m\,s}$	$k_\mathrm{m} = 12.0 \times 10^{-5}\,\mathrm{m\,min^{-1}\,bar^{-1}}$	
$\mathcal{R} = 8.314\,472 \times 10^{-5}\,\mathrm{m^3\,bar\,mol^{-1}\,K^{-1}}$		$M_\mathrm{m} = 0.058\,44\,\mathrm{kg\,mol^{-1}}$	

Table 2.1: Parameter values taken for simulation

2.1.1 Pre-treatment

The pre-treatment is mandatory for every RO plant, whereas it is not for other desalination methods, e.g. thermal processes like the most-used Multi-Stage Flash Distillation (MSF) [EE02]. In contrast to the obligatory pre-treatment to obtain a certain quality of the feed water, the RO membrane separation technology has several advantages compared to the thermal evaporation: The energy consumption and operational costs are less and the water recovery rate is higher [Pér+20]. A complete comparison can be found in [SR14].

The pre-treatment system is applied to assure the RO operation for a substantial period of time, e.g. longer than six months, without the time consuming and expensive cleaning of the membrane. An inadequate pre-treatment of a RO plant would lead to a reduction of the membrane life. Additionally, the plant availability will be shortened due to frequent RO chemical cleanings. [Bad+19]

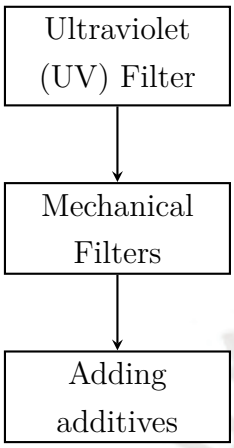

The pre-treatment process treats the feed water before it enters the high pressure pump (see figure 2.1). In the first step of the pre-treatment, the water passes through an UV filter in order to be sterilized. The sterilization is necessary in order to avoid biological fouling, also called biofouling. This biological contamination describes the growth of bacteria on the membrane surface. It depends on the membrane composition as cellulose acetate membranes or polyamide hollow fibers are susceptible to bacteria but thin-film composite membranes, which are used in the considered plant, are quite resistant to a bacterial attack. Beside an UV filter, it is also possible to add chlorine to the water but it must be filtered afterwards. Thus, UV filters are used in the considered plant. [Bak04]

As a second step mechanical filters are applied in order to filter suspended solids and to avoid the deposition of solid particles on the membrane surface which is called fouling. At last, additives are adjoined to the water in the pre-treatment process in order to adjust the pH-value by adding acid, sterilizing the water by adding chlorine or preventing scaling. Scaling means the formation of mineral deposits on a membrane, effecting the permeation rate of the RO system. A measure against scaling comprises an antiscalent additive. [Bak04; Göp21]

Scaling and (Bio-)Fouling inevitably cause the membrane to plug which is described in section 2.1.3.2. The pre-treatment system of the pilot-scale RO plant consists of a feed pump, an UV filter, a set of mechanical filters, namely a multimedia filter and a fine filter, and two additives tanks (see figure 2.5). Additionally, the pre-treatment includes an active carbon filter which removes organic compounds, e.g. pesticides, herbicides and insecticides, and surplus chlorine. [Riv+19]

The multimedia filter consists of several layers of distinct media. In these layers the particles are captured. The multimedia filter can remove particles down to a size of $5 - 10\mu m$. The multimedia filter is described more precisely in [Meh10].

The removal of smaller particles can be improved by using micro- and ultrafiltration, respectively. Both techniques are based on membrane filtration, and their pore size ranges between $0.01 - 0.1\mu m$. [Bad+19]

Due to the small pore size, the porous structure allows the permeability of microsolutes through the membrane. Hence, no representative osmotic pressure is generated across the ultrafiltration membrane on the contrary to RO membranes. [Wan+11]
Compared to media filtration, the membrane filtration is capable of removing more foulants and biopolymers in the water than the media filtration. Moreover, ultrafiltration is very effective for turbidity removal and produces a constant product water quality with low turbidity. Also ultrafiltration membranes can effectively remove viruses which leads to less chlorine use. [Bad+19]

Nevertheless, the pre-treatment has not been modeled in [Göp21] and is neither modeled in this thesis since the influence of the pre-treatment on the desalination process in the interesting range of operation is negligible.

2.1.2 High Pressure Pump Module

The high pressure pump module follows the pre-treatment and is separated into two subsystems: the electrical and the mechanical part. Due to the negligence of the dynamics of the brine valve, the electrical subsystem and therefore the whole system has one input $u = \omega_{el}$. The frequency set point ω_{el} is used by the variable frequency controller to control the electrical motor which is connected to the high pressure pump. By variation of the input, the rotational speed ω_{p} of the mechanical part is affected. The high pressure pump with the rotational speed ω_{p} generates the feed stream Q_{f}:

$$Q_{\mathrm{f}} = \frac{30}{\pi} V_{\mathrm{d}}\, \omega_{\mathrm{p}}. \tag{2.1}$$

Equation (2.1) includes the pump displacement V_{d} which equals the volume of the fluid that the pump delivers per revolution.

The dynamics of the rotational speed ω_{p} of the pump is based on Newton's law of motion:

$$\dot{\omega}_{\mathrm{p}} = \frac{1}{J_{\mathrm{p}}} \left(\underbrace{-\Delta P \frac{5 \times 10^4\, V_{\mathrm{d}}}{\pi}}_{M_p} - d\, \omega_{\mathrm{p}} + \underbrace{\kappa \left(-p\, \omega_{\mathrm{p}} + \omega_{\mathrm{el}}^{*}\, u_{\mathrm{p}} \right)}_{\tau_p} \right) \tag{2.2}$$

with the moment of inertia J_{p} and the friction coefficient d of the pump. The pump generates the torque M_{p} which is expressed as a function of the pressure difference ΔP since the hydraulic power equals the mechanical power. Furthermore, the torque produced by the motor of the pump τ_{p} uses a simplified expression because the frequency converter connected to the motor has a so-called 'volts per hertz' mode. Therefore, the ratio $U_{\mathrm{eff}}/\omega_{\mathrm{p}}$ obeys the proportionality κ with the number of poles of the motor p, the

electrical resistance of the rotor R_r, the mutual inductance between stator and rotor M, the effective voltage of the stator U_eff, and the inductance of the stator L_s:

$$\kappa = \frac{3\,p}{2\,R_\mathrm{r}} \left(\frac{M\,U_\mathrm{eff}}{L_\mathrm{s}\,\omega_\mathrm{el}} \right)^2 . \tag{2.3}$$

The output frequency of the variable frequency controller ω_el has a limit to a certain range and equals to its set point frequency. Thus, it is replaced by the product of the nominal value of the supply frequency ω_el^* and the weighting factor of the frequency u_p which is limited to the range $[0, 1]$.

2.1.3 Membrane Module

The membrane module is the process part in which the RO respectively the desalination takes place. This module is divided into two control volumes V_b and V_p. Both are assumed to be constant and are coupled through the semipermeable membrane. Another assumption is that the flow of water (solvent) and salt (solute) through the membrane occurs independently as stated in the solution-diffusion model in [Kuc15]. Moreover, all fluids are considered as incompressible $\rho = const.$ and have the same density $\rho_\mathrm{f} = \rho_\mathrm{b} = \rho_\mathrm{p}$. Thus, the impact of the salt concentration on the density of the solution is negligible.

2.1.3.1 Reverse Osmosis

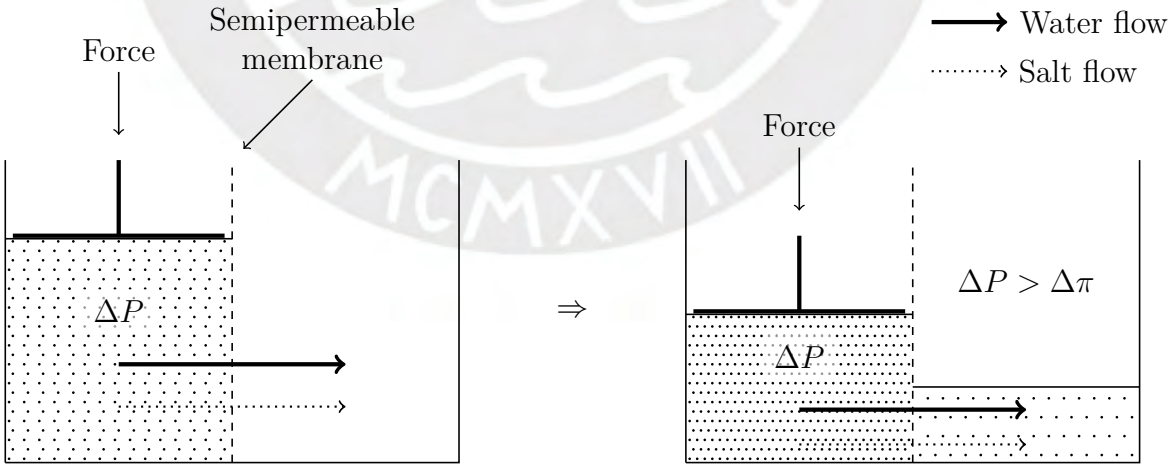

Figure 2.2: Process of reverse osmosis [EE02]

The working principle of the RO can be described as the application of a pressure ΔP which is higher than the osmotic pressure $\Delta\pi$ of the solution to the high concentration

region (see figure 2.2). The osmotic pressure $\Delta\pi$ is influenced by the concentration difference across the membrane and the solution's temperature. Thereby, the hydraulic pressure differential is used to drive the water from regions of high concentration to the ones with low concentration, namely through the membrane. In contrast to osmosis, the direction of the solvent flow changes but the direction of the solute remains the same. The result is purified water called the permeate stream on one side of the membrane, and a more concentrated salt solution on the other side, which is the brine stream. [Göp21; Sta16; CCE06]

Applied to the pilot-scale RO plant displayed in figure 2.1, the pressure ΔP inside the membrane module is generated by the feed stream Q_f with the salt concentration C_f as the membrane with the brine valve acts like a resistance to Q_f. This causes the RO and the feed stream Q_f to separate into the brine stream Q_b and the permeate stream Q_p with the lower concentration of the solute.

Since the control volumes are constant, the mass balance of the control volume on the brine side of the membrane module V_b holds as follows [GKB07]:

$$Q_\mathrm{f} = Q_\mathrm{m} + Q_\mathrm{b} \tag{2.4}$$

$$\dot{C}_\mathrm{b} = \frac{1}{V_\mathrm{b}}(Q_\mathrm{f}\, C_\mathrm{f} - Q_\mathrm{b}\, C_\mathrm{b} - Q_\mathrm{m}\, C_\mathrm{m}). \tag{2.5}$$

The formula (2.4) describes the separation of the feed stream Q_f into the flow passing through the membrane Q_m and the brine stream Q_b. This balance is used to calculate the dynamics of C_b with the formula (2.5). On the other side of the membrane, the balance of the control volume of the solvent and the differential solute can be described as [GKB07]:

$$Q_\mathrm{p} = Q_\mathrm{m} \tag{2.6}$$

$$\dot{C}_\mathrm{p} = \frac{1}{V_\mathrm{p}}(Q_\mathrm{m}\, C_\mathrm{m} - Q_\mathrm{p}\, C_\mathrm{p}). \tag{2.7}$$

However, it is not possible to measure the salt concentration directly. Therefore, the relation between the measurable conductivity of the permeate γ_p and the feed stream γ_f, and the solute concentration is used. Additionally, the constants around the operating points C^*, pH^*, γ^* of the feed stream b_f and the permeate stream b_p are required:

$$\gamma_\mathrm{f} = b_{\mathrm{f}0}\,(C_\mathrm{f} - C_\mathrm{f}^*) - b_{\mathrm{f}1}\,(pH - pH^*) + \gamma_\mathrm{f}^* \tag{2.8}$$

$$\iff C_\mathrm{f} = C_\mathrm{f}^* + \frac{\gamma_\mathrm{f} - \gamma_\mathrm{f}^* + b_{\mathrm{f}1}\,(pH - pH^*)}{b_{\mathrm{f}0}}. \tag{2.9}$$

[Göp21] modeled the hydraulic circuit with an electronic-hydraulic analogy (see figure 2.3) so that the pressure drop corresponds to the electrical potential and the volume flow rate equals the electric current. Thus, the hydraulic pump is a current source

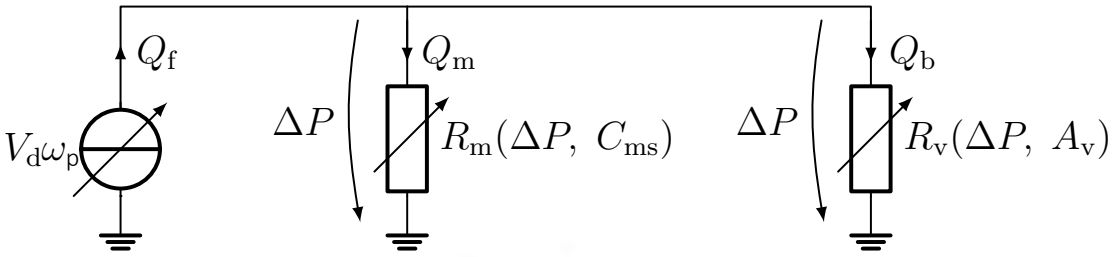

Figure 2.3: Hydraulic network with the electronic-hydraulic analogy [Göp21]

in this analogy and can be adjusted by changing the rotational speed of the pump ω_p. Since the membrane and the valve act like two nonlinear resistors in parallel, the pressure drop ΔP is caused by the flow streaming through the resistors and leads to the following expression for ΔP:

$$\Delta P = \left[\frac{2}{\sqrt{3}}\sqrt{-p}\,\sin\left(\frac{1}{3}\arcsin\left(\frac{3\sqrt{3}q}{2(\sqrt{-p})^3}\right)\right) - \frac{a_2}{3}\right]^2 \tag{2.10}$$

with

$$a_0 = \frac{Q_\mathrm{f}^2}{k_\mathrm{m}A_\mathrm{m}\nu A_\mathrm{v}} + \frac{Q_\mathrm{f}(C_\mathrm{ms}+\alpha)}{\beta\nu A_\mathrm{v}} \tag{2.11}$$

$$a_1 = -\frac{C_\mathrm{ms}+\alpha}{\beta} - \frac{2Q_\mathrm{f}+\alpha}{k_\mathrm{m}A_\mathrm{m}} \tag{2.12}$$

$$a_2 = \frac{\nu A_\mathrm{v}}{k_\mathrm{m}A_\mathrm{m}} - \frac{Q_\mathrm{f}}{\nu A_\mathrm{v}} - \frac{\alpha k_\mathrm{m}A_\mathrm{m}}{\beta\nu A_\mathrm{v}} \tag{2.13}$$

$$p = a_1 - \frac{a_2^2}{3} \tag{2.14}$$

$$q = \frac{2a_2^3}{27} - \frac{a_2 a_1}{3} + a_0. \tag{2.15}$$

The calculation of ΔP underlies the physical assumptions that the values of C_ms, A_v and Q_f are non-negative. Thus, the value of ΔP must be positive as well. If Q_f or C_ms rises, ΔP will increase comparable to the equivalence of an electric resistor $R = \frac{U}{I}$.

The volume stream through the brine valve is defined by the flow coefficient of the valve α_v, the cross sectional area of the valve A_v, the density of the brine stream ρ_b

and the pressure drop ΔP (2.10):

$$Q_{\mathrm{b}} = 0.06\,\alpha_{\mathrm{v}}\sqrt{\frac{2}{\rho_{\mathrm{b}}}}A_{\mathrm{v}}\sqrt{\Delta P}. \tag{2.16}$$

The dynamics of the valve can be expressed with the mechanical time constant of the valve τ_{v}, the nominal value of the cross sectional area of the valve A_{v}^{*} and the opening factor of the valve u_{v} in the range of $[0, 1]$:

$$\dot{A}_{\mathrm{v}} = \frac{1}{\tau_{\mathrm{v}}}\left(-A_{\mathrm{v}} + A_{\mathrm{v}}^{*}\,u_{\mathrm{v}}\right). \tag{2.17}$$

Due to a big value of τ_{v}, the valve is not designed to act fast. Therefore, the dynamics of the brine valve can be neglected which leads to $\dot{A}_{\mathrm{v}} = 0$.

Regarding the solution-diffusion model, the solvent passes through the membrane independently, and thus, the volumetric flow rate flowing through the membrane can be defined with the surface area of the membrane A_{m} and the solvent permeability of the membrane k_{m} [Kim17]:

$$Q_{\mathrm{m}} = k_{\mathrm{m}}\,A_{\mathrm{m}}\,(\Delta P - \Delta\pi). \tag{2.18}$$

In order to calculate Q_{m} (2.18), the osmotic pressure difference $\Delta\pi$ is assumed to be linearly proportional to the solute concentration. The formula (2.19) is also known as Van't Hoff equation. $\Delta\pi$ can be seen as a resistance and is defined by the difference of the solent concentration high and low of the membrane C_{ms} and C_{m} multiplied with the proportionality β consisting of the values of the molar mass of salt M_{m}, the ideal gas constant $\mathcal{R}$, and the temperature of the solvent T [Kim17]:

$$\Delta\pi = \frac{1}{\beta}\left(C_{\mathrm{ms}} - C_{\mathrm{m}}\right) \qquad \text{with } \beta = \frac{M_{\mathrm{m}}}{\mathcal{R}\cdot T}. \tag{2.19}$$

The considered plant operates in RO mode if the osmotic pressure difference $\Delta\pi$ is smaller than the applied pressure difference across the membrane ΔP. Nevertheless, if $\Delta\pi \geq \Delta P$, e.g. when the high pressure pump turns off suddenly, Q_{m} in equation (2.18) becomes negative. Thus, the plant works in osmosis mode.

Due to the independence of the solvent and the solute stream through the membrane, the solute flow Q_{s} can be defined in a similar way to Q_{m} but with the solute permeability of the membrane k_{s}:

$$Q_{\mathrm{s}} = k_{\mathrm{s}}\,A_{\mathrm{m}}(C_{\mathrm{ms}} - C_{\mathrm{m}}). \tag{2.20}$$

Using equations (2.18 - 2.20), the solute concentration on the low side of the membrane C_m can be described as the ratio of the solute flow to the solvent flow [Kim17]:

$$C_\mathrm{m} = \frac{Q_\mathrm{s}}{Q_\mathrm{m}} = \frac{k_\mathrm{s}\, A_\mathrm{m}(C_\mathrm{ms} - C_\mathrm{m})}{k_\mathrm{m}\, A_\mathrm{m}(\Delta P - \Delta\pi)} = \frac{k_\mathrm{s}\, A_\mathrm{m}\,(C_\mathrm{ms} - C_\mathrm{m})}{k_\mathrm{m}\, A_\mathrm{m}\,(\Delta P - \frac{1}{\beta}\,(C_\mathrm{ms} - C_\mathrm{m}))}. \tag{2.21}$$

After the solute molecules have passed through the membrane, it is assumed that the solutes are uniformly mixed in the permeate stream [Kim17]. In order to receive C_m, equation (2.21) is solved explicitly under the assumption that all concentrations are greater than zero:

$$C_\mathrm{m} = \frac{1}{2}\left(C_\mathrm{ms} - \beta\,\Delta P - \alpha + \sqrt{\beta^2\,\Delta P^2 - 2\,\Delta P\,(C_\mathrm{ms} - \alpha)\beta + (C_\mathrm{ms} + \alpha)^2}\right) \tag{2.22}$$
$$\text{with} \quad \alpha = \frac{k_\mathrm{s}}{k_\mathrm{m}}\,\beta.$$

For the calculation of C_ms, a simple approach is chosen from [EE02]:

$$C_\mathrm{ms} = \frac{1}{2}(C_\mathrm{f} + C_\mathrm{b}). \tag{2.23}$$

The salt concentration on the membrane C_ms cannot be equated with C_b since the membrane rejects salt and with it increases the salt concentration on the surface of the membrane. This phenomenon is called Concentration Polarization (CP) and is described in the next section 2.1.3.2.

2.1.3.2 Membrane Fouling and Concentration Polarization

The CP can be described as an uneven concentration distribution near the membrane surface, so that $C_\mathrm{ms} > C_\mathrm{f}$. To describe this phenomenon, a nonlinear PDE is necessary as the CP is a two dimensional problem. Into one dimension, namely the direction of the surface of the membrane, the concentration increases as well as into the direction of the outlet of the brine stream. [Kim17]

The solute build-up by the CP on the membrane surface is considered as reversible and controllable. Possible countermeasures would be the velocity adjustment of the feed stream or using pulsation, ultrasound or an electric field. Compared to that, the membrane fouling is more complex because as described in section 2.1.1 the adhesion of undesirable particles at the membrane is influenced by physical, chemical and biological effects. Thus, the membrane fouling is irreversible and causes the decrease of the membrane permeability. [Sab+01]

The reason for this lies in the trapped particles within the membrane. Therefore, the high-pressure set-point must be increased in order to compensate the fouling effect of the membrane. Otherwise, the flux declines at a constant pressure and the useful filtrate rate decreases as well. However, the adjustment of the pressure should be avoided. Since the lifetime of a membrane is proportional to the particle loading of the feed solution, membrane fouling can be handled by the pre-treatment and should be better monitored. [Bak04]

Without any countermeasure, the membrane is clogged due to fouling or CP and then the membrane normally has to be removed and flushed with a cleaning solution. In order to restore the whole efficiency of the plant, the dynamic process parameters of the plant must be re-determined since they are needed for the light-gray-box model of the plant. [Göp21]

However, it is more efficient to avoid the clogging of the membrane as it reduces the maximal amount of clean water produced by the plant. Therefore, the membrane material (see section 2.1.3.3) and the membrane pre-treatment must be chosen properly. [Sab+01]

In addition, a parameter observer might be possible to supervise the trend of the important parameters for the membrane fouling and the CP in order to maintain an efficient process. As stated in [Kuc15], the change of the water transport coefficient $A = A_\mathrm{m}\, k_\mathrm{m}$ and the salt transport coefficient $K = A_\mathrm{m}\, k_\mathrm{s}$ indicates the degradation, fouling or scaling of the membrane. In order to describe both effects of membrane fouling and CP, the gradually decrease of the membrane area A_m is assumed as time-variant parameter for the pilot-scale RO plant which needs to be observed.

2.1.3.3 Membrane Type and Material

The considered RO plant has two spiral wound modules connected in parallel. It is also possible to combine the modules in series, but additional pressure generation between the connected modules would be necessary which is not given in the pilot set-up. Also the used mathematical model has to be adapted. [Göp21]

Furthermore, the type of the membrane module could be changed from spiral wound to hollow fiber. Hollow fiber membranes are explicitly explained in [Kuc15] and can be described as tubes with an inner diameter in the micrometer range. The outer wall of the tube acts as the membrane. They have the advantage of higher package densities which is the effective membrane area per volume of the membrane module. Compared to that, the used spiral wound membrane module does not consist of tubes but sheets positioned on both sides of a permeate carrier (cf. figure 2.4). This carrier is a nylon

mesh and is used as a spacer between two membrane sheets. [Kuc15]

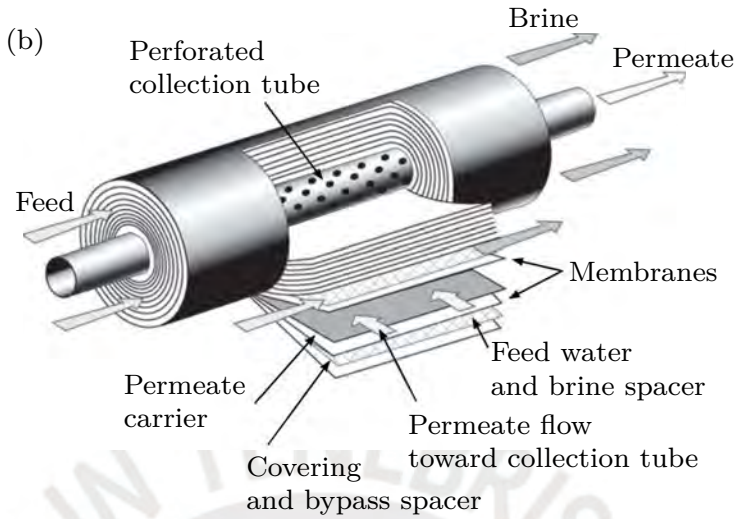

Figure 2.4: Schematic composition of a spiral wound membrane module [Kuc15]

The spacer forms the permeate channel and leads the permeate stream helically to the perforated collection tube in the center of the membrane module and then to the outlet. On the other side of the membrane sheets, the feed/brine spacers are placed in order to provide the channel for the respective stream. Due to the spiral form, various layers are wrapped around the collection tube. Therefore, spiral wound modules compared to hollow fiber modules do not have areas where the water cannot flow properly, and thus, are less sensitive to membrane fouling. [Kuc15; Göp21]

Nevertheless, helical modules are susceptible to CP and could lead to a clogging of the membrane which harms the production of clean water [Bak04]. Due to the parallel set-up, the RO plant can remain in operation during the cleaning of one membrane module. Another positive aspect of the spiral wound modules are the variability of the membrane material. [Göp21]

In the case of the pilot-scale RO plant, the membrane type is a cross linked fully aromatic polyamide composite with the technical designation *Toray TM710D* [TOR19]. This choice can be explained by the required rejection rate of $> 99.3\%$ in order to deliver drinkable water from seawater with only one stage of membrane modules [Göp21]. This rate can be reached with the used type of membrane since the composite membrane *Toray TM710D* obtains a salt rejection of 99.8% [TOR19]. In comparison, the previously developed cellulose acetate membranes only reach a rejection rate of $98-99\%$ and thus are not utilized, although they are cheap in production and robust against chlorine in order to prevent biofouling [Göp21].

However, the most popular RO membrane is the fully aromatic polyamide membrane which is based on 70s technology of interfacial polymerization of a selective layer directly on a porous support [Bak04; Sta16].
The composite membrane consists of a very thin polymer barrier layer ($< 1\mu m$) formed on a thick porous support layer. The thin surface layer allows high water fluxes and a proper rejection of salt which is the aim of an efficient RO process. [CCE06; Wan+11]

There exists an inverse relationship between the applied pressure and the membrane thickness. A thinner membrane needs less pressure to generate a given amount of water. [Sta16] The ratio of membrane surface to volume for a spiral wound module is approximately between $656\frac{m^2}{m^3}$ and $820\frac{m^2}{m^3}$ [Wan+11] and is used for the calculation of the fixed parameters (see table 2.1).

2.2 Sensor Configuration

The sensor configuration of the considered RO plant is depicted in figure 2.5.

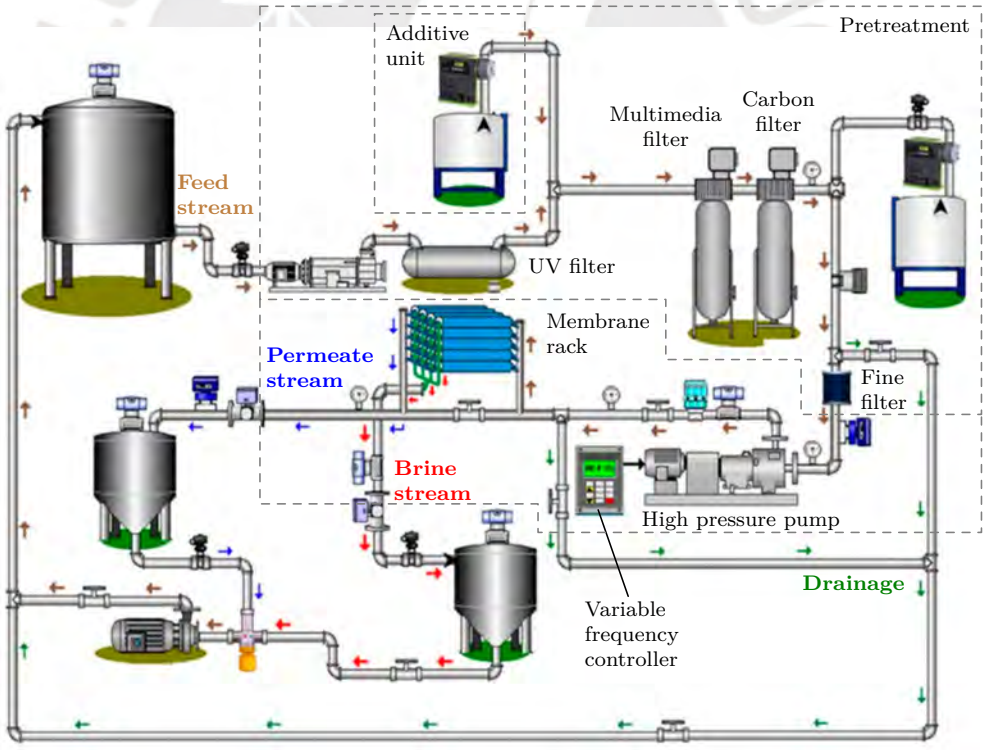

Figure 2.5: Sensor configuration of the RO plant [Riv+19]

The pre-treatment system is explicitly described in section 2.1.1. This part includes a pH sensor after the last tank of additives. The pH measurement is later used for the calculation of the concentration of the feed and permeate stream (cf. equation (2.9)).

Moreover, after each additive tank a dosing pump is installed to control the supply of additives.

The conductivity is measured before the water flows in the high pressure feed pump and after the desalination process, namely the conductivity of the permeate stream. Also a flow sensor is positioned at the outlet of the RO membrane rack. With the values of the conductivity and the flow sensor, the conversion rate can be determined. The permeate conductivity is controlled by the adjustment of the proportional valve in the brine flow which is assumed to have a slow dynamics. In normal operations the proportional valve in the brine stream is opened half by a nominal pressure of $P^* = 20\,\mathrm{bar}$. It is also never completely closed in order to avoid membrane damages. [Riv+19]

Both, a pressure sensor and a flow sensor, are placed at the brine flow outlet. The second pressure sensor of the system is located after the feed water leaves the high pressure feed pump. At the same position, a sensor is put to measure the temperature of the water.

Due to the closed-loop design of the pilot-scale RO plant, drainage and water tanks are necessary since the process is not directly connected to a saltwater source and the water is in a cycle of desalination and salinization [Göp21]. The salt concentration of the feed stream can be replicated by adding Sodium Chloride (NaCl) to the storage tank. Water with the salinity content between $0.5\,\mathrm{kg\,m^{-3}}$ and $30\,\mathrm{kg\,m^{-3}}$ is considered as brackish water. Seawater has a salt content between $30\,\mathrm{kg\,m^{-3}}$ and $50\,\mathrm{kg\,m^{-3}}$ [NW19]. Each tank has a level sensor and either in the inlet or the outlet is put a proportional valve to control the system.

In comparison, a real plant suffers more intensively from changing conditions of the feed water quality, e.g. the temperature, the rate of salinity or other environmental factors, which leads to membrane fouling [FRL17]. However, the dynamics of the pilot-scale RO plant closely resemble the dynamics of a real seawater RO desalination plant. Therefore, the state and parameter estimation of the considered plant gives a good example for a real plant. [Riv+19]

Summarized, the values of pH, γ_f, γ_p, ΔP, Q_p and Q_b can be measured with the sensors. The tasks of the dynamic behavior of the plant are the large time-varying parameters, e.g. the membrane permeability and the surface of the membrane, uncertainties in the model, load disturbances and sensor noise due to the measurement. [FRL17]

2.3 State-space Representation

In figure 2.1 all used variables in the physical context are shown. Aforementioned, the dynamics of the brine valve is neglected, and thus, only one input ω_{el} is considered with a weighting factor u_{p}. As described in the previous section 2.2, the measured variables are listed in green:

Measured Signals:
$$m_1 = pH$$
$$m_2 = Q_{\mathrm{p}}$$
$$m_3 = Q_{\mathrm{b}}$$
$$m_4 = \Delta P$$
$$m_5 = \gamma_{\mathrm{p}}$$
$$m_6 = \gamma_{\mathrm{f}}$$

Inputs $u = u_{\mathrm{p}} \in [0, 1]$

States
$$x_1 = C_{\mathrm{p}}$$
$$x_2 = C_{\mathrm{b}}$$
$$x_3 = \omega_{\mathrm{p}}$$

Output $y = x_1$

The dynamic states of the system are C_{p}, C_{b} and ω_{p}. The output of the system is set equal to the first state C_{p} (see formula (2.27)).

2.3.1 Nonlinear Representation

Based on the formulas of the sections 2.1.2 and 2.1.3.1, the nonlinear state-space representation of the system Σ is given by:

$$\begin{aligned}\dot{x}_1 =& \frac{0.5\,\alpha\,A_{\mathrm{m}}}{V_{\mathrm{p}}}\left(k_{\mathrm{s}} + \Delta P\,k_{\mathrm{m}}\right) + \frac{0.25}{V_{\mathrm{p}}\,b_{\mathrm{f},0}}\Big(A_{\mathrm{m}}\,k_{\mathrm{s}}\,\sigma_1 - 4\,Q_{\mathrm{p}}\,b_{\mathrm{f},0}\,x_1 + A_{\mathrm{m}}\,k_{\mathrm{s}}\,b_{\mathrm{f},0}\Big(C_{\mathrm{f}}^* + x_2 \\ &- \sqrt{(C_{\mathrm{f}}^* + x_2 + \frac{\sigma_1}{b_{\mathrm{f},0}} + 2\,\alpha)^2 + 4\,\beta^2\Delta P^2 - 8\,\beta\,\Delta P\,(0.5\,C_{\mathrm{f}}^* + 0.5\,x_2 + \frac{0.5\,\sigma_1}{b_{\mathrm{f},0}} - \alpha)}\Big)\Big)\end{aligned} \tag{2.24}$$

$$\begin{aligned}\dot{x}_2 =& -\frac{0.499\,\alpha\,A_{\mathrm{m}}}{V_{\mathrm{b}}}\left(k_{\mathrm{s}} + \Delta P\,k_{\mathrm{m}}\right) - \frac{0.0796}{V_{\mathrm{b}}\,b_{\mathrm{f},0}}\Big(12.566\,Q_{\mathrm{b}}\,b_{\mathrm{f},0}\,x_2 \\ &- 120\,V_{\mathrm{d}}\,x_3\,(\sigma_1 + C_{\mathrm{f}}^*\,V_{\mathrm{d}}\,b_{\mathrm{f},0}) + \pi\,A_{\mathrm{m}}\,k_{\mathrm{s}}\Big(C_{\mathrm{f}}^*\,b_{\mathrm{f},0} + b_{\mathrm{f},0}\,x_2 + \sigma_1 \\ &- b_{\mathrm{f},0}\sqrt{(C_{\mathrm{f}}^* + x_2 + \frac{\sigma_1}{b_{\mathrm{f},0}} + 2\,\alpha)^2 + 4\,\beta^2\Delta P^2 - 8\,\beta\,\Delta P\,(0.5\,C_{\mathrm{f}}^* + 0.5\,x_2 + \frac{0.5\,\sigma_1}{b_{\mathrm{f},0}} - \alpha)}\Big)\Big)\end{aligned} \tag{2.25}$$

$$\dot{x}_3 = -\frac{15915\,V_{\mathrm{d}}\,\Delta P + d\,x_3 - c\,(\omega_{\mathrm{el}}^*\,u - p\,x_3)}{J_{\mathrm{p}}} \tag{2.26}$$

$$y = x_1 \tag{2.27}$$

with

$$\sigma_1 = \gamma_\mathrm{f} - \gamma_\mathrm{f}^* + b_{\mathrm{f},1}\ (\mathrm{pH} - \mathrm{pH}^*) \tag{2.28}$$

$$\alpha = \frac{k_\mathrm{s}}{k_\mathrm{m}}\beta \tag{2.29}$$

$$\beta = \frac{M_\mathrm{m}}{\mathcal{R}\,T}. \tag{2.30}$$

The numeric expressions in the state-space representation can be explained with the changed units which have been chosen in order to avoid numerical errors. Due to the CP and the membrane fouling, the parameter $A_\mathrm{m}(t)$ is assumed to be time-variant and should be supervised with the proposed parameter estimator (cf. section 5.3).

This estimator uses the MFM (cf. section 5.2) and thus, requires a modulatable form of the Input/Output (I/O) relation built through the state-space representation. The operation with equations (2.24-2.27) leads to a highly nonlinear I/O relation (B.1) on which the MFM could not be applied easily. Therefore, a linearization of the state-space representation is executed in the following section 2.3.2.

2.3.2 Linearized Representation

Examining the equations (2.24-2.26) closely, the nonlinearity of the states occurs within the discontinuity of the roots. Assuming that the summand $4\,\beta^2\Delta P^2$ dominates numerically, the root can be simplified by using a Taylor series w.r.t. the operating points $\bar{x}_2 = 0.6\,\mathrm{kg\,m^{-3}}$ and $\Delta\bar{P} = 20\,\mathrm{bar}$. The linearized state-space representation of the RO system is given as follows:

$$\begin{aligned}\dot{x}_1 =& \frac{0.5\,\alpha\,A_\mathrm{m}}{V_\mathrm{p}}\left(k_\mathrm{s} + \Delta P\,k_\mathrm{m}\right) + \frac{0.25}{V_\mathrm{p}\,b_{\mathrm{f},0}}\Big(A_\mathrm{m}\,k_\mathrm{s}\,\sigma_1 - 4\,Q_\mathrm{p}\,b_{\mathrm{f},0}\,x_1 \\ &+ A_\mathrm{m}\,k_\mathrm{s}\,b_{\mathrm{f},0}\left(C_\mathrm{f}^* + x_2 - \underbrace{(2\,\beta\,\Delta P - 0.9895\,x_2 - 1.4025)}_{\text{linearized square root}}\right)\Big)\end{aligned} \tag{2.31}$$

$$\begin{aligned}\dot{x}_2 =& -\frac{0.499\,\alpha\,A_\mathrm{m}}{V_\mathrm{b}}\left(k_\mathrm{s} + \Delta P\,k_\mathrm{m}\right) - \frac{0.0796}{V_\mathrm{b}\,b_{\mathrm{f},0}}\Bigg(12.566\,Q_\mathrm{b}\,b_{\mathrm{f},0}\,x_2 - 120\,V_\mathrm{d}\,x_3\,(\sigma_1 + C^*\,V_\mathrm{d}\,b_{\mathrm{f},0}) \\ &+ \pi\,A_\mathrm{m}\,k_\mathrm{s}\left(C_\mathrm{f}^*\,b_{\mathrm{f},0} + b_{\mathrm{f},0}\,x_2 + \sigma_1 - b_{\mathrm{f},0}\,\underbrace{(2\,\beta\,\Delta P - 0.9895\,x_2 - 1.4025)}_{\text{linearized square root}}\right)\Bigg)\end{aligned} \tag{2.32}$$

$$\dot{x}_3 = -\frac{15915\,V_\mathrm{d}\,\Delta P + d\,x_3 - c\,(\omega_\mathrm{el}^*\,u - p\,x_3)}{J_\mathrm{p}} \tag{2.33}$$

$$y = x_1 \tag{2.34}$$

with the equations (2.28-2.30).

In the appendix section B.3, the comparative plots of the evaluated nonlinear and linearized state-space representation are given. After inserting the fixed parameters of table 2.1 into the state-space representations, each dynamics of the states only depend on two variables, i.e. $\dot{x}_1$ needs x_1 and x_2, $\dot{x}_2$ requires x_2 and x_3 and $\dot{x}_3$ depends on x_3 and u. These span a plane in space without nonlinear outliers. The plots of the nonlinear state-space representation (see figures B.1a, B.2a and B.3a) already suggest a linear behavior due to their flat surface area. There is no noticeable difference in the plots of $\dot{x}_1$ (see figures B.1), $\dot{x}_2$ (see figures B.2) and $\dot{x}_3$ (see figures B.3) compared to the nonlinear plots.

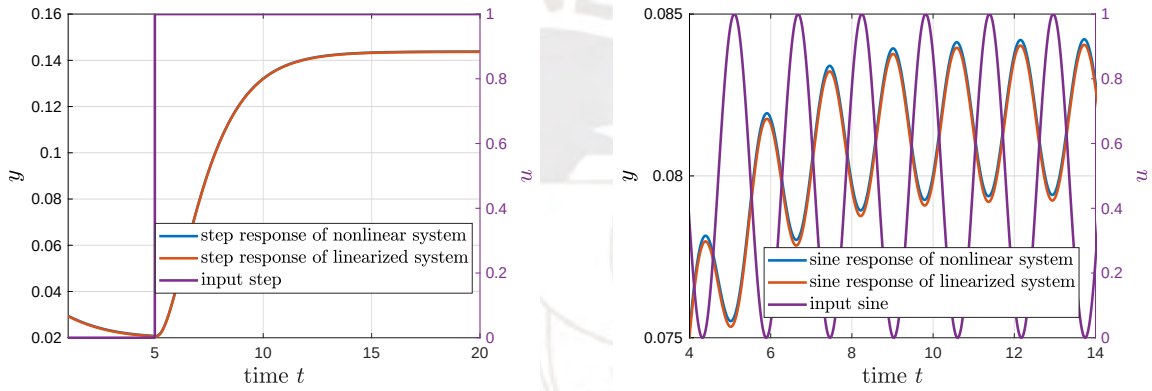

(a) Step input (b) Sine input

Figure 2.6: Comparison of the responses of the nonlinear (2.24-2.27) and the linearized system (2.31-2.34)

This is confirmed by the comparison of the step responses of the nonlinear and the linearized system in figure 2.6a since the step responses are congruent. This approximated linearized form of the state-space model is used in section 5.3 in order to estimate the time-variant parameter A_m.

Also the response of the nonlinear and linearized system to a normalized sine signal with a frequency of $f = 4\,\mathrm{rad\,s^{-1}}$ is analyzed. In figure 2.6b, a small deviation between both responses is recognizable. The operation of the RO system normally includes periodic changes in the rotational speed of the pump ω_p. Therefore, the nonlinear system is directly used for the state estimation in section 5.4 instead of the linearized form.

3 Observability of Nonlinear Systems

There are various reasons why an observer in the control engineering is useful. As stated in [Bes07a], in general three topics are concerned: control, monitoring and fault detection.

Firstly, the more information there is about the states, the more efficient the control of a system can be. Due to missing or expensive sensors or non-measurable states, the states have to be estimated by an observer. With the estimated values, the control signal can be determined and applied to the system in order to control the behavior of the plant. The aim is to stay in the stable part of the closed-loop control system. In the case of the RO plant, the control of the concentration of the permeate stream is required in order to achieve drinkable water.

Secondly, it is useful to monitor the process variables, e.g. in order to prevent the clogging of the membrane. If a certain threshold is reached, the process should be stopped. The requirements of supervision contain a precise estimation of the states in order to achieve the smallest observer error.

The third necessity of an observer belongs to fault detection. Failures as leaks, breaks or sensor errors must be detected before they lead to an irreversible damage. There are distinct methods of fault detection, e.g. applying structural analysis [Pér17; Göp21], using signal models [Ise06] or via state and parameter estimation by an observer with the knowledge of the considered system.

Before implementing an observer, it is important to investigate whether the system is observable. Observability inquires the theoretical, mathematical possibility of the reconstruction of the states $x(t)$ from the input u and the output y of a system in a time interval. Therefore, several observability concepts are introduced in the following section 3.1. Afterwards, these methods are applied symbolically in section 3.2.1 and numerically in section 3.2.2 to the RO plant.

3.1 Observability Definitions

Consider a continuous-time nonlinear dynamical Single-Input Single-Output (SISO) system:

$$\Sigma := \begin{cases} \dot{x}(t) &= f(x(t), u(t)), \quad x(t_0) = x_0 \\ y(t) &= h(x(t)) \quad \text{where } x(t) \in \mathbb{R}^n, u(t) \in \mathbb{R}, y(t) \in \mathbb{R}. \end{cases} \tag{3.1}$$

It is assumed that the functions f and h are known and the input $u(t)$ and the output $y(t)$ are measurable. The solution of the non-homogenous differential equation (3.1) is expressed as $\psi(t; x_0, u(\cdot))$. If it is possible to uniquely determine $x(t_0)$ from the knowledge of $y(t)$ and $u(t)$ at any time interval in $I = [t_0, t_f]$ with $0 \leq t_0 \leq t_f$ and $t \in I$, the system Σ (3.1) is called observable. To assure an explicit solution in the nonlinear case, it is important to introduce the definition of indistinguishability (Definition 3.1.1) in order to be able to differentiate between distinct initial states.

Definition 3.1.1 (Indistinguishability [HK77]). *A pair of initial states $(x_0, x_0') \in \mathbb{R}^n \times \mathbb{R}^n$ is indistinguishable for a system Σ (3.1) if:*

$$\forall u \in \mathcal{U}, \forall t \geq 0, \; h(\psi(t; x_0, u)) = h(\psi(t; x_0', u)). \tag{3.2}$$

A state x is indistinguishable from x_0 if the pair (x_0, x_0') is indistinguishable.

This property is used to define the observability:

Definition 3.1.2 (Observability (resp. at x_0) [Bes07a]). *A system Σ (3.1) is observable (resp. at x_0) if it does not admit any indistinguishable pair (resp. any state indistinguishable from x_0).*

It results that there exists an observer if the system is observable. As this definition 3.1.2 is too general for the practical use, more verifiable concepts of the observability are necessary that are considered in local neighborhoods. In order to distinguish between cases where, for example, certain input signals give rise to such indistinguishable regions, an even more specific definition 3.1.3 is introduced:

Definition 3.1.3 (Weak observability (resp. at x_0) [Bes07a]). *A system Σ (3.1) is weakly observable (resp. at x_0) if there exists a neighborhood U of any x (resp. at x_0) such that there is no indistinguishable state from x (resp. x_0) in U.*

This definition does not hold cases when a trajectory has to go far from U before it is distinguishable between two different states of U. Therefore, a more particular definition is required:

Definition 3.1.4 (Local weak observability (LWO) [resp. at x_0] [Bes07a])**.** *A system Σ (3.1) is Locally Weakly Observable (LWO) (resp. at x_0) if there exists a neighborhood U of any x (resp. of x_0) such that for any neighborhood V of x (resp. x_0) contained in U, there is no indistinguishable state from x (resp. x_0) in V when considering time intervals for which trajectories remain in V.*

In summary, the trajectories in h cannot leave the neighborhood V and every state is distinguishable from its neighbors without 'going too far'. In other words, one can distinguish between any two initial conditions which are close to each other, although there could be other initial conditions which far from each other are indistinguishable.

As a geometrical characterization the observability space is introduced here, which is a subset of the state space.

Definition 3.1.5 (Observation space [Bes07a])**.** *The observation space for a system Σ (3.1) is defined as the smallest real vector space (denoted by $\mathfrak{o}(h)$) of C^∞ functions containing the components of h and closed under Lie derivative along $f_u := f(\cdot, u)$ for any constant $u \in \mathbb{R}^m$ (namely such that for any $\psi \in \mathfrak{o}(h), \mathcal{L}_{f_u}^k \psi \in \mathfrak{o}(h)$, where $\mathcal{L}_{f_u}^k \psi(x) = \frac{\partial \psi}{\partial x} f(x, u)$).*

With definition 3.1.5 and considering constant input values, the observability map includes the output and its derivatives:

Definition 3.1.6 (Observability map [Noa+16b])**.** *According to definition 3.1.5, the related observability map $\mathfrak{o}_k(x) : \mathbb{R}^n \to \mathbb{R}^k$ of the system class Σ (3.1) w.r.t. f_u is defined as:*

$$\mathfrak{o}_k(x) := \begin{pmatrix} y \\ \dot{y} \\ \vdots \\ y^{(k)} \end{pmatrix} = \begin{pmatrix} h(x) \\ \mathcal{L}_{f_u} h(x) \\ \vdots \\ \mathcal{L}_{f_u}^k h(x) \end{pmatrix} = Z \text{ with } Z = \begin{pmatrix} z_0 \\ z_1 \\ \vdots \\ z_{k-1} \end{pmatrix} \tag{3.3}$$

where $\mathcal{L}_{f_u}^k h(x)$ describes the k-th Lie derivative w.r.t. f_u and $k \in \mathbb{N}$.

The observability matrix can be calculated by differentiating the observability map (3.3) w.r.t. the states, i.e. the observability matrix is the Jacobian of the observability map:

Definition 3.1.7 (Observability matrix [Noa+16b])**.** *The observability matrix $\mathcal{O}_k(x) \in$*

$\mathbb{R}^{k\times n}$ *can be calculated as:*

$$\mathcal{O}_k(x) := \frac{\partial \mathfrak{o}_k(x)}{\partial x} = \begin{pmatrix} \frac{\partial}{\partial x}h(x) \\ \frac{\partial}{\partial x}\mathcal{L}_{f_u}h(x) \\ \vdots \\ \frac{\partial}{\partial x}\mathcal{L}^k_{f_u}h(x) \end{pmatrix} \tag{3.4}$$

where $\frac{\partial}{\partial x}(\cdot)$ *stands for the gradient (row vector).*

The observability matrix for a Linear Time-Invariant (LTI) system is equal to the observability matrix according to Kalman. In consideration of the Implicit Function Theorem, the observability matrix can be used to determine local solvability of the nonlinear system for the state x. Therefore, the following theorem 3.1.1 is introduced:

Theorem 3.1.1 (Observability rank condition (resp. at x_0) [Noa+16b])**.** *The system* Σ *(3.1) is LWO at* $x_0 \in \mathbb{R}^n$ *if* $\exists k \in \mathbb{N}$ *such that for all constant* $u \in \mathbb{R}^p$*:*

$$\mathcal{O}_k(x_0) \in \mathbb{R}^{k\times n} \quad \textit{and} \quad rk(\mathcal{O}_k(x_0)) = n. \tag{3.5}$$

If this holds for all $x_0 \in \mathbb{R}^n$*, the system is globally weakly observable.*

The nonlinear system is locally observable at x_0 if for some value of k the observability matrix is at least injective. From the Cayley-Hamilton theorem it is sufficient to check $k = n-1$ where n stands for the order of the system Σ. Practically, one has to calculate the determinant of the observability matrix in order to evaluate the observability rank condition (theorem 3.1.1). In the LTI case, a fulfilled rank condition of the observability matrix according to Kalman implies that the pair (A, C) is called observable.

Until now only constant inputs have been considered although the influence of some inputs can harm the observability of a system. Therefore, analytic conditions for observability have to be introduced in order to involve the impact of the input on a nonlinear system.

Definition 3.1.8 (Universal inputs (resp. on $[0,t]$) [Bes07a])**.** *An input* u *is universal (resp. on* $[0,t]$*) for system* Σ *(3.1) if* $\forall x_0 \neq x_0', \exists \tau \geq 0$ *(resp.* $\exists \tau \in [0,t]$*) so that* $h(\psi(\tau; x_0, u)) \neq h(\psi(\tau; x_0', u))$*.*
An input u *is a singular input if it is not universal.*

In order to simplify the observability of a nonlinear system, singular inputs which are difficult to handle should be avoided.

Definition 3.1.9 (Uniformly observable systems (resp. locally) [Bes07a]). *A system is Uniformly Observable (UO) if every input is universal (resp. on* $[0, t]$*).*

The property of UO can be checked with any pair of distinct states. Hence, the universality is assured over time, the observability is independent of its inputs.

In general, systems are input dependent. Therefore, it is always important to investigate whether this creates unobservable spaces. The most practice oriented criterion belongs to the theorem 3.1.1 which is easier verifiable than the UO concepts and is sufficient in the most cases, e.g. for non-uniformly observers as typically corresponding to the case of Kalman observers for Linear Time-Variant (LTV) systems [KB61; Bes07a]. Based on this, there exist various approaches on the observability of nonlinear systems, e.g. stronger concepts of the observability in [Bes07a] or the concept of the infinitesimal observability in [GK01], but these are not considered here due to the application.

If the system is stated as observable, there exists an asymptotic observer. The aim of an asymptotic observer is the convergence of the observer error $e(t) := \hat{x}(t) - x(t)$ to the equilibrium $e = 0$. Therefore, the definition of [Bes07a] is modified:

Definition 3.1.10 (Asymptotic observer). *Considering a system* Σ *(3.1), an observer is given by an auxiliary system:*

$$\dot{X}(t) = F(X(t), u(t), y(t), t) \tag{3.6}$$

$$\hat{x}(t) = H(X(t), u(t), y(t), t) \tag{3.7}$$

such that with the observer error $e(t) := \hat{x}(t) - x(t)$*:*

$$(i) \quad e(0) = 0 \Rightarrow e(t) = 0, \ \forall t \geq 0; \tag{3.8}$$

$$(ii) \ \lim_{t \to \infty} \|e(t)\| = 0. \tag{3.9}$$

If (ii) *holds for any* $x(0), \hat{x}(0)$*, the observer is global. Moreover, if* (ii) *is valid with an exponential convergence, the observer is exponential. If* (ii) *holds with a convergence rate which can be tuned, the observer is tunable.*

In this thesis, the EKF is applied as an asymptotic observer (see section 4) based on the definition 3.1.10. Comparatively, MFs are used to create a non-asymptotic observer in section 5.

3.2 Observability Analysis of the Reverse Osmosis Plant

As a basis, the nonlinear state-space representation (2.24-2.27) of the RO system of the section 2.3 is used. The observability of the linear state-space representation can be derived from the observability analysis of the nonlinear system. The observability evaluation is divided into the symbolic and the numerical analysis which are outlined in the following two subsections.

3.2.1 Symbolic Analysis

The calculation of the observabiliy matrix $\mathcal{O}(x)$ (cf. definition 3.1.7) of the considered system corresponds to the derivatives of the observability map $\mathfrak{o}(x)$ (cf. definition 3.1.6) w.r.t. the states $x = [x_1, x_2, x_3]^\top$:

$$\mathcal{O}(x) = \begin{pmatrix} 1.0 & 0 & 0 \\ -\frac{Q_\mathrm{p}}{V_\mathrm{p}} & \frac{0.25\,A_\mathrm{m}\,k_\mathrm{s}}{V_\mathrm{p}} - \frac{0.125\,A_\mathrm{m}\,k_\mathrm{s}\,\sigma_3}{V_\mathrm{p}\,\sigma_2} & 0 \\ \frac{{Q_\mathrm{p}}^2}{{V_\mathrm{p}}^2} & * & \frac{2.3873\,A_\mathrm{m}\,V_\mathrm{d}\,k_\mathrm{s}\,\sigma_1}{V_\mathrm{b}\,V_\mathrm{p}\,b_{\mathrm{f},0}} - \frac{1.1937\,A_\mathrm{m}\,V_\mathrm{d}\,k_\mathrm{s}\,\sigma_3\,\sigma_1}{V_\mathrm{b}\,V_\mathrm{p}\,b_{\mathrm{f},0}\,\sigma_2} \end{pmatrix} \tag{3.10}$$

with

$$\sigma_1 = \gamma_\mathrm{f} - \gamma_\mathrm{f}^* + b_{\mathrm{f},1}\,(\mathrm{pH} - \mathrm{pH}^*) + C_\mathrm{f}^*\,b_{\mathrm{f},0} \tag{3.11}$$

$$\sigma_2 = \sqrt{\left(C_\mathrm{f}^* + x_2 + \frac{\sigma_1}{b_{\mathrm{f},0}} + 2\alpha\right)^2 + 4\beta^2\Delta P^2 - 8\beta\Delta P\left(0.5\,C_\mathrm{f}^* + 0.5\,x_2 + \frac{0.5\,\sigma_1}{b_{\mathrm{f},0}} - \alpha\right)} \tag{3.12}$$

$$\sigma_3 = 2\,C_\mathrm{f}^* + 2\,x_2 + \frac{2\,\sigma_1}{b_{\mathrm{f},0}} - 4\,\beta\,\Delta P + 4\,\alpha \tag{3.13}$$

$$\alpha = \frac{k_\mathrm{s}}{k_\mathrm{m}}\beta \tag{3.14}$$

$$\beta = \frac{M_\mathrm{m}}{\mathcal{R}\,T}. \tag{3.15}$$

Since the resulting matrix (3.10) is a lower triangular matrix, it is only necessary to verify that the elements on the diagonal are different from zero in order to ensure that the determinant of the matrix is non-zero. Since the input u occurs only in the last state x_3, which in turn appears only linearly in state x_2, the observability map and matrix are independent of the input and thus autonomous.

Obviously, the rank criterion (see theorem 3.1.1) for this observability matrix is not fulfilled if one of the parameters k_s, V_d or A_m is equal to zero. The volume of the pump displacement is assumed to be constant and thus will never be zero apart from the

situation when the pump is broken. This scenario is excluded in this thesis. However, the parameters of the membrane k_s and A_m can reach zero if the membrane is clogged due to membrane fouling or CP (see section 2.1.3.2). That means that a clogged membrane must be avoided in order to keep the system observable.

3.2.2 Numerical Analysis

Inserting the values of the parameter table 2.1, the observability matrix only depends on the measurements γ_f, pH and ΔP, the time-variant parameter A_m and the state x_2 (see formula (A.1) in the appendix). Based on this evaluated observability matrix (A.1), plots with possible unobservable spaces are generated which are shown in figure 3.1. Since the values of γ_f and pH do not change highly in the considered system, they are assumed to be a constant measurement of $\gamma_f = 0.1\,\mathrm{S\,m^{-1}}$ and $pH = 7$.

The remaining three variables are considered in the range of a lower and upper limit which are set in table 3.1. The maximum limit of A_m belongs to the nominal value A_m^*

Variable	**Minimum**	**Maximum**	**Unit**
A_m	0	16	$[\mathrm{m^2}]$
ΔP	0	20	[bar]
x_2	0	5	$[\mathrm{kg\,m^{-3}}]$

Table 3.1: Simulation area for observability study

that stands for the completely particle free membrane surface taken from [TOR19].
The generated pressure difference and the concentration of the brine stream depend on whether brackish or seawater is desalinated. A higher salt concentration of the feed stream requires a greater value of the pressure difference in order to produce the same amount of desalinated water. Since the feed stream of the considered pilot-scale plant is brackish water produced by adding NaCl manually, the upper limit of ΔP and C_b have been chosen to $\Delta P_{max} = 20\,\mathrm{bar}$ and $x_2 = C_{b,max} = 5\,\mathrm{kg\,m^{-3}}$.
Physically, the minimum limit of the membrane surface A_m and the brine concentration C_b are equal to zero. The lower limit of the pressure difference is also set to zero since it is assumed to operate the plant in RO mode.

The figure 3.1a proves the symbolic evaluation of section 3.2.1 that $A_m = 0$ will lead to an unobservable RO system. In this plot, the value of C_b is fixed to $x_2 = 0.6\mathrm{kg\,m^{-3}}$. Furthermore, $\Delta P = 0$ leads to a determinant of the observability matrix equal to zero. This is confirmed by the figure 3.1b which demonstrates the relation of the variable ΔP and the second state C_b. In this plot, the surface of the membrane is assumed

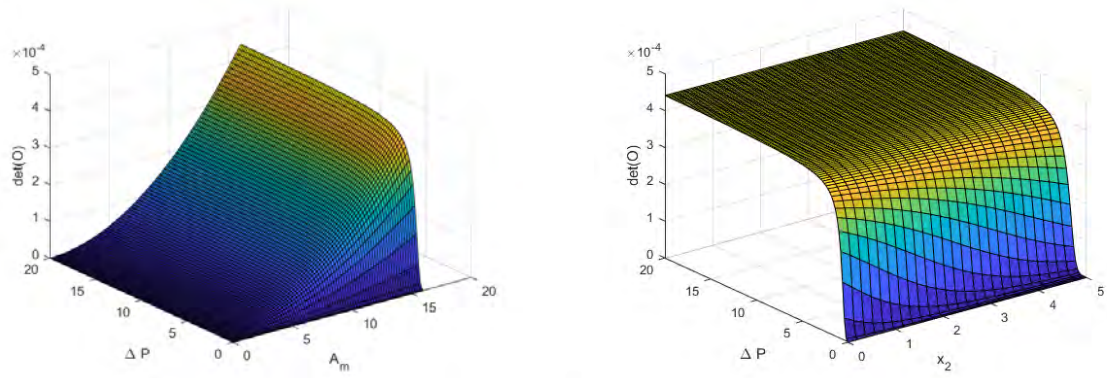

(a) (b)

Figure 3.1: Determinant of the observability matrix evaluated with ΔP, x_2 and A_m

to be equal to the nominal value $A_\mathrm{m}^* = 16\mathrm{m}^2$. Moreover, it becomes obvious that the values of the second state x_2 do not harm the observability of the system as no value in the range of $[0, 5]$ leads to an observability matrix with a rank smaller than $n = 3$. Noticeable are the generally small values for the determinant which lead to a condition number of the observability matrix $\kappa(\mathcal{O}) \approx 7.85 \times 10^5$. This can be explained by the small inserted variables (cf. table 2.1) and the dimension of the chosen units. Therefore, the invertibility as well as its error susceptibility are within a tolerable range and only zero-valued determinants create a non observable space.

Summarized, if the RO plant is in running mode, the rank criterion (theorem 3.1.1) is fulfilled, and thus, the system is LWO. Since the observability map is autonomous of the input u, the map has an unique solution for the states for any given input. Therefore, there are no singular inputs and the RO system is even UO. [Bes07a]

If the system is observable w.r.t. to theorem 3.1.1, the system can be converted by a state transformation into a more manageable form, i.e. there exists a normal observable form of the system which is useful in the design of nonlinear observers. Analogous to the exact input-state linearization for the controller design, an exact estimation error linearization can be performed for the observer design, as shown in [KR85]. Thereby, a diffeomorphism for state and output transformation have to be found which, on the one hand, can only be done for a very restrictive class of systems. On the other hand, this leads to a solution problem of partial differential equations and thus is very complex. Another concept of a normal observable form is depicted in [GB81] and comprises a partial linearization of the system and the transformed state can be built from the observability map (3.3). If the input affine normal observable form is not given, the state transformation can still be performed with similar statements, i.e. it is possible

to reconstruct the state x in a locally weakly sense from the output y which will be used in section 5.4.1 to build an I/O relation of the system. This relation is essential for the construction of the observer with MFs.

4 Extended Kalman-Bucy Filter

The EKF belongs to the asymptotic observers (cf. definition 3.1.10) and is a stochastic approach. This thus provides a basis of comparison to the non-asymptotic MF observer approach proposed in chapter 5. In the following chapter, the EKF is explained and the local convergence proof is given in 4.3.

In 1960 Kalman published his paper [Kal60] about a recursive solution to the discrete time linear filtering and prediction problem. This original theory of the Kalman Filter (KF) is based on a discrete dynamic system with additive white noise which models unpredictable disturbances. One year later in 1961 Kalman and Bucy released together their "New Results in Linear Filtering and Prediction Theory" [KB61] describing the Kalman-Bucy Filter as the continuous time version of the KF.

The proposed KF has the same structure of a Luenberger observer [Bes07a]. Both are asymptotic observers based on definition 3.1.10. In contrast to the fixed matrix gain of the Luenberger observer due to the choice of the eigenvalues of the estimation error dynamics, the KF determines the matrix gain in such a way that the influence of the noise is minimal. The KF is a predictor-corrector type estimator, which means it is a recursive procedure consisting of a time update ('predict') and a measurement update ('correct') that is optimal in the sense of minimizing the estimated error covariance. This optimization problem has a closed-form solution, namely in the form of the solution of the Riccati Differential Equation (RDE).

When the considered system is nonlinear, an extension of the KF is necessary which was first published by Gelb in 1979 [Gel+01]. This extension includes the linearization via a first order approximation of the Taylor series along the trajectory in each time step and the observer gain is determined by the optimization of a cost function. Advantageously, normally distributed stochastic disturbances can be taken into account, and thus, a certain robustness can be achieved. Therefore, an explicit description of this EKF follows in this chapter and is applied to the nonlinear RO plant in chapter 6.

Julier and Uhlmann proposed a further improvement of the EKF in [JU04] called the Unscented KF. This approach propagates the mean and covariance information through nonlinear transformation in order to avoid the linearization step of the EKF. Hence, their method is presented to be easier to implement and more accurate since the estimation of the considered systems is reliable even if the system is far from linear. Due to the nearly linear behavior of the RO plant (cf. section 2.3.2), the EKF provides

good results, and thus, the Unscented KF is not further considered in this thesis.

4.1 Definition

The general nonlinear system (3.1) is extended to:

$$\Sigma := \begin{cases} \dot{x}(t) &= f(x(t), u(t)) + w(t), \quad x(t_0) = x_0 \\ y(t) &= h(x(t)) + v(t) \end{cases} \tag{4.1}$$

with the process noise $w(t)$ and the measurement noise $v(t)$. This measurement noise $v(t)$ comprises the simulation of disturbances of the sensor system which manipulates the system output y. The process noise $w(t)$ is an additive or multiplicative perturbation of the system model that includes external influences or parameter uncertainties. Both noises are assumed to be a Gaussian white noise with the following characteristics [Bes07a]:

- The expectation of the white noise has zero mean and is unbiased:

$$E(w(t)) = 0, \quad E(v(t)) = 0. \tag{4.2}$$

- The stochastic processes w.r.t. process and measurement noise are uncorrelated:

$$E(w(t_1)\, v^\top(t_2)) = 0, \quad E(v(t_1)\, w^\top(t_2)) = 0 \qquad \forall t_1, t_2. \tag{4.3}$$

- The process noise is itself uncorrelated in time and has the covariance matrix Q:

$$E(w(t_1)\, w^\top(t_2)) = Q\, \delta(t_1 - t_2), \quad Q^\top = Q \geq 0. \tag{4.4}$$

- The measurement noise is itself uncorrelated in time and has the covariance matrix R:

$$E(v(t_1)\, v^\top(t_2)) = R\, \delta(t_1 - t_2), \quad R^\top = R \geq 0. \tag{4.5}$$

- Both noise variables have a normal probability distribution.

The covariance matrices Q and R serve as setting parameters of the observer and can be determined with the power density spectrum, i.e. with the Fourier transform of the autocorrelation function of the respective processes. The design of these matrices R and Q require experience since they are normally unknown in practice. Hence, they

are often estimated as a positive semi-definite diagonal matrix based on the amplitude of the noise. In the simplest case, they are assumed to be unitary matrices.

The estimation equation of the KF can formally be applied to this nonlinear situation, thus the EKF is defined as follows.

Definition 4.1.1 (EKF [Bes07a])**.** *Considering a system Σ (3.1), the corresponding EKF with covariances $Q = Q^\top \geq 0, R = R^\top > 0$ and the forgetting factor $\lambda \geq 0$ is given by*

$$\dot{\hat{x}} = f(\hat{x}(t), u(t)) - K\Big(h(\hat{x}(t)) - y(t)\Big) \quad \text{with } K = P(t)C(t)^\top R^{-1} \tag{4.6}$$

$$\dot{P}(t) = A(t)P(t) + P(t)A(t)^\top - P(t)C(t)^\top R^{-1}C(t)P(t) + Q + \lambda P(t) \tag{4.7}$$

where the linearization

$$A(t) := \frac{\partial f}{\partial x}\Big|_{(\hat{x}(t),u(t))}, \quad C(t) := \frac{\partial h}{\partial x}\Big|_{(\hat{x}(t))} \tag{4.8}$$

is applied.

The worse the measurement quality of the respective sensor is, the larger the values of the measurement noise variance matrix R should be made. However, bigger entry values of R lead to a smaller Kalman gain K, i.e. the adaption to process changes occurs more slowly. Nevertheless, the gain K is very sensitive to the measurement noise variance matrix R, especially when R has small entries.
The diagonal entries of the process noise covariance matrix Q should be the larger, the more transient or the worse modeled the dynamics of the respective state is expected to be. It is recommended to tune the covariance matrices during tests and simulations.

The error covariance $P(t)$ is the only positive semi-definite solution ($P^\top = P \geq 0$) of the RDE $\dot{P}(t)$ (cf. equation (4.7)). The RDE is solvable depending on Q, i.e. Q should be well known. Additionally, it holds $P(0) = P^\top(0) > 0$. Next to $P(t)$, the EKF has a second solution $\hat{x}(t)$.

The EKF is a predictor-corrector procedure that depends only on the previous estimation state following the Markov Property. It is a great advantage of the KF that, in addition to the estimation of a state, it also provides deviation information in the form of the stochastic variance. This contributes a kind of quality measure of one's estimate.

The Jacobian matrices $A(t)$ and $C(t)$ (4.8) result from a first-order Taylor approximation, i.e. the nonlinear trajectory is linearized at each sampling time point around the current reference point $\hat{x}(t)$ and the current input signal $u(t)$. If the system includes discontinuities, e.g. root function, this might lead to problems since these functions

reach infinite slopes and thus are non Lipschitz continuous. Furthermore, since the Taylor expansion is a linear process, the estimation with the EKF only gets relatively close to the true value as long as the system equations are nearly linear and continuous.

Another disadvantageous aspect covers the performance of the EKF which relies on the state and observation noise. If the two noise covariance matrices R and Q are not accurately enough estimated, errors would be accumulated and as a result, the EKF would diverge. These phenomena could be avoided by using the Unscented KF, which has the same computation complexity as the EKF.

Another problem regards to the assumption that the filter is bounded to Gaussian white noise with zero mean. This can vary from reality, because the ideal coincidence does not occur but mostly a systematic deviation of it, thus a correlation is always present.

Nevertheless, the EKF shows sufficient results on the considered RO plant in order to compare it with the proposed Extended Modulation Filter (EMF) in chapter 6. In total, the general system is built by a differential equation of the order $\frac{1}{2}n^2 + \frac{3}{2}n$ due to the RDE and the EKF differential equation, which should be solved simultaneously since $A(t)$ and $C(t)$ depend on $\hat{x}(t)$ and $u(t)$. The order of the general system grows very strongly with the order of the system n. Thereby, the complexity of the solution of the RDE rises by in the case of higher dimensional systems. [Mor14]

4.2 Structure

The figure 4.1 gives an overview about the prediction-correction procedure of the EKF. Due to simplicity, the time dependency is neglected in this figure.

As first step of the EKF recursion, the covariance matrices R and Q and the initial values of $\hat{x}_0$ and P_0 have to be chosen. Using the measurements of the input u of the nonlinear system and the estimated $\hat{x}$, the actual state dynamic $\dot{\hat{x}}$ and the output $\hat{y}$ can be predicted.

The values of the Jacobian matrices $A(t)$ and $C(t)$ are updated with the estimated $\hat{x}$ and the measured u since they change continuously due to the new linearization in each time step. Therefore, the RDE $\dot{P}(t)$ is resolved online in order to determine the stationary value of $P(t)$. This numerical solution of the RDE is given by means of an integration process, e.g. the Runge-Kutta method. The Kalman gain $K(t)$ is computed with the fixed process noise covariance matrix R, the error covariance matrix $P(t)$ estimated in the previous time step and the newly calculated Jacobian $C(t)$ w.r.t. the output $y(t)$.

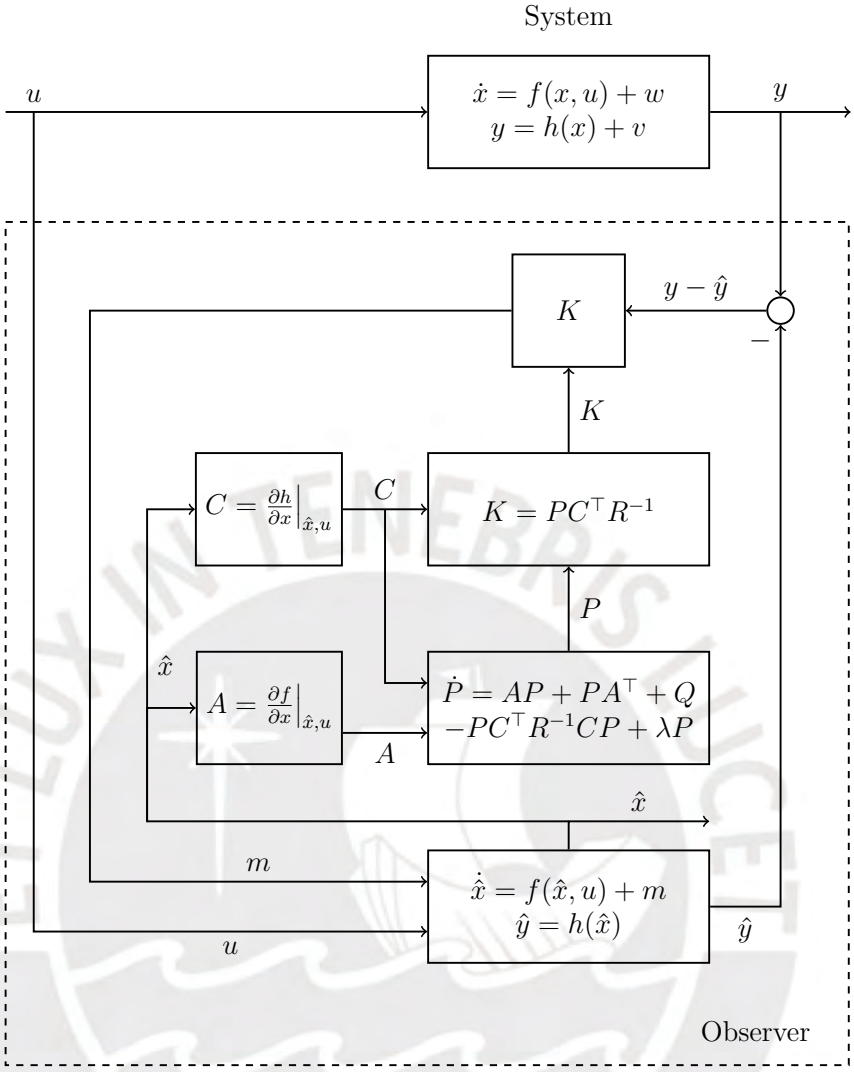

Figure 4.1: Structure of the EKF

In the last step of the correction phase, the new value for the state dynamics $\dot{\hat{x}}(t)$ is computed by adding the predicted value of the state dynamics to the correction factor $m(t) = K(t)\, e_{\mathrm{y}}(t)$ consisting of the product of the Kalman gain $K(t)$ and the output error $e_{\mathrm{y}}(t) = y(t) - \hat{y}(t)$. Also the RDE $\dot{P}(t)$ is calculated in order to compute a new $P(t)$ for the next time step.

4.3 Convergence Analysis

In [Kre03] the convergence analysis of the EKF is subject to the assumption that the considered system (4.1) is UO for any input and the system equations f, h satisfy the Lipschitz condition. In general, the convergence can be assured only locally and is based

on the Lyapunov theorem of stability [Kha02]. The forgetting factor λ is set to zero in order to analyze the classical Kalman observer. The dynamics of the estimation error $e(t) = \hat{x}(t) - x(t)$ is given by

$$\dot{e}(t) = f(\hat{x}(t), u(t)) - f(x(t), u(t)) + K(h(x(t)) - h(\hat{x}(t))) + \xi(t)\,, \quad e(t_0) = e_0 \tag{4.9}$$

with the perturbation

$$\xi(t) = K(t)\, v(t) - w(t). \tag{4.10}$$

Furthermore, it is assumed that $x(t), u(t), K(t), v(t), w(t)$ are bounded and that the system is $\mathcal{C}^2$. Using a Taylor series around the equilibrium $e = 0$, it follows:

$$\dot{e}(t) = [A(t) - K(t)\, C(t)]e(t) + \eta(e,t) + \xi(t) \tag{4.11}$$

$$\begin{aligned}\eta(e,t) = {} & f(\hat{x}(t), u(t)) - f(x(t), u(t)) \\ & + K(h(x(t)) - h(\hat{x}(t))) - [A(t) - K(t)\, C(t)]e(t)\end{aligned} \tag{4.12}$$

$$\eta(0,t) = 0. \tag{4.13}$$

By the mean value theorem, η and ξ are bounded:

$$||\eta(e,t)|| \leq k_1\, ||e(t)||^2\,, \quad ||\xi(t)|| \leq k_2. \tag{4.14}$$

It is considered a quadratic Lyapunov function candidate for the observer error equation

$$V(t,e) = e^\top(t) P^{-1}(t) e(t) \tag{4.15}$$

which is positive definite and decrescent. This condition is fulfilled if the pair $(A(t), C(t))$ is uniformly completely observable such that the following holds

$$l_1 ||e(t)||^2 \leq V(t,e) \leq l_2 ||e(t)||^2. \tag{4.16}$$

Moreover, the candidate satisfies the condition $V(t,0) = 0$. According to the Lyapunov's stability theorem (see [Kha02]), the derivative of the Lyapunov candidate $\dot{V}$ must be negative definite which is shown as follows under consideration that

$$\frac{d}{dt} P^{-1}(t) = -P^{-1}(t) \frac{dP(t)}{dt} P^{-1}(t)\,: \tag{4.17}$$

$$
\begin{aligned}
\dot{V} &= \dot{e}^\top(t)P^{-1}(t)e(t) + e^\top(t)P^{-1}\dot{e}(t) + e^\top(t)\frac{d}{dt}P^{-1}(t)e(t) \\
&= e^\top(t)(A(t) - K(t)C(t))^\top P^{-1}(t)e(t) + e^\top(t)P^{-1}(t)(A(t) - K(t)C(t))e(t) \\
&\quad - e^\top(t)P^{-1}(t)\frac{dP(t)}{dt}P^{-1}(t)e(t) + 2e^\top(t)P^{-1}(t)(\eta(e,t) + \xi(t)) \\
&= e^\top(t)P^{-1}(t)\Bigg[P(t)A^\top(t) + A(t)P(t) - P(t)C^\top(t)R^{-1}C(t)P(t) \\
&\quad - P(t)C^\top(t)R^{-1}C(t)P(t) - \frac{dP}{dt}\Bigg]P^{-1}(t)e(t) + 2e^\top(t)P^{-1}(t)\xi(t) \\
&= -e^\top(t)P^{-1}(t)QP^{-1}(t)e(t) - e^\top(t)C^\top(t)R^{-1}C(t)e(t) + 2e^\top(t)P^{-1}(t)\eta(e,t) \\
&\quad + 2e^\top(t)P^{-1}(t)\xi(t) \\
&\leq -c_1||e(t)||_2^2 + c_2||e(t)||_2^3 + c_3||e(t)||_2||\xi(t)||_2. \qquad (4.18)
\end{aligned}
$$

Hence, the estimation error dynamics is Input-to-State-Stable (ISS) of small gain w.r.t. $\xi(t)$ [Kha02]. For small initial conditions and small perturbations ξ, the error $e = 0$ is a locally exponentially stable equilibrium if $\xi = 0$. Furthermore, if $\xi \to 0$, then $e \to 0$ and if ξ is bounded, e remains bounded. [Mor14]

Therefore, it is obvious that the EKF is an asymptotic observer. The EKF fulfills the optimal state estimator problem which determines the state x as an estimated value $\hat{x}$ dynamically from the knowledge of u and the measured values of y so that the error expectation is minimized and the estimation error dynamics is asymptotically stable. However, this local convergence underlies the assumptions of UO and a Lipschitz-continuous system description. If the considered system is only LWO or has definition gaps in the system equations, the asymptotic convergence of the estimation error could be disturbed. Moreover, the derivative of the Lyapunov candidate $\dot{V}$ (4.18) can be influenced by a great perturbation $\xi(t)$ and thus can imperil the local convergence.

5 Adaptive Observer with Modulating Functions

Originally, the MFM was proposed by Shinbrot [Shi54] as a method of moment functionals in order to estimate parameters of linear differential equation models. A historical background of the years 1954 - 1990 w.r.t. the MFs can be found in [PR93].
In [RU06] Rao and Unbehauen reviewed state and parameter estimation methods using MFs for LTI systems in continuous-time in comparison to discrete-time such as Kalman filtering. The advantage of retaining in the continuous-time formalism belongs to using physical laws in which the system is originally modeled. Moreover, the discretization and the associated mapping problems such as non-minimum-phase sampling zeros are omitted. However, time-derivatives still have to be considered for estimating parameters and states.

If the explicit time-derivatives of the measured signals are subject to noise, this will lead to errors of the observation process. In order to avoid the derivation of measurements, the repeated integration method [MF72] or the Poisson moment functional approach [RU06] can be used. Another opportunity consists in using MFs whose horizon of integration is fixed or receding. In contrast, the repeated integration method and the Poisson moment functional method have an expanding integration horizon and disadvantageously require all initial conditions of the signal which the MFM does not due to the elimination of the initial conditions by the convolution with the known MF. This integration process can be seen as a Finite Impulse Response (FIR)-filter which obtains a non-asymptotic solution of the estimation problem in finite-time. On the contrary, common differential observers, e.g. Luenberger or Kalman observers (cf. chapter 4), are based on the definition 3.1.10 of asymptotic observers. These observers provide the convergence of an estimated state to the real state when time goes to infinity. Nevertheless, in some applications it is necessary that the algorithm may converge in finite-time for a fast estimation in on-line applications which is provided by a non-asymptotic approach like the estimation method based on MFs [Gha+20].

In [Liu+14] the MFM is extended to estimate the state and the unknown input of a LTV system. One year later in 2015, the extension of the MFM to jointly estimate the states and parameters of a nonlinear system was published in [JR15]. This paper is based on the regressor form of the system and the least-squares observer concept.

The proposition in this thesis for a simultaneous parameter and state estimation of a nonlinear system is a real-time capable approach which uses a hierarchical structure. Firstly, the unknown parameters are estimated, and subsequently, the state observer uses the parameter estimation in order to observe the system states. The idea of the parameter estimator is based on [Noa+16a], namely avoiding the inversion of matrices and receiving a stable estimation. Instead of using a nonlinear gradient algorithm as in [Noa+16a], the modulation is combined with the EKF. The state observer has a closed-loop design and uses the Taylor series to obtain a regressor form of the nonlinear system on which the MFM is applied.

Due to the linearization of the nonlinear system, the approach is generally applicable unless discontinuities occur. This represents the same restriction as with the EKF. In general, the use of the MFM in the observer design comprises several advantages. The approach is robust against measurement noise, real-time capable and non-asymptotic. Thus, it provides an accurate estimation in an arbitrarily fast manner. Additionally, it is efficient to implement and the MFs provide tuning possibilities, e.g. the function shape or the moving horizon length.

In the first section 5.1 of this chapter, the MF and its characteristics are defined. Subsequently, the MFM is explained in section 5.2. These basics are used in section 5.3 for the parameter estimation approach and in section 5.4 for the closed-loop design of the state observer EMF. In section 5.5, the combination of the proposed parameter estimator and the state observer EMF is introduced in order to receive a nonlinear adaptive observer.

5.1 Definition of Modulating Functions

Jouffroy and Reger defined in [JR15] the MF referring to the characteristic boundary conditions as follows:

Definition 5.1.1 (Modulating Function)**.** *For a fixed time horizon length $T > 0$, the function $\varphi \in \mathcal{C}^n([0,T],\mathbb{R})$ is called Modulating Function (MF) of order $n \in \mathbb{N}$ if*

$$\varphi^{(i)}(0) \cdot \varphi^{(i)}(T) = 0 \quad \forall i \in \{0, 1, \cdots, n-1\}. \tag{5.1}$$

Furthermore, it is called

1. *Total Modulating Function (TMF) if*

$$\varphi^{(i)}(0) = \varphi^{(i)}(T) = 0 \quad \forall i \in \{0, 1, \cdots, n-1\}, \tag{5.2}$$

2. Left Modulating Function (LMF) if

$$\varphi^{(i)}(0) = 0,\ \varphi^{(i)}(T) \neq 0 \quad \forall i \in \{0, 1, \cdots, n-1\}. \tag{5.3}$$

The related modulation operator $L^i : \mathcal{L}_2^{loc} \to \mathbb{R}$ *is applied to a function* $f \in \mathcal{L}_2^{loc}$ *in the following manner:*

$$L^i[f](t) = (-1)^i \langle \varphi^{(i)}, f \rangle = (-1)^i \int_{t-T}^{t} \varphi^{(i)}(\tau - t + T)\, f(\tau)\, d\tau \tag{5.4}$$

where a receding horizon can be realized by using the short form notation $L^i[f] = L^i[f](\tau)\ \forall \tau \leq 0$.

Summarized, the MF is a constructed, state-independent, sufficiently smooth function. In general, TMFs are applied for estimating parameters and LMFs are employed to observe states since the right boundary values $\varphi^{(i)}(T)$ are used for the actual state estimation. The application of the MFM with both functions TMF and LMF requires a regressor form (5.12) of the differential equation which is explained in the following section 5.2.

5.2 Modulating Function Method

The states of a system can sufficiently be described by the output y as well as its derivatives and is also dependent on the system input u. One way to determine the states, when they are not measurable, is by directly differentiating the output. However, small perturbations in the system output lead to noisy derivatives, which complicate the estimation. Therefore, it is useful to estimate the states and parameters with the MFM in order to avoid differentiating noisy signals. The procedure of the MFM is described in [BK20] and is applied in the combination with the EKF in section 5.3 and with the EMF in section 5.4.

For the application of the MFM to linear systems, the differential equation of the system should have the following form of a linear I/O equation:

$$\sum_{i=0}^{n} a_i\, y^{(i)}(t) = \sum_{j=0}^{m} b_j\, u^{(j)}(t) \qquad , m \leq n. \tag{5.5}$$

In the case of nonlinear systems, it becomes more difficult to state an adequate structure. If the nonlinear system is composed of integrable, convolvable or e-convolvable signals (see definition 5.2.1), the MFM is applied by a skillful transformation of the

nonlinearities or a time-variant modulation with a projection approach (cf. [CTR14; Web17]).

Definition 5.2.1. *For a given function $q \in \mathcal{C}^i([0,T],\mathbb{R}^p)$ and parameter $a \in \mathbb{R}$ define:*

- *Linear signal with $p = 1$:* $\xi(t) = a\, q^{(i)}(t)$
- *Integrable signal:* $\xi(t) = a\, g^{(i)}(q(t))$
- *Convolvable signal:* $\xi(t) = a\, h(q(t))\, g^{(i)}(q(t))$
- *E-convolvable signal:* $\xi(t) = a\, h^{(i)}(q(t))\, g^{(i)}(q(t))$

with $g, h \in \mathcal{C}^i(\mathbb{R}^p,\mathbb{R})$ arbitrary functions [CTR14].

In order to omit the exhausting characterization of the nonlinearities in the I/O relation, the MFM should be applied directly to the system. This is one of the objectives of the proposed approaches.

The MFM uses MFs to transform a signal over a certain time interval $[t-T,t]$ and finally receives an algebraic system of equations. The transformation of a signal f with a MF φ comprises the multiplication of the signal with the predefined modulation kernel and the integration over a fixed-time moving horizon interval:

$$\begin{aligned}\langle \varphi, f^{(i)} \rangle &:= \int_{t-T}^{t} \varphi(\tau - t + T)\, f^{(i)}(\tau) d\tau \\ &= (-1)^i \int_{t-T}^{t} \varphi^{(i)}(\tau - t + T)\, f(\tau) d\tau =: (-1)^i \langle \varphi^{(i)}, f \rangle. \end{aligned} \tag{5.6}$$

This equation shows the central property of the modulation, namely transferring derivatives from a measured signal to the known MF in order to avoid the noise differentiation. Another result of the MFM is the loss of the unknown initial and final conditions due to the inclusion of the boundary conditions of the MFs and the application of the integrations by parts formula. [JR15]

Examining the homogeneous boundary value conditions of a TMF (5.2), the boundary values vanish and the modulation operator (5.4) can be applied for the parameter estimation. For the state estimation, a LMF is necessary which leads to a modified modulation operator (cf. lemma 5.2.1) since the difference between a TMF and a LMF lies in the boundary value condition of the function at the right boundary T. There, the function must be different from zero as stated in the condition (5.3). Thus, the partial integration preserves the boundary values that ultimately provide the state estimate.

Lemma 5.2.1. *For a signal $f \in \mathcal{C}^i$, the modulation operator (5.4) of order $n \in \mathbb{N}$ fulfills $\forall i \leq k$:*

$$L^0[f^{(i)}] = \begin{cases} L^i[f] & : TMF \\ L^i[f] + \sum_{n=1}^{i} (-1)^{n-1} \varphi^{(n-1)}(T)\, f^{(i-n)}(t) & : LMF. \end{cases} \tag{5.7}$$

The proof of lemma 5.2.1 is outlined in [Web17]. Exemplified, the modulation operator for a LMF and $n \in \{0, 1, 2, 3\}$ is calculated as follows:

$$L^0[f] = \int_{t-T}^{t} \varphi(\tau - t + T)\, f(\tau) d\tau \tag{5.8}$$

$$L^1[f] = -\int_{t-T}^{t} \dot{\varphi}(\tau - t + T)\, f(\tau) d\tau + y(t)\, \varphi(T) \tag{5.9}$$

$$L^2[f] = \int_{t-T}^{t} \ddot{\varphi}(\tau - t + T)\, f(\tau) d\tau + \dot{f}(t)\, \varphi(T) - f(t)\, \dot{\varphi}(T) \tag{5.10}$$

$$L^3[f] = -\int_{t-T}^{t} \dddot{\varphi}(\tau - t + T)\, f(\tau) d\tau + \ddot{f}(t)\, \varphi(T) - \dot{f}(t)\, \dot{\varphi}(T) + f(t)\, \ddot{\varphi}(T). \tag{5.11}$$

With the modulation operator L, the differential equation (5.5) can be converted into an algebraic system of equations. This can be solved for either the desired parameters or the estimated states.

5.3 Parameter Estimation

Common approaches to estimate parameters with MFs comprise a least-squares algorithm (see e.g. [DU96]), a Gramian approach (see e.g. [JR15]) or a gradient descent (see e.g. [RM15; Noa+16a]). All mentioned estimators require a regression structure involving time-derivatives w.r.t. the input and the output as follows:

$$\zeta(t) := \eta(t)^\top \theta_0, \tag{5.12}$$

where $\theta_0 \in \mathbb{R}^n$ are the parameters, $\eta(t) \in \mathbb{R}^n$ is the regressor and $\zeta(t) \in \mathbb{R}$ is the measured signal [RM15].

Due to the parameter nonlinearity of the nonlinear I/O relation of the RO plant (B.1), the classification as integrable or (e-)convolvable signals (cf. definition 5.2.1) and the handling with the MFM is not obvious. The reformulation of the nonlinear I/O equation (B.1) into a polynomial form in θ with a factorization method would require a quadratic operation which leads to numerical inequalities. Hence, the I/O relation (B.3) built from the linearized state-space representation (see section 2.3.2) is

used which is state linear and only nonlinear in the parameters.

The proposed input-output parameter estimator consists of the modulation of the system I/O relation with a TMF in order to obtain the time-derivatives of the measured signals. The modulated signals are the input of the EKF that estimates the parameter state. Therefore, the proposed parameter estimator is called State - **D**ecoupled Parameter Estimation via **M**odulated **R**egression (DMR).

5.3.1 Persistence of Excitation

A major factor of estimating parameters belongs to the persistence of excitation w.r.t. the input signal which is defined as follows:

Definition 5.3.1 (Persistent Excitation [Bes07b])**.** *A signal* $\varsigma : \mathbb{R}^+ \to \mathbb{R}^r$ *satisfies the property of persistent excitation if there exists* $T, k_1, k_2 > 0$ *such that* $\forall t \geq 0$*:*

$$k_1 I_r \geq \int_t^{t+T} \varsigma(\tau)^\top \varsigma(\tau)\, d\tau \geq k_2 I_r. \tag{5.13}$$

In other words, the input signal has to be sufficiently rich in order to receive an observed response which comprises the necessary information to execute the estimation process. If the input signal is universal (cf. definition 3.1.8) and thus not singular, the input is considered to be persistent, e.g. a signal consisting of filtered white noise. The aim of such a sufficiently rich input signal is the approach of the estimated parameters to the true values. [Lju99]

5.3.2 Structure of the Parameter Estimator

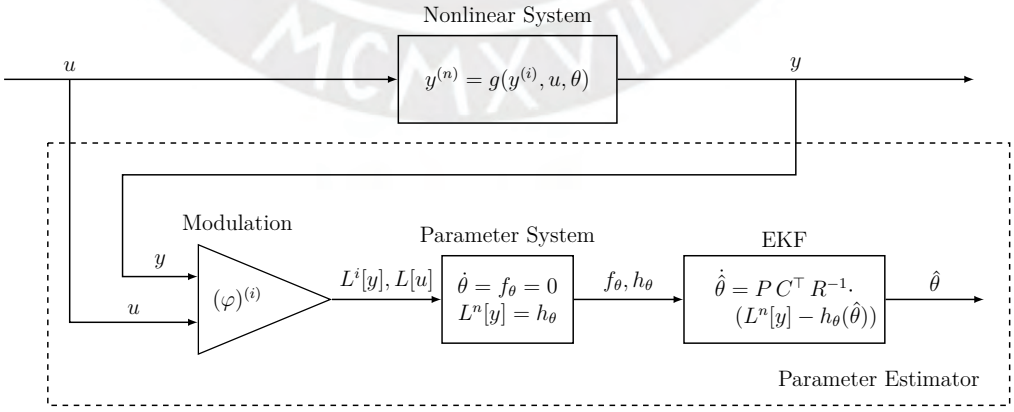

Figure 5.1: Structure of the parameter estimator with $i \in \{0, 1, \cdots, n-1\}$

The proposed DMR employs the measured signals of the nonlinear system and is a combination of the MFM and the EKF used as linearization-based recursive least squares algorithm (see figure 5.1). The design of this parameter estimator is based on a linearized state-space representation with a possible parameter depending offset (5.14-5.15) in order to apply the MF. The modulation depicted in figure 5.1 is explained more precisely in section 5.4.7. The parameter system is constructed of the internal model f_θ (5.19) and the output equation h_θ (5.18) which in turn ared used for the dynamic regression of the EKF (5.21-5.23).

In general, the output dynamics of the EKF uses the dynamics of the system which are represented by the n-th derivative of the output. The linearized representation of the considered RO system (2.31-2.34) can be put in a general linear SISO system form with the offset $E(\theta)$:

$$\dot{x}(t,\theta) = A(\theta)x(t) + B(\theta)u(t) + E(\theta) \tag{5.14}$$

$$y(t,\theta) = C(\theta)x(t) + D(\theta)u(t). \tag{5.15}$$

with the states $x \in \mathbb{R}^n$, input $u \in \mathbb{R}$, output $y \in \mathbb{R}$, matrices $A \in \mathbb{R}^{n\times n}$, $C \in \mathbb{R}^{n\times n}$ and vectors $B \in \mathbb{R}^n, D \in \mathbb{R}^n$. Differentiating the output n-times:

$$\underbrace{\begin{pmatrix} y \\ \dot{y} \\ \vdots \\ y^{(n-1)} \\ y^{(n)} \end{pmatrix}}_{\begin{pmatrix} Z \\ y^{(n)} \end{pmatrix}} = \underbrace{\begin{pmatrix} C \\ CA \\ \vdots \\ CA^{n-1} \\ CA^n \end{pmatrix}}_{\begin{pmatrix} \mathcal{O} \\ CA^n \end{pmatrix}} x + \underbrace{\begin{pmatrix} D & 0 & \cdots & 0 \\ CB & D & \ddots & 0 \\ CAB & \ddots & \ddots & \\ \vdots & & & D \\ CA^{n-1}B & \cdots & CAB & CB \end{pmatrix}}_{\begin{pmatrix} \Gamma \\ \gamma \end{pmatrix}} \underbrace{\begin{pmatrix} u \\ \dot{u} \\ \vdots \\ u^{(n-1)} \end{pmatrix}}_{U} + \underbrace{\begin{pmatrix} 0 \\ CE \\ CAE \\ \vdots \\ CA^{n-1}E \end{pmatrix}}_{\begin{pmatrix} \Upsilon \\ \upsilon \end{pmatrix}}, \tag{5.16}$$

Z can be used to express the states x only with the output y, its derivatives $\dot{y}, \cdots, y^{(n-1)}$, the input u and the unknown parameter θ in order to obtain a differential parameterization. This underlies the assumption of a non-singular observability matrix $\mathcal{O}$ that is fulfilled if the system (5.14-5.15) is observable which has been investigated in section 3.2. The n-th order dynamics of the output constitutes the I/O relation:

$$y^{(n)} = C\,A^n \underbrace{\mathcal{O}^{-1}\left(Z - \Gamma \cdot U - \Upsilon\right)}_{=x(y,\cdots,y^{(n-1)},u,\theta)} + \gamma \cdot U + \upsilon. \tag{5.17}$$

Since the I/O dynamics (5.17) is only nonlinear in the parameters, this form is suitable to modulate the equation with a MF. By this, the derivatives of the unknown output derivatives are shifted to the known MF and the parameter θ is separated from the modulation operator under the assumption that the parameters are constant. For the modulation, a TMF φ is considered and the nonlinear output equation for the parameter θ is given as follows:

$$h_\theta(t,\theta) = L^n[y] = C\,A^n\,\mathcal{O}^{-1}\left(L^i[y] - \Gamma \cdot L^i[u] - \varphi(t)\cdot\Upsilon\right) + \gamma \cdot L^i[u] + \varphi(t)\cdot\upsilon \quad (5.18)$$

with $i = 0, \cdots, n-1$. This modulated output $h_\theta(t,\theta)$ is without signal derivatives and the nonlinear parameters θ can be extracted from the modulation integrals.

The number of the used TMFs depends on the number of parameters that have to be estimated. Thereby, the minimum number of MFs is equal to the number of unknowns. Using a greater number of MFs than unknowns can improve the estimations, e.g. in consideration of noise. [BK20]

The constant parameters imply that the dynamics of the parameter state is assumed to be zero. Therefore, the internal model is stated as follows:

$$f_\theta(t,\theta) = \dot{\theta}(t) = 0. \quad (5.19)$$

In chapter 4, the procedure of the EKF is explained which is applied to the parameter system consisting of the internal model (5.19) and the nonlinear parameter output equation (5.18). Due to

$$A(t) = \left.\frac{\partial f_\theta(t,\theta)}{\partial\theta}\right|_{\theta=\hat{\theta}} = 0, \quad (5.20)$$

the dynamic regression with the EKF of the parameter system f_θ, h_θ declines to:

$$C(t) = \left.\frac{\partial h_\theta(t,\theta)}{\partial\theta}\right|_{\theta=\hat{\theta}} \quad (5.21)$$

$$\dot{P}(t) = Q - P(t)C(t)^\top R^{-1}C(t)P(t) + \lambda P(t) \quad (5.22)$$

$$\dot{\hat{\theta}} = P(t)C(t)^\top R^{-1}\left(L^n[y] - h_\theta(t,\hat{\theta})\right). \quad (5.23)$$

In summary, the proposed parameter estimation for θ only requires the measurements of the output y and the input u with persistent excitation and thus can be used stand-alone. Moreover, the DMR is real-time capable and is used in section 5.5 to build an adaptive observer architecture.

5.4 Extended Modulation Filter

The fundamental idea of the EMF is based on the EKF. However, instead of linearizing the state-space representation of the system at each time step and doing a one step prediction using the RDE, the I/O relation of the system (5.24) is linearized and the MFM is applied. The advantages of the MFM comprise a certain robustness against noise and numerical stability due to the algebraic approach through integral transformation [Noa+16a]. With each new measurement, the linearization is adopted using the measured signals and the observed states because of the information processing over a moving horizon. The new states are estimated with the MFM using a Generalized Modulating Function (GMF) defined in section 5.4.3. The proposed structure of the real-time capable EMF has a closed-loop design (see section 5.4.4). Furthermore, an improvement of the EMF w.r.t. the linearization step is proposed in section 5.4.6. Also the numerical implementation of the approach is explained (see section 5.4.7) and an error analysis of the EMF is provided in section 5.4.5.

5.4.1 Input-Output Relation

If the considered system does not yet have the form of an I/O equation, the state-space representation of the SISO system (3.1) has to be transferred in the requested form of a linear I/O relation. To achieve this, a diffeomorphism of the observability map (definition 3.1.6) can be used. If there exists an inverse function of the observability map $\mathfrak{o}$, the states x can be determined with the knowledge of the output y and its derivatives. Thus, the I/O equation is calculated as follows:

$$y^{(n)} = \mathcal{L}_f^n h(\mathfrak{o}^{-1}(Z)) \tag{5.24}$$

with the Lie derivatives $\mathcal{L}_f h(x) := \frac{\partial h(x)}{\partial x} f(x)$ and successively $\mathcal{L}_f^k h(x) := \mathcal{L}_f(\mathcal{L}_f^{k-1} h(x))$. Thus, a nonlinear system is globally observable when the mapping $Z = \mathfrak{o}(x)$ has an unique solution for all x. Unfortunately, for most cases of nonlinear systems this inverse function is difficult to calculate or even sometimes impossible to compute because of singularities or high computational costs. Nevertheless, it is possible to check the local properties considering the implicit function theorem. Therefore, an approximation

around a working point $\bar{x}$ with the first-order Taylor series is applied [Kha02]:

$$x = \mathfrak{o}^{-1}(Z) \approx \bar{x} + \left[\frac{\partial \mathfrak{o}_k(x)}{\partial x}\right]^{-1}\Bigg|_{x=\bar{x}} \cdot (Z - \bar{Z}) = x_{\text{approx}} \tag{5.25}$$

$$y^{(n)}_{\text{approx}} \approx \mathcal{L}_f^n h \left(\bar{x} + \left[\frac{\partial \mathfrak{o}(x)}{\partial x}\right]^{-1}\Bigg|_{x=\bar{x}} \cdot (Z - \bar{Z})\right) = g(y, \dot{y}, \ddot{y}, \cdots, y^{(n-1)}, u). \tag{5.26}$$

It is obvious that only the inverse of the observability matrix (definition 3.1.7) is required, which is easier to compute due to its quadratic form. The achieved I/O equation (5.26) is still nonlinear and represents the dynamics of the system. In addition, the form examined in this thesis is restricted to the measurable output y as well as its derivatives and the measurable input u. On the contrary, the derivatives of the input are not included in the I/O equation (5.26). When considering errors, the transformation error due to the approximation of the states x_{approx} (5.25) must be taken into account which is analyzed in section 5.4.5.

To be able to handle all nonlinearities that occur in the I/O relation (5.26), these have to be linearized around the working points of $\bar{Z} = [\bar{z}_1, \cdots, \bar{z}_{n-1}]^\top$ and $\bar{u}$. The working point of the input $\bar{u}$ is the actual input measurement of the nonlinear system, whereas for the working points of the output and its derivative $\bar{Z}$, the estimated state values of the previous time step are used. Again a first-order Taylor series is applied for the linearization [Kha02]:

$$\begin{aligned} y^{(n)}_{\text{lin}} &= g(\bar{Z}, \bar{u}) - \sum_{i=0}^{n-1} \underbrace{\frac{\partial g(Z,u)}{\partial y^{(i)}}\Bigg|_{\bar{Z},\bar{u}}}_{a_{i+1}} \cdot (\bar{z}_i - y^{(i)}) - \underbrace{\frac{\partial g(Z,u)}{\partial u}\Bigg|_{\bar{Z},\bar{u}}}_{b} (\bar{u} - u) + \xi(t) \\ &= a(t)^\top Z + b(t)^\top u + \underbrace{g(\bar{Z}, \bar{u}) - a(t)^\top \bar{Z} - b(t)^\top \bar{u}}_{=:\varepsilon(t)} + \underbrace{\xi(t)}_{\text{H.O.T.}} . \end{aligned} \tag{5.27}$$

The result is the required system form of a linear I/O equation (5.27) which corresponds to the required form (5.5). The advantage of this form is the convenient application of the MFM due to the regressor form. The Jacobians $a(t), b(t)$ and the summands including the operating points $\varepsilon(t)$ build the time-variant linearization parameters which need to be updated in each modulation horizon. The linearization error $\varepsilon(t)$ and the H.O.T. error $\xi(t)$ are outlined in section 5.4.5. The difference between the two errors is that the linearization error ε is determinable and used for the estimation, whereas the H.O.T. error is not known.

5.4.2 State Estimation

Applying the MFM with a LMF (see section 5.2) to the linearized I/O relation (5.27) of a nonlinear system, the algebraic system of equation is created as follows:

$$L^n[y] - \sum_{i=0}^{n-1} a_{i+1}(t)\, L^i[y] = b(t)\, L^0[u] + L^0[\varepsilon]. \tag{5.28}$$

In the case of the RO plant, the used modulation operators are derived w.r.t. to lemma 5.2.1 by means of the integration by parts with LMFs as outlined in the exemplified formulas (5.8-5.11). These operators with the fixed right boundary values of the MF unequal to zero have to be inserted in the algebraic system of equations (5.28) in order to solve the system for the output and the unknown output derivatives. Exemplarily, the modulated equation for the RO system is stated as follows:

$$\begin{aligned} &- \langle \dddot{\varphi}, y\rangle + \ddot{y}(t)\,\varphi(T) - \dot{y}(t)\,\dot{\varphi}(T) + y(t)\,\ddot{\varphi}(T) + a_3(t)\,\left(\langle \ddot{\varphi}, y\rangle + \dot{y}(t)\,\varphi(T) - y(t)\,\dot{\varphi}(T)\right) \\ &+ a_2(t)\,\left(-\langle \dot{\varphi}, y\rangle + y(t)\,\varphi(T)\right) + a_1(t)\langle \varphi, y\rangle = -b(t)\langle \varphi, u\rangle + \langle \varphi, \varepsilon\rangle. \end{aligned} \tag{5.29}$$

In order to obtain the unknown variables Z, the algebraic system (5.28) is restructured to:

$$\begin{aligned} &\underbrace{\left(\langle \dddot{\varphi}, y\rangle - a_3(t)\,\langle \ddot{\varphi}, y\rangle + a_2(t)\,\langle \dot{\varphi}, y\rangle - a_1(t)\langle \varphi, y\rangle - b(t)\langle \varphi, u\rangle + \langle \varphi, \varepsilon\rangle\right)}_{q(y,\varphi,a,b,\varepsilon)} = \\ &\underbrace{\left(\ddot{\varphi}(T) - a_3(t)\,\dot{\varphi}(T) + a_2(t)\,\varphi(T) \qquad a_3(t)\,\varphi(T) - \dot{\varphi}(T) \qquad \varphi(T)\right)}_{\delta(\varphi,a)} \underbrace{\begin{pmatrix} y(t) \\ \dot{y}(t) \\ \ddot{y}(t) \end{pmatrix}}_{Z}. \end{aligned} \tag{5.30}$$

On the one hand, the summands independent of the estimates form the scalar q. Hence, q only includes the modulated signals and the linearization parameters $a(t)$ and $b(t)$. On the other hand, the δ-vector consists of the right boundary values of the MF and its derivatives and also the linearization parameters $a(t)$ which are the Jacobians of the I/O equation (5.26) w.r.t. the output and its derivatives.

As postulated in [JR15], the number of MFs is at least equal or higher than the number of unknowns in the system. The number of estimated variables in (5.29) corresponds to the order of the system. In the case of the considered RO plant, three variables, namely the output and its first and second derivatives, will be estimated using the MFM. Thus, q is extended to a vector $Q \in \mathbb{R}^n$ and δ to a squared matrix

$\Delta \in \mathbb{R}^{n\times n}$. In the example of the RO system, the algebraic system of equations solved for the unknowns is formulated as:

$$\underbrace{\begin{pmatrix} \hat{y}(t) \\ \dot{\hat{y}}(t) \\ \ddot{\hat{y}}(t) \end{pmatrix}}_{\hat{z}} = \underbrace{\begin{pmatrix} \ddot{\varphi}_1(T) - a_3(t)\dot{\varphi}_1(T) + a_2(t)\varphi_1(T) & a_3(t)\varphi_1(T) - \dot{\varphi}_1(T) & \varphi_1(T) \\ \ddot{\varphi}_2(T) - a_3(t)\dot{\varphi}_2(T) + a_2(t)\varphi_2(T) & a_3(t)\varphi_2(T) - \dot{\varphi}_2(T) & \varphi_2(T) \\ \ddot{\varphi}_3(T) - a_3(t)\dot{\varphi}_3(T) + a_2(t)\varphi_3(T) & a_3(t)\varphi_3(T) - \dot{\varphi}_3(T) & \varphi_3(T) \end{pmatrix}^{-1}}_{\Delta^{-1}(\varphi,a)} \cdot$$
$$\underbrace{\begin{pmatrix} \langle \dddot{\varphi}_1, y\rangle - a_3(t)\langle \ddot{\varphi}_1, y\rangle + a_2(t)\langle \dot{\varphi}_1, y\rangle - a_1(t)\langle \varphi_1, y\rangle - b(t)\langle \varphi_1, u\rangle + \langle \varphi_1, \varepsilon\rangle \\ \langle \dddot{\varphi}_2, y\rangle - a_3(t)\langle \ddot{\varphi}_2, y\rangle + a_2(t)\langle \dot{\varphi}_2, y\rangle - a_1(t)\langle \varphi_2, y\rangle - b(t)\langle \varphi_2, u\rangle + \langle \varphi_2, \varepsilon\rangle \\ \langle \dddot{\varphi}_3, y\rangle - a_3(t)\langle \ddot{\varphi}_3, y\rangle + a_2(t)\langle \dot{\varphi}_3, y\rangle - a_1(t)\langle \varphi_3, y\rangle - b(t)\langle \varphi_3, u\rangle + \langle \varphi_3, \varepsilon\rangle \end{pmatrix}}_{Q(y,\varphi,a,b,\varepsilon)}. \tag{5.31}$$

The solution for the output and its derivatives requires the inverse of the Δ-matrix. During the online procedure, this could lead to singularities of the matrix due to the insertion of the newly calculated linearization parameters in each time step. A possible solution, outlined in the following section 5.4.3, includes the use of GMFs instead of LMFs in order to obtain mixed boundary conditions such that the invertability of the Δ-matrix is guaranteed.

5.4.3 Mixed Boundary Conditions

Originally, the GMF has been used to design fractional order differentiators (cf. [LL15; WLB17]). In [Tia+19] the MFM is extended with the GMF in order to provide algebraic integral formulas by eliminating unknown boundary values. In the context of the EMF, the GMFs should be applied to build the system of equations more skillfully for a better conditioning of the Δ-matrix. It also ensures that the Gaussian-algorithm used to numerically solve the algebraic equation always finds a symbolic inverse.

The definition of a GMF in [Tia+19] is extended to a set of GMFs as follows:

Definition 5.4.1 (Generalized Modulating Function)**.** *For a fixed time horizon length $T > 0$, the function $\varphi \in \mathcal{C}^n([0,T],\mathbb{R})$ is called MF of order $n \in \mathbb{N}$ if*

$$\varphi^{(i)}(0) \cdot \varphi^{(i)}(T) = 0 \quad \forall i \in \{0, 1, \cdots, n-1\}. \tag{5.32}$$

Furthermore, it is called a set of k GMFs if additionally $\forall k \leq n,\ k \in \mathbb{N}$*:*

$$\varphi_{\mathrm{k}}^{(i)}(T) = 1, \quad \textit{if} \quad i = n - k, \tag{5.33}$$

$$\varphi_{\mathrm{k}}^{(i)}(T) = 0, \quad \textit{else.} \tag{5.34}$$

The observation of states, while using GMFs instead of LMFs, is guaranteed due to the one right boundary value equal to one (5.33) of each GMF in a set of GMFs.

For instance, the conditioning constraints of the set of three GMFs for the RO system comprise, on the one hand, the left boundary values of the GMF:

$$\varphi_{\mathrm{i}}(0) = \dot{\varphi}_{\mathrm{i}}(0) = \ddot{\varphi}_{\mathrm{i}}(0) = 0 \qquad \text{with } i = 1, 2, 3. \tag{5.35}$$

On the other hand, the right boundary values differ w.r.t. to the number of the GMF in the set:

$$\varphi_1(T) = \dot{\varphi}_1(T) = 0 \qquad \varphi_2(T) = \ddot{\varphi}_2(T) = 0 \qquad \dot{\varphi}_3(T) = \ddot{\varphi}_3(T) = 0$$
$$\ddot{\varphi}_1(T) = 1 \qquad \dot{\varphi}_2(T) = 1 \qquad \varphi_3(T) = 1$$

This leads to a lower triangular Δ-matrix:

$$\Delta(a) = \begin{pmatrix} 1 & 0 & 0 \\ -a_3(t) & -1 & 0 \\ a_2(t) & a_3(t) & 1 \end{pmatrix} \tag{5.36}$$

which fulfills a determinant $\det(\Delta) = -1$. The determinant is independent of the linearization parameter $a(t)$, i.e. the inversion of Δ is guaranteed during the online simulation. The matrix only relies on the parameter $a(t)$ which is obtained by linearizing the nonlinear I/O w.r.t. the output and its derivatives.

5.4.4 Structure of the EMF

In figure 5.2, the concept of the EMF is shown. The first step consists in linearizing the nonlinear I/O relation (5.26) of the considered system in order to receive the target structure of the EMF which is a linear I/O equation (5.27) (cf. section 5.4.1). This linear equation provides a straightforward application of the MFM. The linearization parameters $a(t), b(t)$ are the Jacobians of the nonlinear I/O relation (5.26) w.r.t. to the output, its derivative and the input, respectively. The parameter $\varepsilon(t)$ consists of

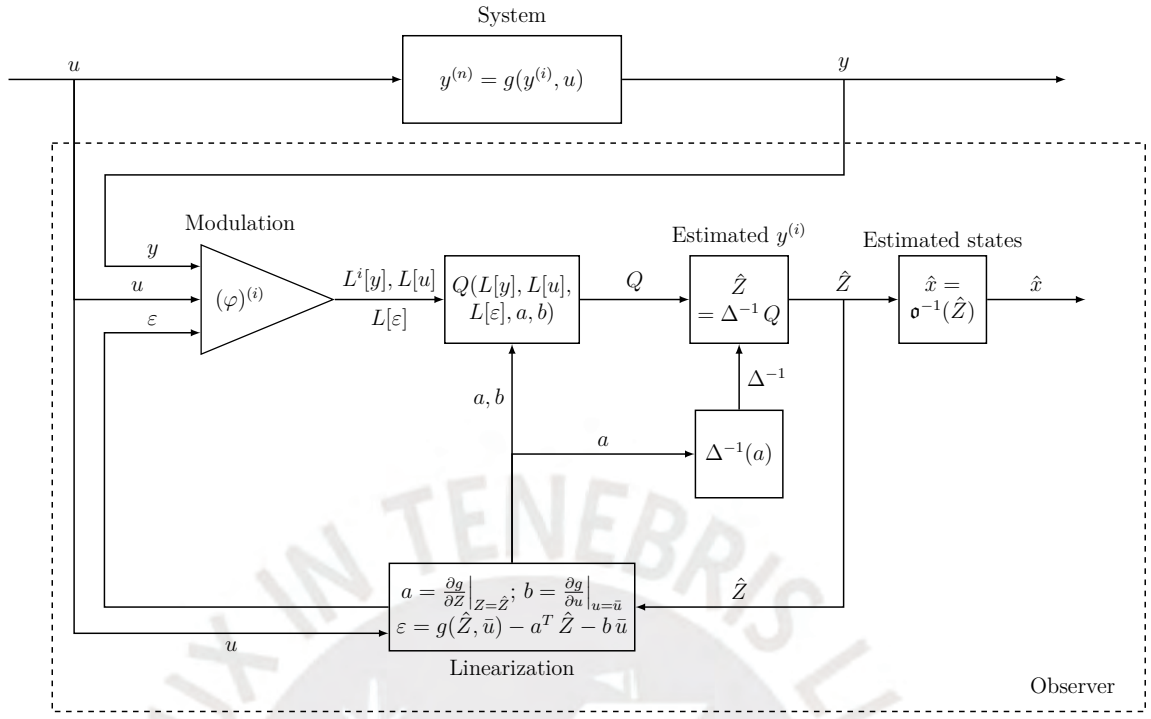

Figure 5.2: Structure of the EMF with $i \in \{0, 1, \cdots, n-1\}$

the summands of the Taylor series that include the operating point around which the I/O equation has been linearized. These parameters have to be recalculated in each time interval. However, it is assumed that the linearization parameters $a(t), b(t), \varepsilon(t)$ are constant over the modulation interval $[t-T, t]$. This assumption of constancy is considered in more detail in the following section 5.4.5.

Subsequently, the measured signals of the input $u(t)$ and the output $y(t)$ of the nonlinear system and the linearization parameter $\varepsilon(t)$ are modulated over a moving horizon which produces the modulation operators $L[u], L[\varepsilon], L^i[y]$ with $i = 0, 1, \cdots, n-1$. These are required to calculate the matrix Q (cf. example equation (5.31)) together with the linearization parameters $a(t)$ and $b(t)$.

In order to obtain the whole algebraic system of equations, the inverse of the Δ-matrix with the calculated $a(t)$ has to be determined. Using GMFs, the lower triangular Δ-matrix can be easily inverted offline also for higher orders n and the linearization parameters $a(t)$ must be only inserted during the online procedure. Moreover, if the system is of order $n = 2$, the Δ-matrix is equal to its inverse.

The estimation of the output and its derivatives $\hat{Z} = [\hat{y}, \dot{\hat{y}}, \cdots, \hat{y}^{(n-1)}]^\top$ is obtained by the product of the inverse of Δ with Q:

$$\hat{Z} = \Delta^{-1}(a) \cdot Q(L[y], L[u], L[\varepsilon], a, b). \tag{5.37}$$

These estimates constitute the new working points which are used in the next time step to be linearized around in order to determine $a(t), b(t)$ and $\varepsilon(t)$.

In the last step, the estimated values of $\hat{Z}$ can be used to compute the estimated states $\hat{x}$. This can be done by inserting $\hat{Z}$ into the inverse function of the observability map (3.3). If this might not be possible due to the nonlinearities as explained in section 5.4.1, the proposed approximation (5.25) can be used.

5.4.5 Error Analysis

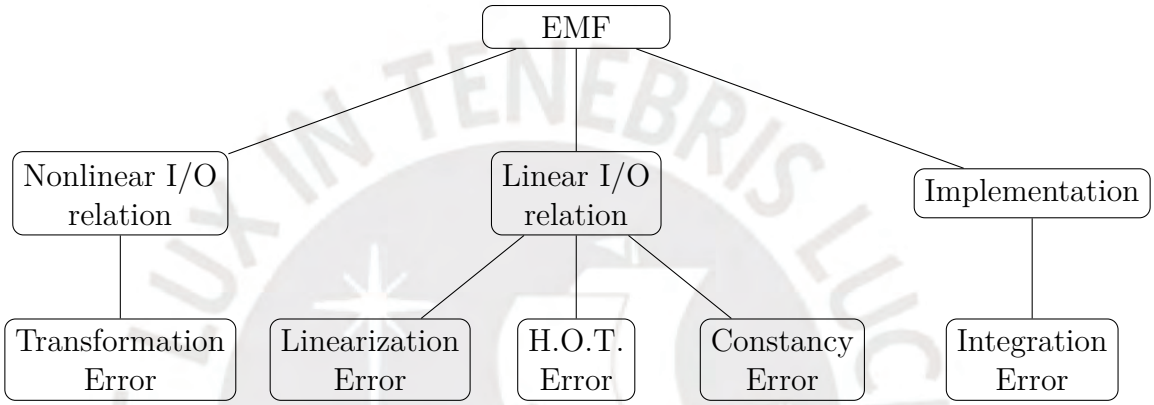

Figure 5.3: Error analysis of the EMF

The errors concerning the EMF are summarized in figure 5.3. If the system is not yet available in I/O form, it must be transformed from its state-space representation. If additionally the inverse function of the observability map is difficult to calculate, the proposed local solution in section 5.4.1 has to be applied, i.e. the approximation of the states (5.25) is determined with the Taylor series around the working point $\bar{x}$. This working point $\bar{x}$ is chosen in the beginning of the calculations and cannot be changed afterwards. Otherwise, the offline calculations must be repeated. Therefore, a proper selection of this value $\bar{x}$ is important. However, the working point $\bar{x}$ cannot be chosen perfectly, and thus, this transformation error is present during the entire observation procedure.

In addition to the transformation error due to the unique choice of the working point $\bar{x}$, the linearization error $\varepsilon(t)$ from the linearized I/O relation (5.27) has to be examined:

$$\varepsilon(t) = g(\bar{Z}, \bar{u}) - a(t)^\top \bar{Z} - b(t)^\top \bar{u}. \tag{5.38}$$

This error can be improved by using the Iterated Extended Modulation Filter (IEMF) which is proposed in the following section 5.4.6. The iteration belongs to the lineariza-

tion step in order to improve the estimated value $\hat{Z}$.

Moreover, the linearization (cf. formula (5.27)) includes the H.O.T. error which can be analyzed with:

$$\xi(t) = g(Z,u) - a(t)^\top Z - b(t)^\top u - \varepsilon(t). \tag{5.39}$$

Nevertheless, the H.O.T. error cannot be minimized by using a higher order of the Taylor series since this would lead to new nonlinearities due to mixed terms with the output, its derivatives and the input.

As outlined in section 5.4.4, the moving horizon window of the MFM is slided over the trajectories of the measured input and output signals in order to apply the MFM. During an estimation step, it is assumed that the linearization parameters a, b, ε are constant. This leads to the constancy error which could be improved in further work with a projection approach in order to obtain a time-variant parameter influence in the moving horizon.

Furthermore, the implemented EMF generates a numerical integration error while using the trapezoidal rule (cf. section 5.4.7). An improvement represents the change of the Newton-Cotes formula, e.g. to the use of the Simpson's rule. Another more precise method represents the Gaussian integration method. [SB80] The test of different integration methods can also be part of further work.

5.4.6 Iterated EMF

In order to minimize the linearization error by applying the first-order Taylor series to the nonlinear I/O system equation, an improvement of the EMF is proposed in this section. The idea is to recursively modify the center point of the Taylor expansion and to achieve an 'one-step-convergence' of the estimation error within one time step. This is possible due to the non-asymptotic approach.

The IEMF is an extension to the structure of the EMF explained in section 5.4.4. The iterated steps can be seen in figure 5.4 and consist in repeating the linearization with the estimated $\hat{Z}$ in order to minimize the estimation error $e_\mathrm{Z} = Z - \hat{Z}$. This is accomplished by recalculating the linearization parameters which are assumed constant in the considered horizon interval. Subsequently, the revised linearization parameters lead to an improved estimation $\hat{Z}$.

The most computational part of the online estimation by the EMF, namely the modulation of the measured signals u and y, is executed only once in the modulation horizon $[t-T, t]$. Nevertheless, the iteration loop includes the modulation of the linearization parameter ε, but due to the constancy assumption, the convolution of the ε with the

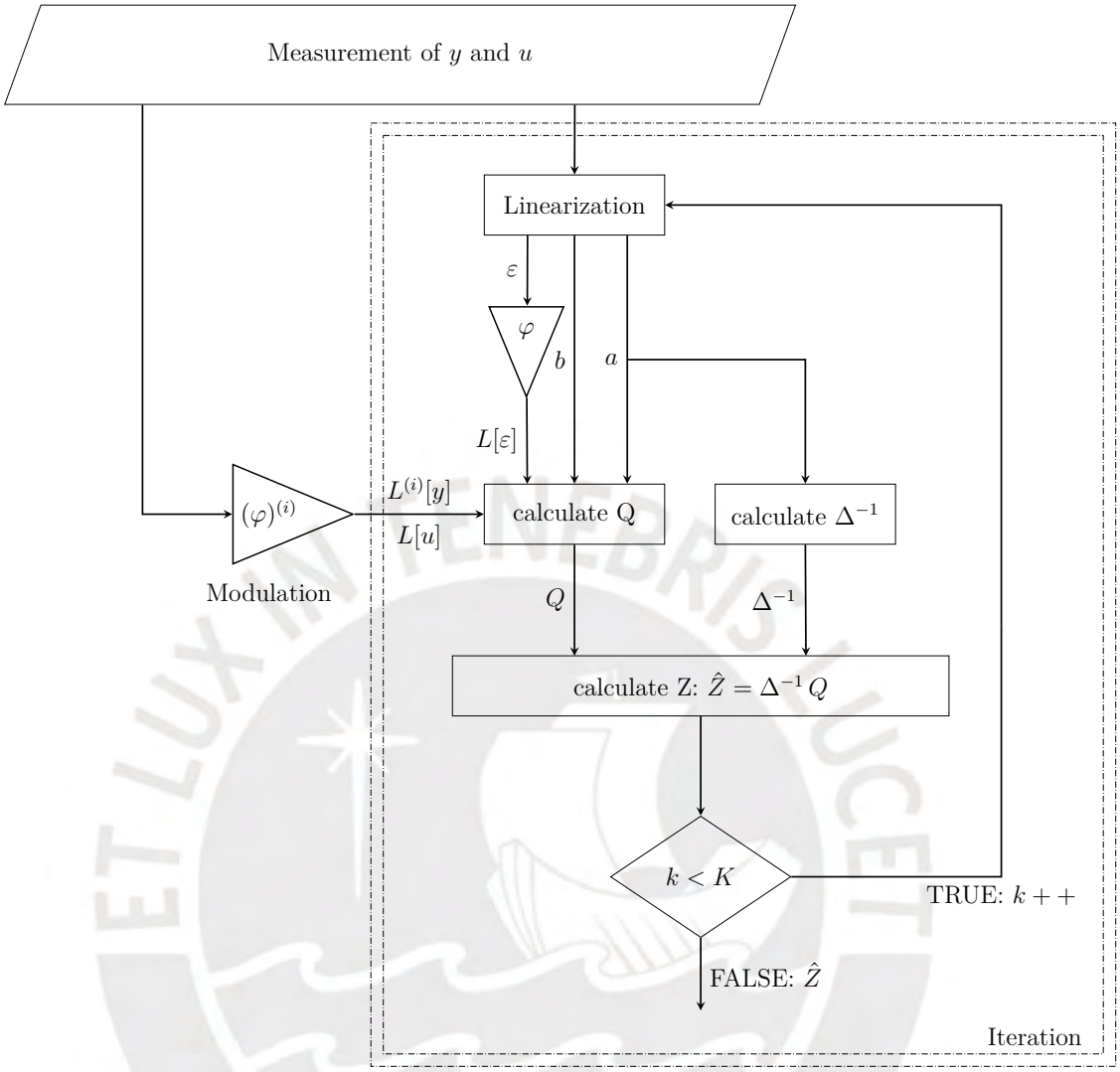

Figure 5.4: Structure of the IEMF

MF is a low cost calculation.

The iteration number K must be chosen beforehand and can only be adapted offline. The higher the number K is, the more increase the computational requirements but at the same time the linearization error ε declines. Therefore, the iteration number K must be adjusted to the system under this consideration.

5.4.7 Numerical Implementation

The numerical implementation of the proposed state observer is divided into the offline calculations and the online procedure. Primarily, the required nonlinear I/O equation (5.26) for the state observation is determined. Also the Jacobians $a(Z, u, \theta)$ and

$b(Z, u, \theta)$ of the system equation (5.27) can be pre-calculated such that only an online insertion of the estimated values $\hat{Z}$, the measured input signal u and the estimated parameter value θ is required.

Furthermore, the used MFs are chosen w.r.t. the tuning parameters that include the modulating sampling time T_{MF}, the length of the moving horizon window T and the kernel shape. In particular, the construction of the GMF is stated in the proposition 5.4.1.

Proposition 5.4.1 (Construction of GMF [Tia+19]). *Let $T \in \mathbb{R}_+, K \in \mathbb{N} \setminus \{0\}, n \in \mathbb{N}$ with $n \leq K-1$. For $i = 0, \cdots, K-1$, let φ_{i} be a left K^{th} order modulation function on $[0, T]$. Then, let us consider the following function: $\forall \tau \in [0, t]$,*

$$\varphi(\tau) = \sum_{i=0}^{K-1} \lambda_{\mathrm{i}}\, \varphi_{\mathrm{i}}(\tau). \tag{5.40}$$

If the coefficient vector $\lambda = (\lambda_0, \cdots, \lambda_{\mathrm{K}-1})^T$ is the unique solution of the following linear system:

$$B\lambda = b_{\mathrm{n}} \tag{5.41}$$

where $B \in \mathbb{R}^{K \times K}$ assumed to be invertible, and $b_n \in \mathbb{R}^K$ are defined as follows: for $k, i = 0, \cdots, K-1$,

$$B(k, i) = \varphi_{\mathrm{i}}^{(k)}(T) \tag{5.42}$$

and for $k = 0, \cdots, K-1$,

$$b_{\mathrm{n}}(k) = \begin{cases} 1, & \text{if } k = n \\ 0, & \text{else} \end{cases} \tag{5.43}$$

then φ is a $(K, n)^{th}$ order generalized modulating function on $[0, T]$.

Beside the definition, the proof of the construction of the GMF can also be found in [Tia+19].

The kernel of the MF consists of an orthonormal basis $\Phi = \{\Phi_1, \cdots, \Phi_N\} \subset \mathcal{L}_2^{loc}([0, T], \mathbb{R})$ with an unweighted inner product space:

$$\langle \Phi_i, \Phi_j \rangle = \int_0^T \Phi_i(\tau)\Phi_j(\tau)d\tau = \begin{cases} 1 & : i = j \\ 0 & : i \neq j \end{cases}. \tag{5.44}$$

The GMF is built w.r.t. the Gram-Schmidt process that is described in detail in [Lyc20].

The modulation of a signal is numerically implemented by an integral function ap-

proximation. Hence, the realization of the receding horizon MF operator as an FIR filter by a discrete-time integral approximation for a signal $y : \mathbb{R}_0^+ \to \mathbb{R}$ is given as follows:

$$\begin{aligned} L^i[y] &= (-1)^i \int_{t-T}^{t} \varphi^{(i)}(\tau - t + T)\, y(\tau)\, d\tau \\ &\approx (-1)^i\, T_s \sum_{k=0}^{N} W_{\mathrm{k}}\, \varphi^{(i)}(k\, T_s)\, y((l - N + k)\, T_{\mathrm{s}}) \\ &= (K_{\mathrm{MF}}^0 \cdots K_{\mathrm{MF}}^N) \begin{pmatrix} y(l-N) \\ \vdots \\ y(l) \end{pmatrix} =: K_{\mathrm{MF}}\, Y \end{aligned} \tag{5.45}$$

with

- current time $t = l\, T_{\mathrm{s}}$ where $l \in \mathbb{N}$,
- number of approximation steps $N \in \mathbb{N}$ and
- step size T_{s} with $T = N\, T_{\mathrm{s}}$.

The modulation vector K_{MF} consists of N time samples as the filter coefficients. The numerical approximation of the filter coefficients is performed in this thesis by a forward integration rule, namely the trapezoidal rule which is one of the Newton–Cotes formulas [SB80]. The vector Y contains the memory of the saved measured values over the moving horizon. The implementation of the modulation of the signal y can be summarized as depicted in figure 5.5. The filtering characteristics of a zero-order modulation operator correspond to a low-pass filter, whereas a MF is generating measures of the derivatives of a signal equal to a band-pass filter [PR93].

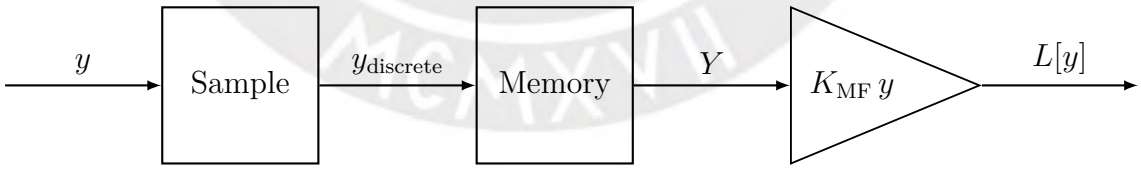

Figure 5.5: Numerical implementation of the modulation operator

5.5 Joint Parameter and State Estimation

The design of the proposed nonlinear adaptive observer combines the input-output based parameter identification DMR (see section 5.3) with the time-variant state observer called EMF (see section 5.4). By using MFs and a closed-loop design of the EMF,

a real-time capable adaptive observer architecture is achieved which is illustrated in figure 5.6. Both, the parameter estimator and the state observer, can act autonomously.

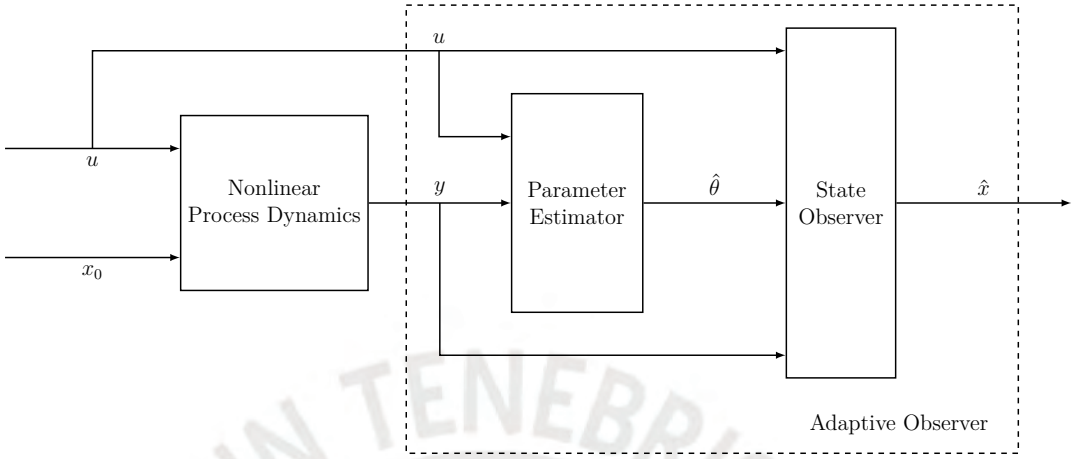

Figure 5.6: Structure of the adaptive observer

However, the state observer requires a parameter value. An extension of the system with a parameter state is not recommended since this would increase the order of the required output derivatives and thus, unnecessarily rise the complexity and the computational burden. Therefore, the proposed structure of the approach is advantageous since the parameter estimation does not depend on the result of the state observation like the coupled EKF.

The performance of the adaptive non-asymptotic observer is tested in the following chapter 6 where it is additionally compared to the well-known asymptotic observer EKF. For state and parameter estimation, all measurements of the last integration horizon T are needed, i.e. only from the time T the results is reliable. Thus, the system has to be pre-initialized and it is recommended to choose the horizon for the DMR smaller than for the state observer: $T_{\mathrm{DMR}} < T_{\mathrm{EMF}}$ sucht that the state observer can directly use the parameter estimation.

In general, the moving horizon length T must be large enough to contain sufficient information. However, if the system has a fast dynamics, the horizon must be adapted to a smaller T to be able to react to the dynamics. This compromise is part of the tuning procedure w.r.t. the MFM in order to obtain a robust implementation. Also the kernel function of the MF can be varied, e.g. polynomial, Fourier, etc. In contrast to the EKF, this approach does not need to solve a RDE in each time step. Instead of that, an algebraic system of equations with an efficient implementation of the numerical integrals has to be solved.

6 Comparative Simulations

In order to validate the properties of the proposed adaptive observer, the approach of the decoupled parameter and state estimator using MFs is compared to the industrial standard observer EKF. The programming, the graphical representation as well as the evaluation are done in MATLAB® and SIMULINK®.

Firstly, the preliminaries for the simulations are provided in section 6.1. Secondly, in section 6.2 the observers are used in several simulation scenarios with distinct parameter behavior and noise influence in order to show their characteristics.

6.1 Preliminaries

Beside the constant parameters of the plant set in table 2.1, it is assumed that the measured signals $m_1 - m_6$ are constant during the simulations. They are listed in the following table 6.1:

Description	Variable	Value	Unit
pH-value	pH	7	
Permeate Flow Rate	Q_p	0.00681	$\mathrm{m}^3/\mathrm{min}$
Brine Flow Rate	Q_b	0.1	$\mathrm{m}^3/\mathrm{min}$
Pressure Difference	ΔP	20	bar
Conductivity of Feed Stream	γ_f	0.1	$\mathrm{S\,m}^{-1}$

Table 6.1: Measured signals for the simulation

Furthermore, the initial values of the states x_0 are chosen in advance to receive the approximated nonlinear I/O relation (5.26) in the offline calculations. They are set to $x_0 = [0.5, 0.5, 0.5]^\top$ to form a basis for a comparison of both adaptive observers. This leads to a transformation error (cf. section 5.4.5) w.r.t. the considered input signals u_1 and u_2 (see figures 6.3) that influences the estimation by the EMF. In figure 6.1a, the transformation w.r.t. the operating point input u_1 produces an error of $e_{\mathrm{trans,x_3}} \approx -0.001$, whereas in figure 6.1b the impact of the moving input can be seen in the transformation errors.

Also the initial values of the output and its derivatives are selected for the first run of the EMF. In this case, $Z_0 = [0, 0, 0]^\top$ is used to linearize the nonlinear I/O equation of the

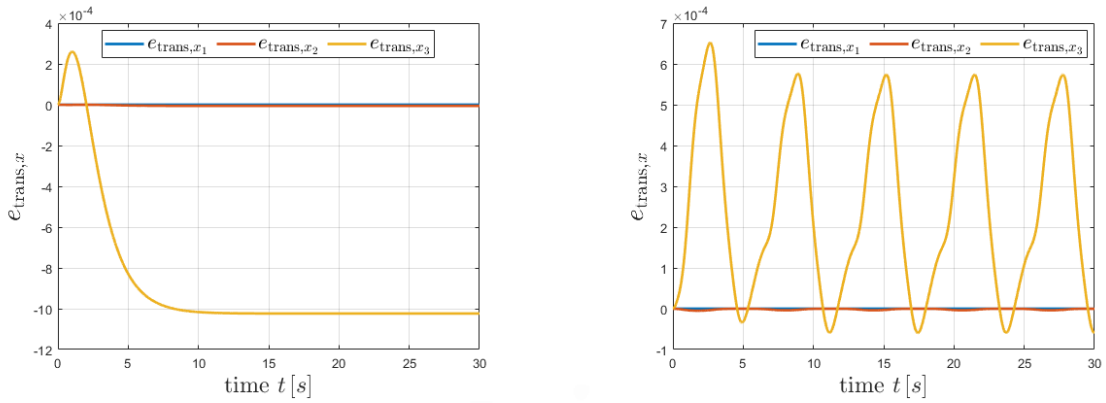

(a) u_1 (b) u_2

Figure 6.1: Transformation error by developing the nonlinear I/O relation (5.26) from the state-space representation (2.24-2.26)

system (5.26) in order to obtain the linear I/O relation (5.27). Hence, the linearization parameters a, b, ε, which are assumed constant in each moving horizon window of the MFM, imply an incorrect estimation of the output value y and its first and second derivatives $\dot{y}, \ddot{y}$ (cf. section 5.4.4). That is the reason why in the first interval with the moving horizon length T the estimation is peaking and only for $t > T$ the estimation is reliable.
Moreover, the initial value of the parameter is set to $A_{\text{m},0} = 0.5 \cdot A_{\text{m}}^*$.

The modulation related sampling time of the TMF is chosen to $T_{\text{TMF}} = 1 \times 10^{-2}\,\text{s}$. Due to the dynamics of the state, the modulation related sampling time of the GMF is adopted smaller to $T_{\text{GMF}} = 1 \times 10^{-3}\,\text{s}$. Both MFs are based on polynomials with an orthonormal basis and exemplified functions can be seen in figure 6.2 which are used in the following simulations. The moving horizon with the length T of the MFs is adjusted during the simulations in order to receive the best possible results of the MFM.

The EKF used for the parameter estimation by the DMR in the proposed adaptive observer employs the values of the covariances matrices $Q_{\text{DMR}} = 10$, $R_{\text{DMR}} = 0.05$ and the forgetting factor is set to $\lambda_{\text{DMR}} = 5$. In this case, the matrices are single valued since only one parameter is estimated.

The chosen time-variant parameter of the plant is the changing surface area of the membrane A_{m} due to the CP and the membrane fouling as explained in section 2.1.3.2. The nominal value, which corresponds to the particle clean surface membrane area, is set to $A_{\text{m}}^* = 16\,\text{m}^2$. During the operation, this parameter declines because more and more particles accumulate on the membrane surface. In the following section, three parameter scenarios are considered. Firstly, the parameter A_{m} is fixed to its nominal

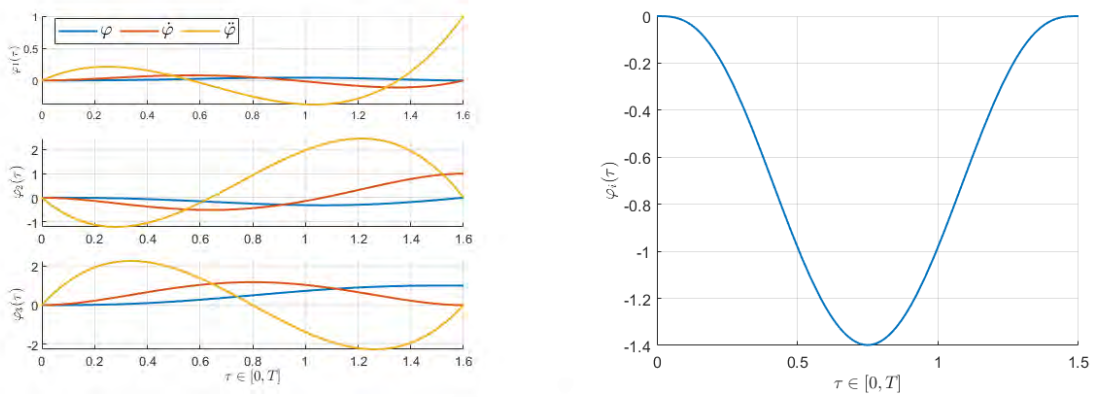

(a) GMFs (b) TMF

Figure 6.2: Set of three GMFs for the state observation with the EMF and one TMF for parameter estimation with the DMR

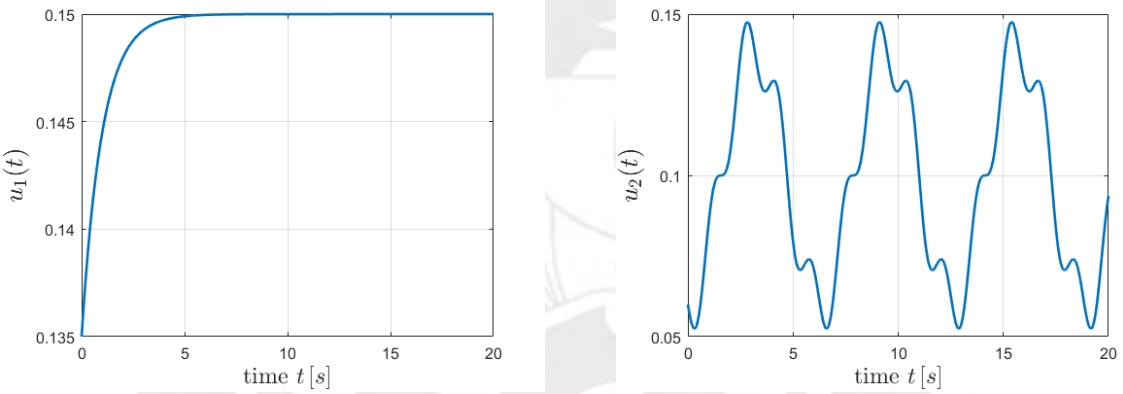

(a) Operating Point Input (b) Excitation Mode Input

Figure 6.3: Input signals for the operating point and the excitation mode scenarios

value A_{m}^{*} and thus represents the optimal case. Secondly, there is a sudden decrease in the parameter value from A_{m}^{*} to $A_{\mathrm{m}} = 15\,\mathrm{m}^2$. Thirdly, the parameter reduces steadily comparable to a ramp. This comes closest to the physical degradation.

In each scenario two distinct input cases are executed. These include the operation around the operating point with the input $u_1 = \frac{3}{20} - \frac{3\,\mathrm{e}^{-t}}{200}$ and in a dynamical mode with an alternating input $u_2 = \frac{1}{10} - \frac{\cos(t)}{25} - \frac{\sin(4\,t)}{100}$ (see figures 6.3).
In figure 6.3a the exponential rise of the input is shown which is directly applied to the rotational speed of the pump ω_{p}. After the exponential rise of the signal, it reaches the set point and remains at this operating point.
The excitation mode in figure 6.3b shows the increase and decrease of the input which directly affects the pump speed ω_{p} by the changing input u. Thereby, the system gets

dynamical and the entire operating spectrum of the pump is reproduced.

Additionally, in each scenario the measured signals are exposed to noise. The applied noise is a zero-mean white Gaussian noise which is low-pass filtered. The low-pass filter is of first order (transfer function $G(s) = \frac{1}{1+s}$) and is applied in order to receive similar noise as in [Riv+19] which has used real-time data of the considered RO plant of the *PUCP*.

6.2 Scenarios

In the following part, the coupled EKF (cf. chapter 4) is contrasted with the proposed adaptive observer of chapter 5. Different scenarios concerning the RO plant are simulated. These comprise the constant parameter scenario in section 6.2.1, the step (see section 6.2.2) and the gradual decrease of the parameter value which is outlined in section 6.2.3. Both inputs of figure 6.3 are simulated each time. Moreover, the observers are analyzed under noise affection in section 6.2.4.

6.2.1 Constant Parameter

In this section, the general behavior of the RO plant is considered as well as the characteristics of the observers in an optimal environment without the CP and the membrane fouling.

Operating Point Input The coupled EKF estimates both states and parameter due to the extension by the parameter as fourth state with the parameter dynamics equals zero. The covariances R_{EKF} and Q_{EKF} are unitary matrices and the forgetting factor is chosen to $\lambda_{\mathrm{EKF}} = 3.5$. The smaller the forgetting factor, the slower the convergence of the estimation error, which has been proven during the tuning of the coupled EKF.

Physically, the behavior of the RO plant can be analyzed in figure 6.4a. Due to the rise of the rotational speed of the pump $x_3 = \omega_{\mathrm{p}}$, the RO process starts. In the operating point of the plant, two streams with a constant concentration are produced. The first state x_1 represents the concentration of the permeate stream C_{p} which is lower as the brine stream concentration $x_2 = C_{\mathrm{b}}$. Hence, the brine stream carries the salt particles out of the membrane. In this simulation, the product of the process $y = x_1$ is drinkable fresh water with a concentration $C_{\mathrm{p}} < 0.5\,\mathrm{kg\,m^{-3}}$.

In figure 6.4a the observation of the states $\hat{x}_1 - \hat{x}_3$ and the parameter $\hat{\theta}$ is shown in comparison to their real trajectories. The estimation error converges to zero at $t \approx 8\,\mathrm{s}$

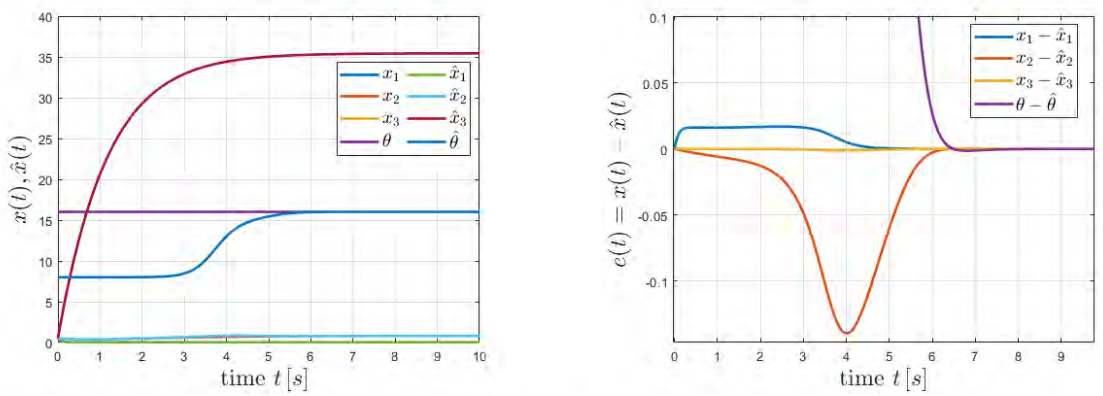

(a) State estimation

(b) Zoom in the state estimation error

Figure 6.4: State and parameter estimation by the coupled EKF with u_1, $\lambda_{\text{EKF}} = 3.5$ and constant parameter

which is depicted in figure 6.4b.

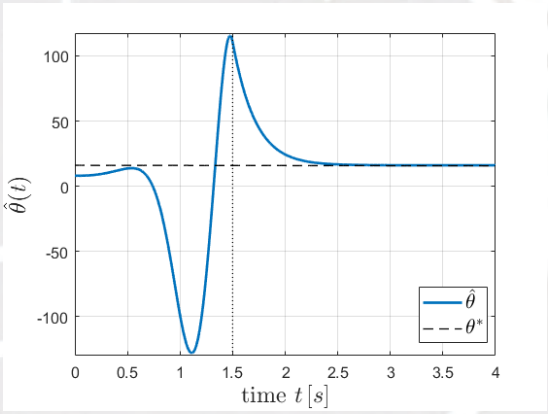

Figure 6.5: Parameter estimation by the DMR with u_1 and constant parameter

In contrast, the parameter estimator of the proposed adaptive observer DMR shows a direct convergence to the optimal value after the moving horizon length of $T = 1.5\,\text{s}$ (see figure 6.5). Thereafter, the value of the parameter can be used for the state estimation shown in figure 6.6.

The state observation in figure 6.6 is based on the estimated values of $\hat{Z}$ which represents the output and its derivatives. The error of the calculated $\hat{Z}$ is shown in figure 6.7a. Noticeable is the peak at $t = 0.74\,\text{s}$ which implies a great state estimation error of $e_{x_3} \approx 15.3 \times 10^6$ (in figure 6.6a) due to the transformation (cf. formula (5.25)). Hence, these estimations in the first interval should not be used for further applications, for instance in the control or the fault detection.

In the first interval of the sliding window, the peaking of the estimation is obvious.

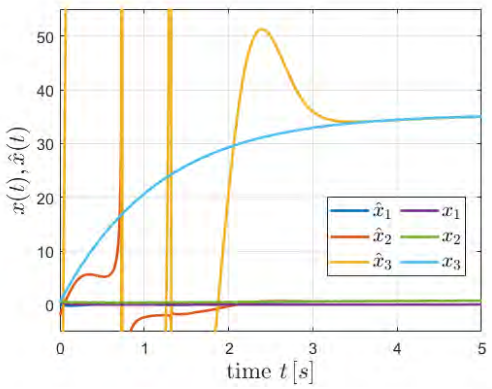

(a) Comparison of the real and estimated states

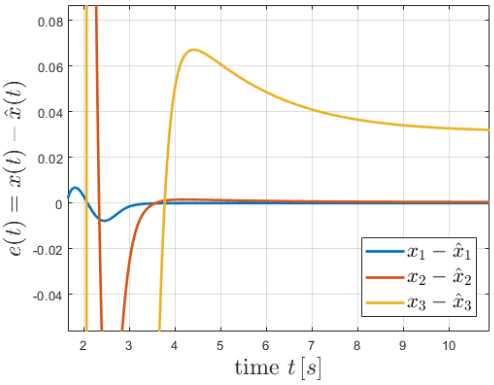

(b) State estimation error

Figure 6.6: State estimation by the EMF with u_1 and constant parameter

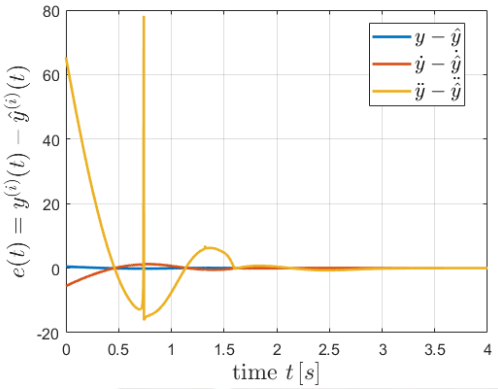

(a) Estimation error by the EMF

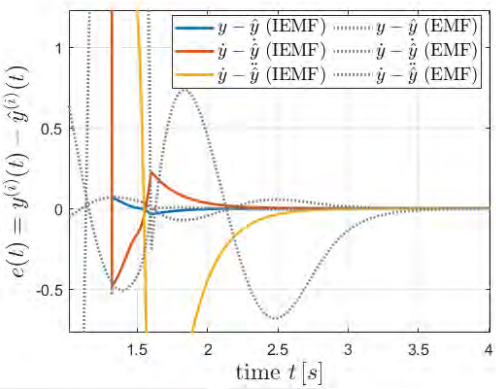

(b) Comparison of the Z estimation error by the IEMF and the EMF

Figure 6.7: Estimation error of the output and its derivatives by the EMF and IEMF with u_1 and constant parameter

After the DMR delivers a reliable estimation, the state observer error of the first and second states $\hat{x}_1, \hat{x}_2$ also tend to zero (see figure 6.6b). The larger the derivative of the signal, the more difficult is the estimation. Therefore, the second derivative has an offset of $e_{\ddot{y}} \approx 1.8 \times 10^{-4}$ (cf. figure 6.7) which becomes larger by the transformation to the states $e_{x_3} \approx 0.031$ (see figure 6.6b).
However, the estimation process with the proposed adaptive observer is faster than the observation with the coupled EKF and shows good results for $t > 4\,\mathrm{s}$.

The improvement using the IEMF instead of the EMF with an iteration number of $K = 5$ is shown in the figure 6.7b. Due to the 'one-step convergence' by means of the iteration of the linearization step, the estimation error tends even faster to zero. The

choice of the iteration number is a tradeoff between the rise of the computational costs and the exactness of the 'one-step convergence'. Therefore, only the IEMF will be used in the following since the performance exceeds that of the EMF.

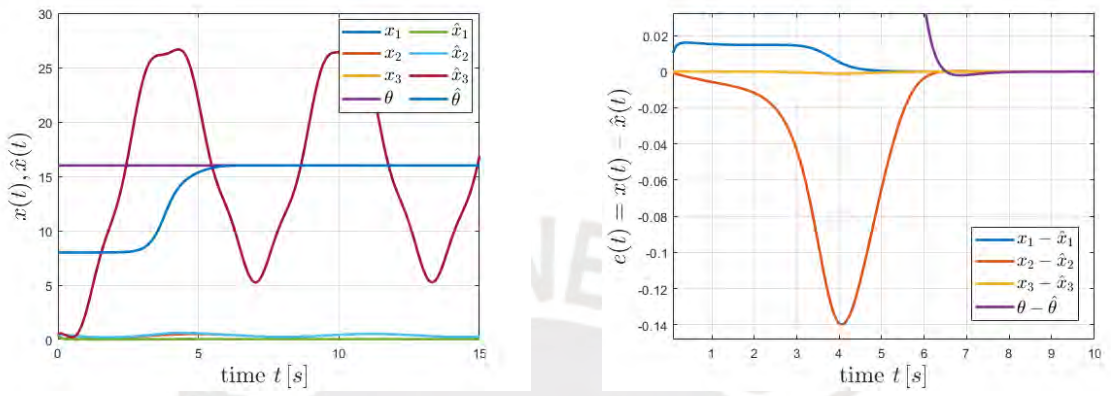

(a) State estimation

(b) Zoom in the state estimation error

Figure 6.8: State and parameter estimation by the coupled EKF with u_2, $\lambda_{\text{EKF}} = 3.5$ and constant parameter

Excitation Mode Input The coupled EKF shows similar results as with the input of exponential rise up to the set point but needs longer ($t \approx 9\,\text{s}$) to converge in all four states (cf. figure 6.8).

Examining the proposed adaptive observer with MFs, the parameter estimation is equal to the one in the case of the operating point input. Thus, figure 6.5 represents the same result as with the excitation input and it can be stated that the DMR is less sensitive to the input.

The estimation of the output and its derivatives using the IEMF shows a convergence of the estimation error after the first moving horizon window $t > T = 1.6\,\text{s}$ (cf. figure 6.9a). Examing the zoom figure 6.9b, the varying input is displayed in the estimation especially of the second derivative $\ddot{\hat{y}}$. Transforming the output estimates into the state observations by using formula (5.25), the estimation error increases (see figure 6.10b). In percentage terms, the estimate of $\hat{x}_3$ is off by approximately $0.18 - 0.7\,\%$ from the real value x_3. Due to the change in the rotational speed of the pump ω_p, the first and second states, which are the concentrations of the permeate and the brine stream C_p and C_b, are also changing.

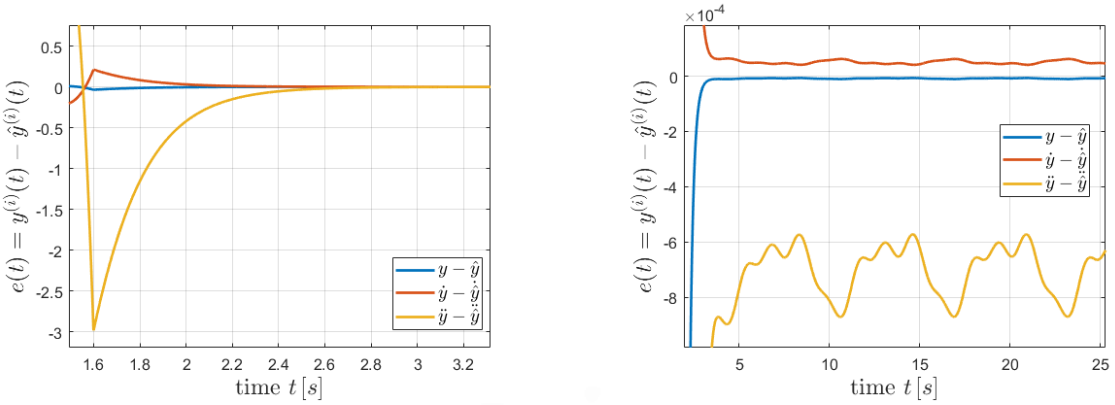

(a) Error convergence after $t > T$

(b) Zoom in the figure 6.9a

Figure 6.9: Estimation of the output and its derivatives by the IEMF with u_2 and constant parameter

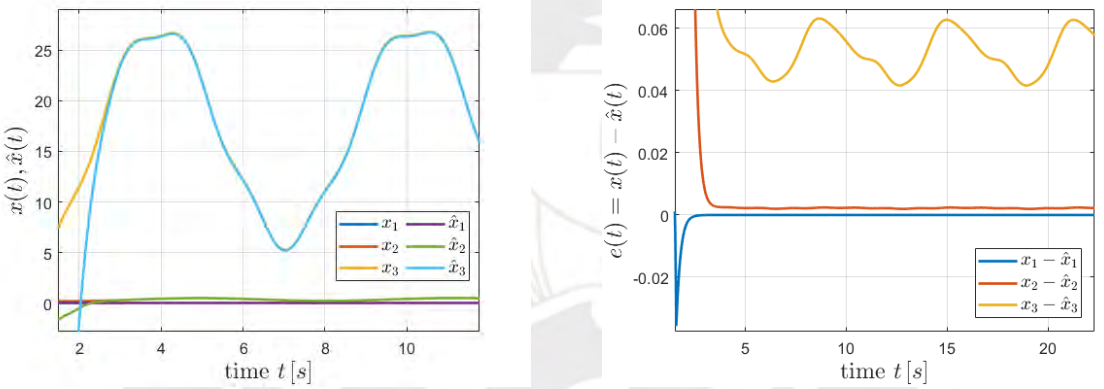

(a) Comparison of real and estimated states

(b) Zoom in state estimation error

Figure 6.10: State estimation by the IEMF with u_2 and constant parameter

6.2.2 Step Decline in Parameter

In each simulation, a parameter step from $A_\mathrm{m}^* = 16\,\mathrm{m}^2$ to $A_\mathrm{m} = 15\,\mathrm{m}^2$ at $t = 10\,\mathrm{s}$ is executed in order to rebuild a sudden deposit on the membrane surface. Physically, the reduction of the membrane surface A_m leads to a decrease of the permeate volume stream Q_p, whereas the volumetric flow rate of the brine stream Q_b will rise. Therefore, the ratio of $\dfrac{Q_\mathrm{b}}{Q_\mathrm{p}}$ will increase and with it the pressure difference across the membrane ΔP. At the end of this effect chain, the output of the system $y = x_1 = C_\mathrm{p}$ will decline and at the same time less fresh water is produced.

Operating Point Input In the direct comparison of the DMR with the coupled EKF in the figure 6.11, it is noticeable that the proposed parameter observer DMR overswings the optimal value more than the coupled EKF estimation. Especially, in the beginning

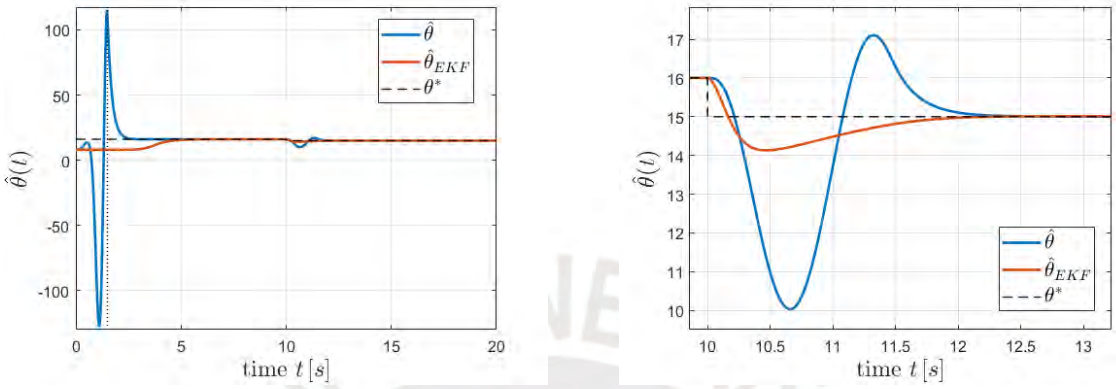

(a) Parameter Estimation (b) Zoom in the figure 6.11a

Figure 6.11: Comparison of the parameter estimation with u_1 and step decline of the parameter at $t = 10\,\mathrm{s}$

of the observation $t < T$ the peak of $\hat{\theta}$ is seven times higher than the optimal value, but after the first moving horizon interval of the MFM the estimated value converges faster than the estimation of the coupled EKF. After the step at $t = 10\,\mathrm{s}$, both estimations tend to the new value of the surface area with the same speed but the parameter value $\hat{\theta}$ of the DMR overswings more (see figure 6.11b). If the parameter step increases, the peaks of the overshoots will also rise.

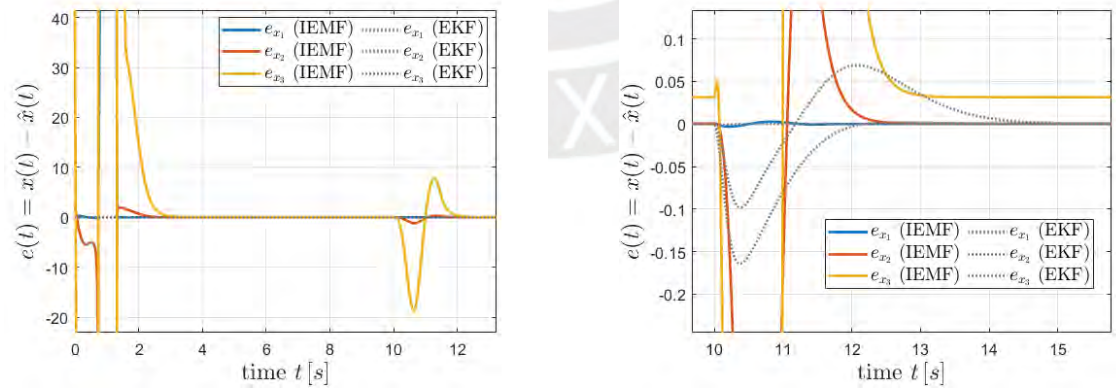

(a) State estimation error (b) Zoom in the figure 6.12a at the parameter step

Figure 6.12: Comparison of the IEMF and the coupled EKF with u_1 and step decline of the parameter at $t = 10\,\mathrm{s}$

The direct contrasting of both considered state observers in figure 6.12 demonstrates similar results as the parameter comparison: the EMF shows bigger overshoots until the new value of the parameter is used for the solution of the system of equations (5.31). Figure 6.12b visualizes the zoom in figure 6.12a at $t = 10\,\mathrm{s}$ where the convergence of the states after the step is visible. Again the state observations of the EMF is faster than of the coupled EKF. However, there is still the offset of the estimated value $\hat{x}_3$ by the EMF as detected in section 6.2.1.

Excitation Mode Input Similar results are obtained while using the dynamic input which can be seen in the figures C.4 in the appendix. The only difference to the plots in the previous paragraph (see figures 6.12) with the static input is the moving estimates $\hat{x}$ of the EMF due to the ups and downs of the input, whereas the coupled EKF observation is not influenced.

6.2.3 Gradual Decrease in Parameter

The proposed gradual decline in the parameter A_m is simulated by a ramp function and represents the real case of the CP and the fouling of the membrane. This process does not occur suddenly but gradually, i.e. the deposit takes place evenly. Thus, the membrane surface becomes less with increasing time by a decline rate of $\dot{\theta} = -0.1$. This will show the adaptability of the observer approaches.

Operating Point Input The forgetting factor of the coupled EKF is adjusted to $\lambda_\mathrm{EKF} = 1.2$. Figure 6.13a illustrates that the parameter state can follow the gradual decline of the parameter A_m. In the zoomed figure 6.13b, the state estimation error of the coupled EKF shows the convergence of the states $\hat{x}_1 - \hat{x}_3$. However, the parameter state has a constant offset of $e_\theta = -0.09$. If the forgetting factor is chosen $\lambda_\mathrm{EKF} > 1.2$, the second and third states will diverge slightly. Therefore, $\lambda_\mathrm{EKF} = 1.2$ is chosen, but this results in a slower convergence of the states than in the previous scenarios with the constant parameter or the step decline in the parameter.

Also the proposed adaptive observer requires an adaption of its tuning parameters. Using the moving horizon window length $T_\mathrm{TMF} = 1.5\,\mathrm{s}$ of the DMR applied in the previous plots, a clear deviation from the desired parameter value is recognizable in figure 6.14a. This generates a falling state estimation error of $\hat{x}_3$ (see figure 6.14b). One possible solution includes the tuning of the MF horizon length in order to receive more information for the parameter estimator DMR. The use of a length of $T_\mathrm{TMF} = 3.3\,\mathrm{s}$ leads to a more exact estimation of the parameter decline $\hat{\theta}$ (cf. figure 6.15a), also in

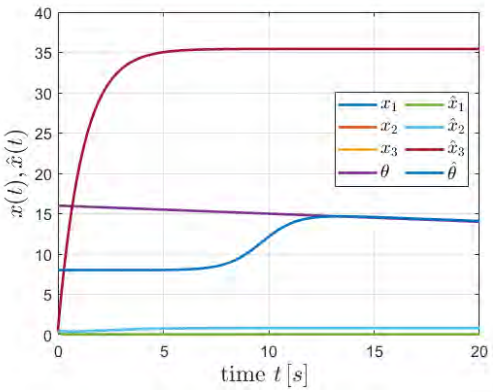

(a) State estimation

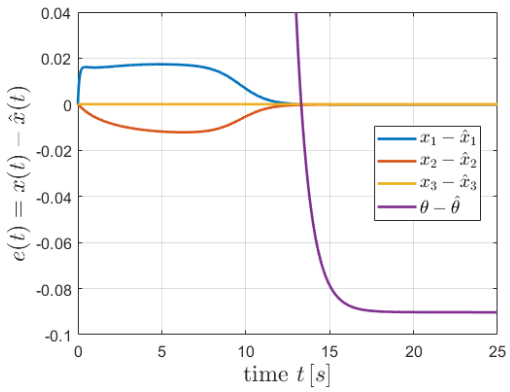

(b) Zoom in the state estimation error

Figure 6.13: State and parameter estimation by the coupled EKF with u_1, $\lambda_{\mathrm{EKF}} = 1.2$ and gradually decreasing parameter

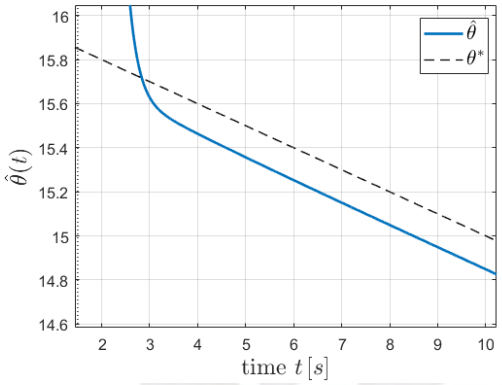

(a) Parameter estimation offset

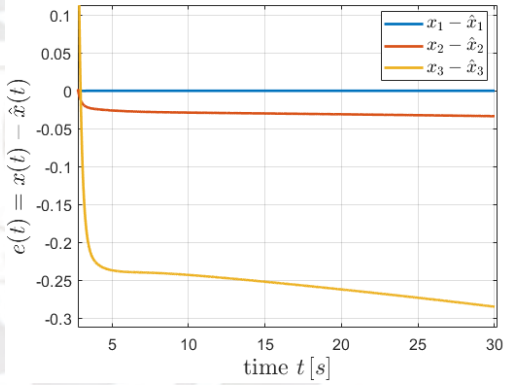

(b) State Estimation error with diverging e_{x_3}

Figure 6.14: Parameter estimation and state error by the proposed adaptive observer with u_1, $T_{\mathrm{TMF}} = 1.5\,\mathrm{s}$ and gradually decreasing parameter

comparison with the coupled EKF estimate $\hat{\theta}_{EKF}$. However, after the transformation of the estimated output and its derivatives to the states, there is a constant offset of the third state outlined in figure 6.15b. Nevertheless, the non-asymptotic estimation is still faster than the asymptotic estimation by the coupled EKF (cf. figures 6.15).

Excitation Mode Input When the rotational speed of the pump $\omega_{\mathrm{p}} = x_3$ turns up and down (see figure 6.16a), the parameter estimation with the coupled EKF shows a dynamic parameter state estimation error in figure 6.16b.

In comparison, the parameter value by the DMR $\hat{\theta}$ is faster and closer to the gradually decreasing optimal value θ^* as the coupled EKF estimate $\hat{\theta}_{\mathrm{EKF}}$ (see figure 6.17a). The

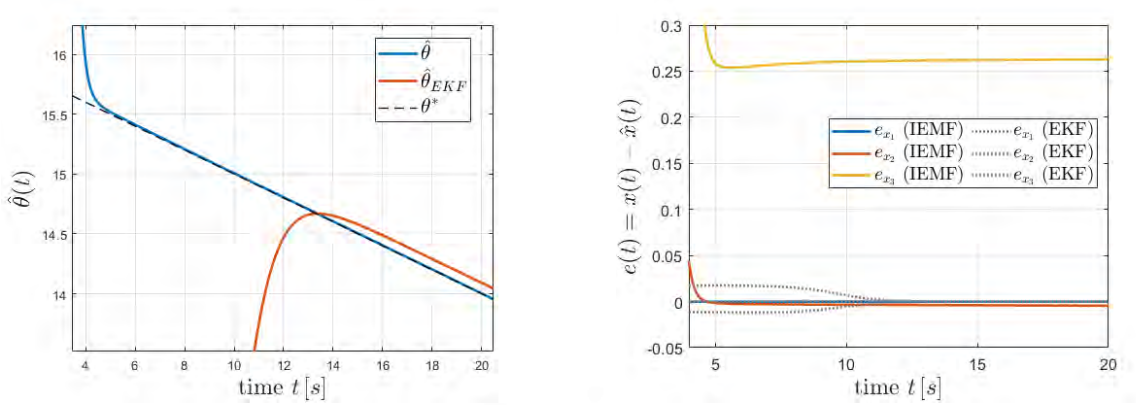

(a) Parameter Estimation (b) Comparison of the State Estimation Error

Figure 6.15: Comparison of the IEMF and the coupled EKF with u_1, $T_{\text{TMF}} = 3.3\,\text{s}$ and gradually decreasing parameter

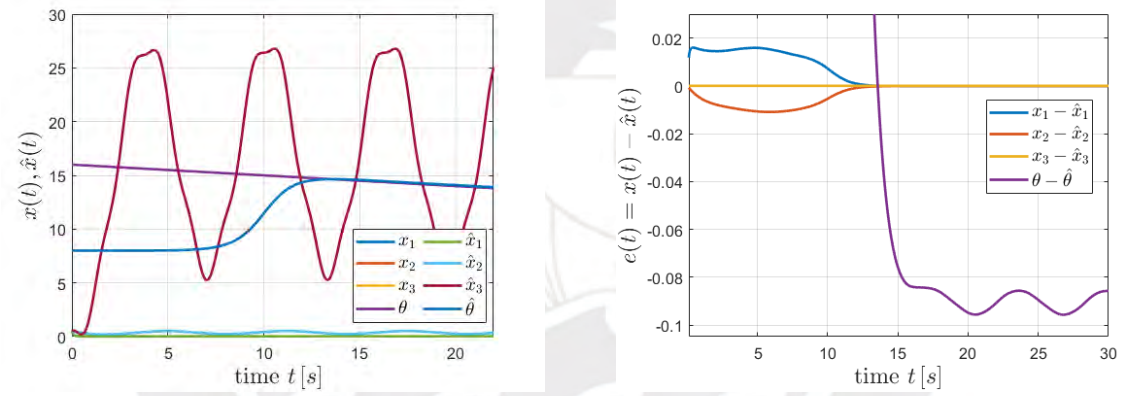

(a) State estimation (b) State estimation error

Figure 6.16: State and parameter estimation by the coupled EKF with u_2, $\lambda_{\text{EKF}} = 1.2$ and gradually decreasing parameter

figure 6.17b displays the state estimation error by the EMF which is bigger than in figure 6.10b due to the additional inaccuracy in the parameter estimation with the unknown decline rate.

6.2.4 Noise Impact

In order to investigate the properties of the observers under noise impact, the variance of the considered noise is chosen to $\text{Var} = 5 \times 10^{-4}$. The bigger the variance of the noise is, the bigger is the noise-ratio level. Furthermore, the noise signal is also low-pass filtered. This scenario represents a good feasibility study of the observers in a practical

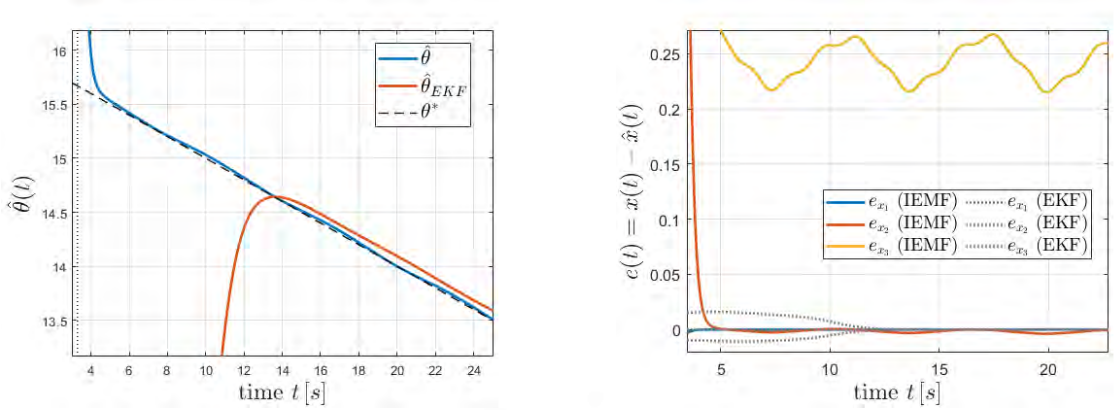

(a) Parameter estimation (b) State Estimation Error

Figure 6.17: Comparison of both observers with u_2, $T_{\text{TMF}} = 3.3\,\text{s}$ and gradually decreasing parameter

environment of the considered RO plant (cf. [Riv+19]). The noise analysis is restricted to the impingement of noise on the output y since it is assumed that the input signal u is well known.

Operating Point Input The output signal with noise y_n is displayed in the figure 6.18b. In comparison with the noise-free output signal y, a signal-to-noise-ratio can be calculated and in the case of the operating point input u_1 the ratio amounts to $SRN \approx 43\,\text{dB}$. The estimated parameters using the measured output, which is subject

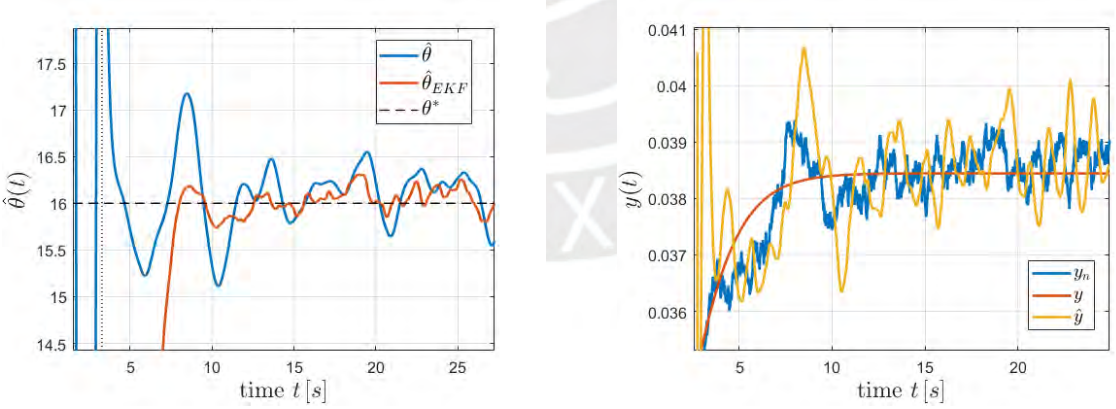

(a) Parameter Estimation (b) Output signal

Figure 6.18: Comparison of parameter and output estimation with u_1, $T_{\text{TMF}} = 3.3\,\text{s}$, $\lambda_{\text{EKF}} = 2$, constant parameter and noise impact

to noise, are displayed in figure 6.18a. The amplitude of the estimated value with the coupled EKF $\hat{\theta}_{EKF}$ is less influenced by the noise than with the DMR although

the impact depends on the chosen forgetting factor λ_{EKF} of the coupled EKF. Since the EMF uses the estimated parameter value $\hat{\theta}$, the estimations of the output and its derivatives are also affected next to the output with noise. Thus, the estimation errors

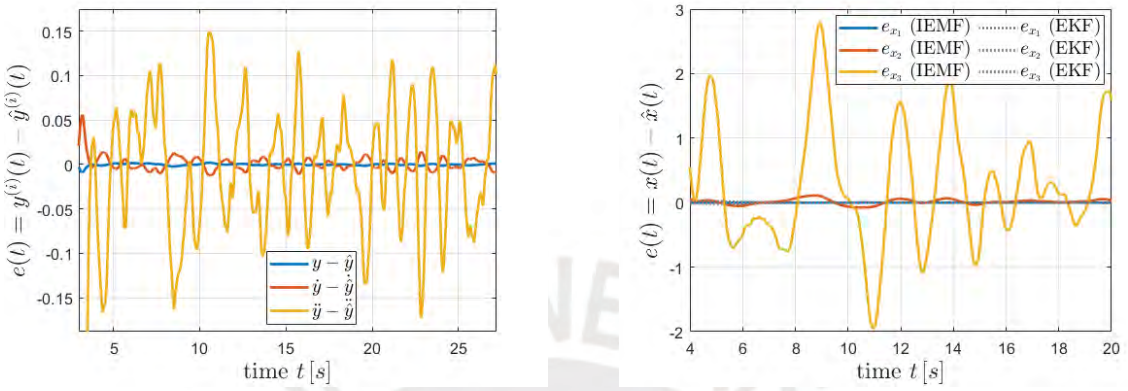

(a) Output Estimation Error by the IEMF (b) Comparison of the State Estimation Error

Figure 6.19: Comparison of the IEMF and the coupled EKF with u_1, $T_{\text{TMF}} = 3.3\,\text{s}$, $\lambda_{\text{EKF}} = 2$, constant parameter and noise impact

of $y^{(i)}$ are noisy as well (see figure 6.19a). The greater the degree of derivation is, the bigger is the noise influence. Hence, the third state is very noisy which can be seen in figure 6.19b.

Examining the figure 6.18b closely, a time lag between the output with noise (in blue) and the estimated value (in yellow) is noticeable. However, the noise effect on the state estimates with the coupled EKF are minor, since the idea of the EKF is based on the occurrence of Gaussian white noise. In order to affect the estimation of the EKF with noise, the variance has to be increased or a distinct type of noise has to be used.

Excitation Mode Input Applying the dynamical input u_2, the parameter and state estimates do not show significant differences to the scenario with the operating point input (cf. figures C.5).

Step Decline in Parameter Including the parameter step at $t = 10\,\text{s}$, the peak of the DMR in the following sliding window increases but the estimate adapts to the step (cf. figures 6.20). In the figure 6.20a, the influence of the noise to the coupled EKF is shown which overlaps the estimate of the DMR. Adapting the forgetting factor of the coupled EKF to $\lambda_{\text{EKF}} = 1.2$, the impact by means of the noise is lowered (cf. figure 6.20b). It follows that the moving of the estimated parameter $\hat{\theta}_{EKF}$ around the new

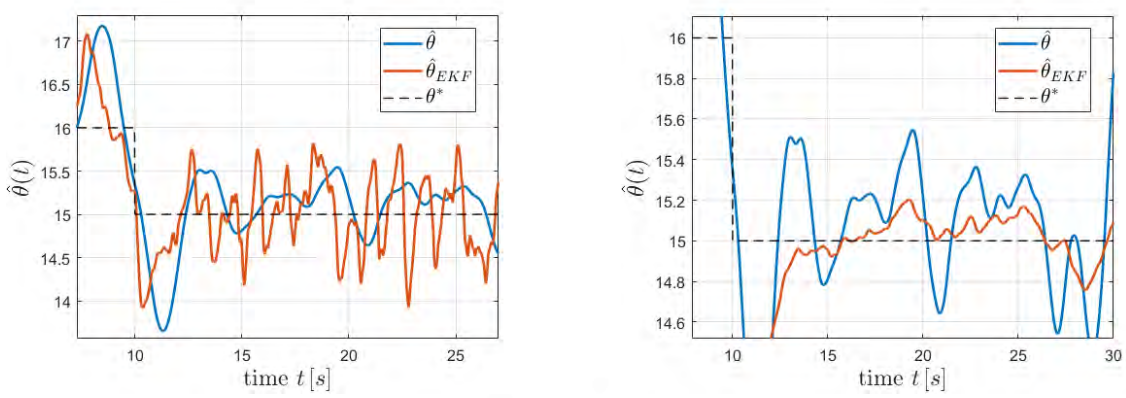

(a) $\lambda_{\mathrm{EKF}} = 3.5$ (b) $\lambda_{\mathrm{EKF}} = 1.2$

Figure 6.20: Comparison of the parameter estimation by the IEMF and the coupled EKF with u_1, $T_{\mathrm{TMF}} = 3.3\,\mathrm{s}$, step decrease and noise impact

nominal value $A_{\mathrm{m}} = 15\,\mathrm{m}^2$ is smaller than the overshoots of the parameter value $\hat{\theta}_{DMR}$ of the combined modulation filter and the EKF approach.

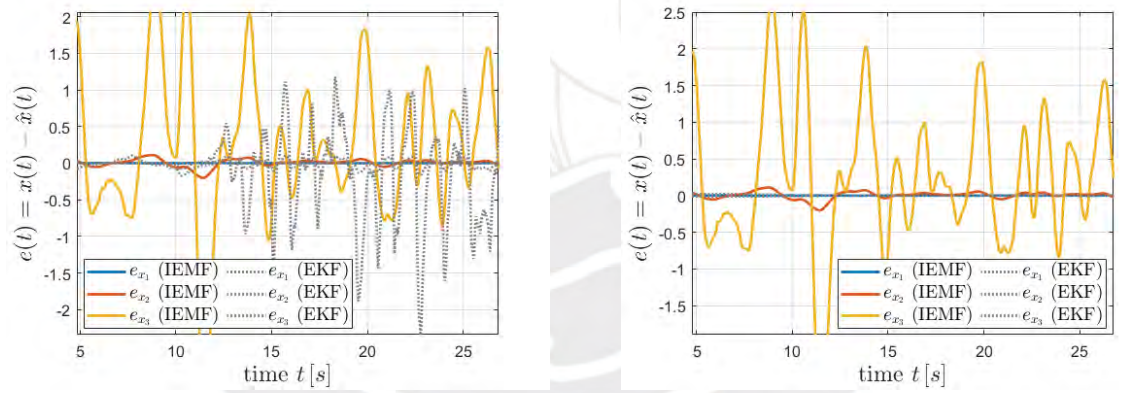

(a) $\lambda_{\mathrm{EKF}} = 3.5$ (b) $\lambda_{\mathrm{EKF}} = 1.2$

Figure 6.21: Comparison of the state estimation error by the IEMF and the coupled EKF wit u_1, $T_{\mathrm{TMF}} = 3.3\,\mathrm{s}$, step decrease and noise impact

Beside the noise influenced parameter estimation due to $\lambda_{\mathrm{EKF}} = 3.5$ (see figure 6.20a), the coupled EKF shows an increased state estimation error in figure 6.21a. The adjustment of the forgetting factor lowers the noise influence on the state estimations which is shown in figure 6.21b. Thus, the estimation error of the IEMF is bigger than the one of the coupled EKF.

Gradual Decrease in Parameter A similar behavior is determined during the gradual decline of the parameter $\theta = A_{\mathrm{m}}$ by a ramp function in figure C.6. The estimated

parameters $\hat{\theta}_{EKF}$ and $\hat{\theta}_{DMR}$ can follow the slow decline of the membrane surface value (cf. C.6a) but the amplitude of the state estimation error of the EMF increases which is displayed in figure C.6b. The state estimation errors e_{x_1}, e_{x_2} and e_{x_3} of the coupled EKF are less influenced since this state observer does not depend on the estimated parameter value.

7 Conclusion and Outlook

The proposed nonlinear adaptive observer (cf. chapter 5) shows a sufficiently satisfying observation behavior w.r.t. the considered RO plant which is mathematically modeled in chapter 2. The results of the observability analysis (cf. chapter 3) are used to apply the common EKF to the desalination plant as a basis for comparison.

The MF based adaptive observer consists of a hierarchical structure of the joint parameter and state estimation as described in section 5.5. The parameter estimator DMR applies the MFM to a system in regressor form and estimates the parameter values with an EKF. In the case of the RO plant, the linearized I/O relation (B.3) is linear in the output, its derivatives $y^{(i)}$ and the input u but nonlinear in the parameter θ. However, the state observer approach EMF can be generally applied to a nonlinear SISO system of the form $y^{(n)} = g(y^{(i)}, u, \theta)$ with $i = 0, 1, \cdots, n-1$ due to the linearization with the Taylor series (cf. equation (5.27)). Nevertheless, the linearization can also lead to definition gaps when the system has non-Lipschitz points in state-space. The EKF has the same disadvantage, but with the MFM there is no need to differentiate noisy signals. Also the estimation result of the EKF depends on the noise, since it is a stochastic approach. If the noise is unknown, the estimate can even diverge. In comparison, the proposed observer is based on integration, and thus, provides in theory a perfect suppression for non-autocorrelated noise. However in the RO example, the measured output signal y with the applied noise has a greater impact on the estimates by the MF observer approach than on the EKF due to the use of a Gaussian white noise (cf. figure 6.18a and figure 6.19b).

Moreover, the simulations show a moving estimation by the EMF due to the excitation input (see figures 6.9b and 6.10b). The peaks in the first interval of the MFM occur due to the initial error in the algebraic equation (5.31). This error disappears when the first reliable estimate is used for the linearization of the nonlinear I/O equation (5.27). A possible improvement of the proposed estimation scheme could include the estimation of the initial values in order to enhance the estimate of the first interval. Another possibility constitutes the use of a receding moving horizon interval in the beginning.

The major advantage of the proposed nonlinear adaptive observer consists in the fast estimation. The first reliable estimates are obtained after the moving horizon window at $t > T$. In comparison, the coupled EKF needs more time to estimate the parameter state θ. However, both observers struggle with the ramp decline in the parameter and

create an offset in the parameter and state estimates (cf. section 6.2.3). The reason lies in the assumption of the constant parameter.

An additional advantage of the proposed state observer structure (see section 5.4.4) is related to the computational costs since no RDE has to be solved at each iteration like the EKF does. The computationally costly parts of the MFM can be done offline. For instance, the preliminaries to receive the nonlinear I/O relation (5.26) is computed only once. Furthermore, the selection of the initial values and the parameters of the MF, which includes the tuning possibilities, e.g. the kernel function, the horizon length T and the modulation sampling time T_{MF}, are calculated offline. Thereby, the well conditioned Δ-matrix by means of GMFs (cf. section 5.4.3) can be inverted beforehand and only the calculated linearization parameter a has to be inserted online.

The proposed state observer EMF shows no direct convergence of the state estimation error in contrast to an asymptotic observer like the EKF, e.g. in figure 6.6b. These inaccuracies occur due to the transformation error, the assumption of constancy of the linearization parameters a, b, ε within a horizon window $[0, T]$, the linearization and H.O.T. error by the Taylor series, and the integration error by the numerical implementation (cf. section 5.4.5). Therefore, the IEMF, an improvement of the EMF, is proposed in order to obtain a 'one-step convergence' by means of an iteration over the linearization and estimation calculations (cf. section 5.4.6).

With the achieved observation accuracy of the rotational pump speed ω_{p}, it is possible to improve the proposed fault detection in [Göp21] by isolating all occurring faults. Moreover, the clogging of the membrane can be monitored with the parameter estimator DMR, which is investigated by a simulative step decrease and a declining ramp for a gradual particle deposition. This could be improved by estimating the decline rate of the membrane surface due to the CP and the membrane fouling and using it for the internal model (5.19) of the DMR. Also additional parameters as the membrane permeability coefficients k_{s} and k_{m} could be included in the parameter estimation process in order to differ between the CP and the membrane fouling.

Further works could consider an improvement of the EMF by means of a time-variant approach of the linearization parameters by projection and the change of the integration method. If the system has faster dynamics, the appeared error could increase. A countermeasure would be the separation of the moving horizon window T into smaller intervals and the estimation of the new values in each interval. This idea could also improve the constancy error due to the assumption of the piecewise constant linearization parameters over each modulation interval.

Appendix

A Determinant of the Observability Matrix

Evaluated determinant of observability matrix (A.2) of the RO system with inserted parameters of the table 2.1:

$$
\begin{aligned}
\det(\mathcal{O}) = \Big(& 2.2677 \times 10^{-6}\, {A_\mathrm{m}}^2 \left(-0.258 + 0.05\,\mathrm{pH} + \gamma_\mathrm{f} \right) \left(1.4026 \times 10^{-6}\, \Delta P \right. \\
& - 2.9733 \times 10^{-6}\, \gamma_\mathrm{f} - 1.4866 \times 10^{-7}\, \mathrm{pH} - 2.9733 \times 10^{-7}\, x_2 + 2.9733 \times 10^{-7} \cdot \\
& \sqrt{4.4448 - 2.1083\,\mathrm{pH} + 0.25\,\mathrm{pH}^2 - 42.165\,\gamma_\mathrm{f} + 10.0\,\gamma_\mathrm{f}\,\mathrm{pH} + 100.0\,{\gamma_\mathrm{f}}^2 + 28.792\,\Delta P} \\
& \overline{-4.7173\,\Delta P\,\mathrm{pH} - 94.345\,\Delta P\,\gamma_\mathrm{f} + 22.252\,\Delta P^2 - 4.2165\,x_2 + 1.0\,\mathrm{pH}\,x_2} \\
& \left. \overline{+20.0\,\gamma_\mathrm{f}\,x_2 - 9.4345\,\Delta P\,x_2 + {x_2}^2} + 6.2684 \times 10^{-7} \right)^2 \Big) \cdot \\
& \Big(3.9293 \times 10^{-13} - 1.8638 \times 10^{-13}\,\mathrm{pH} + 2.2101 \times 10^{-14}\,\mathrm{pH}^2 - 3.7275 \times 10^{-12}\,\gamma_\mathrm{f} \\
& + 8.8402 \times 10^{-13}\,\gamma_\mathrm{f}\,\mathrm{pH} + 8.8402 \times 10^{-12}\,{\gamma_\mathrm{f}}^2 + 2.5452 \times 10^{-12}\,\Delta P \\
& - 4.1702 \times 10^{-13}\,\Delta P\,\mathrm{pH} - 8.3403 \times 10^{-12}\,\Delta P\,\gamma_\mathrm{f} + 1.9672 \times 10^{-12}\,\Delta P^2 \\
& - 3.7275 \times 10^{-13}\,x_2 + 8.8402 \times 10^{-14}\,\mathrm{pH}\,x_2 + 1.768 \times 10^{-12}\,\gamma_\mathrm{f}\,x_2 \\
& - 8.3403 \times 10^{-13}\,\Delta P\,x_2 + 8.8402 \times 10^{-14}\,{x_2}^2 \Big)^{-1}
\end{aligned}
\tag{A.1}
$$

General determinant of the observability matrix (3.10) of the RO system:

$$
\begin{aligned}
&\det(\mathcal{O}) = \frac{1}{V_\mathrm{b}\, {V_\mathrm{p}}^2\, b_{\mathrm{f},0}} \\
&\Big(\sigma_1^2\, {\gamma_{\mathrm{f,st}}}^2\, {k_\mathrm{m}}^2 - 2.0\,\sigma_1^2\,\gamma_\mathrm{f}\,\gamma_{\mathrm{f,st}}\,{k_\mathrm{m}}^2 + \sigma_1^2\,{\gamma_\mathrm{f}}^2\,{k_\mathrm{m}}^2 + 2.0\,\sigma_1^2\,b_{\mathrm{f},1}\,\gamma_{\mathrm{f,st}}\,{k_\mathrm{m}}^2\,\mathrm{pH_{st}} \\
&- 2.0\,\sigma_1^2\,b_{\mathrm{f},1}\,\gamma_{\mathrm{f,st}}\,{k_\mathrm{m}}^2\,\mathrm{pH} - 2.0\,\sigma_1^2\,b_{\mathrm{f},1}\,\gamma_\mathrm{f}\,{k_\mathrm{m}}^2\,\mathrm{pH_{st}} + 2.0\,\sigma_1^2\,b_{\mathrm{f},1}\,\gamma_\mathrm{f}\,{k_\mathrm{m}}^2\,\mathrm{pH} + \sigma_1^2\,{b_{\mathrm{f},1}}^2\,{k_\mathrm{m}}^2\,{\mathrm{pH_{st}}}^2 - 2.0\,\sigma_1^2\,{b_{\mathrm{f},1}}^2\,{k_\mathrm{m}}^2\,\mathrm{pH}\,\mathrm{pH_{st}} \\
&+ \sigma_1^2\,{b_{\mathrm{f},1}}^2\,{k_\mathrm{m}}^2\,\mathrm{pH}^2 - 2.0\,C_{\mathrm{f,st}}\,\sigma_1^2\,b_{\mathrm{f},0}\,\gamma_{\mathrm{f,st}}\,{k_\mathrm{m}}^2 - 4.0\,M_\mathrm{m}\,\sigma_1\,b_{\mathrm{f},0}\,\gamma_{\mathrm{f,st}}\,k_\mathrm{m}\,k_\mathrm{s} + 2.0\,C_{\mathrm{f,st}}\,\sigma_1^2\,b_{\mathrm{f},0}\,\gamma_\mathrm{f}\,{k_\mathrm{m}}^2 + 4.0\,M_\mathrm{m}\,\sigma_1\,b_{\mathrm{f},0}\,\gamma_\mathrm{f}\,k_\mathrm{m}\,k_\mathrm{s} + 4.0\,M_\mathrm{m}\,\sigma_1\,b_{\mathrm{f},0}\,\Delta P\,\gamma_{\mathrm{f,st}}\,{k_\mathrm{m}}^2 \\
&- 4.0\,M_\mathrm{m}\,\sigma_1\,b_{\mathrm{f},0}\,\Delta P\,\gamma_\mathrm{f}\,{k_\mathrm{m}}^2 - 2.0\,C_{\mathrm{f,st}}\,\sigma_1^2\,b_{\mathrm{f},0}\,b_{\mathrm{f},1}\,{k_\mathrm{m}}^2\,\mathrm{pH_{st}} + 2.0\,C_{\mathrm{f,st}}\,\sigma_1^2\,b_{\mathrm{f},0}\,b_{\mathrm{f},1}\,{k_\mathrm{m}}^2\,\mathrm{pH} - 4.0\,M_\mathrm{m}\,\sigma_1\,b_{\mathrm{f},0}\,b_{\mathrm{f},1}\,k_\mathrm{m}\,k_\mathrm{s}\,\mathrm{pH_{st}} \\
&+ 4.0\,M_\mathrm{m}\,\sigma_1\,b_{\mathrm{f},0}\,b_{\mathrm{f},1}\,k_\mathrm{m}\,k_\mathrm{s}\,\mathrm{pH} + 4.0\,M_\mathrm{m}\,\sigma_1\,b_{\mathrm{f},0}\,b_{\mathrm{f},1}\,\Delta P\,{k_\mathrm{m}}^2\,\mathrm{pH_{st}} - 4.0\,M_\mathrm{m}\,\sigma_1\,b_{\mathrm{f},0}\,b_{\mathrm{f},1}\,\Delta P\,{k_\mathrm{m}}^2\,\mathrm{pH} + {C_{\mathrm{f,st}}}^2\,\sigma_1^2\,{b_{\mathrm{f},0}}^2\,{k_\mathrm{m}}^2 + 4.0\,C_{\mathrm{f,st}}\,M_\mathrm{m}\,\sigma_1\,{b_{\mathrm{f},0}}^2\,k_\mathrm{m}\,k_\mathrm{s} \\
&+ 4.0\,{M_\mathrm{m}}^2\,{b_{\mathrm{f},0}}^2\,{k_\mathrm{s}}^2 - 4.0\,C_{\mathrm{f,st}}\,M_\mathrm{m}\,\sigma_1\,{b_{\mathrm{f},0}}^2\,\Delta P\,{k_\mathrm{m}}^2 + 8.0\,{M_\mathrm{m}}^2\,{b_{\mathrm{f},0}}^2\,\Delta P\,k_\mathrm{m}\,k_\mathrm{s} + 4.0\,{M_\mathrm{m}}^2\,{b_{\mathrm{f},0}}^2\,\Delta P^2\,{k_\mathrm{m}}^2 - 2.0\,\sigma_1^2\,b_{\mathrm{f},0}\,\gamma_{\mathrm{f,st}}\,{k_\mathrm{m}}^2\,x_2 + 2.0\,\sigma_1^2\,b_{\mathrm{f},0}\,\gamma_\mathrm{f}\,{k_\mathrm{m}}^2\,x_2 \\
&- 2.0\,\sigma_1^2\,b_{\mathrm{f},0}\,b_{\mathrm{f},1}\,{k_\mathrm{m}}^2\,\mathrm{pH_{st}}\,x_2 + 2.0\,\sigma_1^2\,b_{\mathrm{f},0}\,b_{\mathrm{f},1}\,{k_\mathrm{m}}^2\,\mathrm{pH}\,x_2 + 2.0\,C_{\mathrm{f,st}}\,\sigma_1^2\,{b_{\mathrm{f},0}}^2\,{k_\mathrm{m}}^2\,x_2 + 4.0\,M_\mathrm{m}\,\sigma_1\,{b_{\mathrm{f},0}}^2\,k_\mathrm{m}\,k_\mathrm{s}\,x_2 \\
&- 4.0\,M_\mathrm{m}\,\sigma_1\,{b_{\mathrm{f},0}}^2\,\Delta P\,{k_\mathrm{m}}^2\,x_2 + \sigma_1^2\,{b_{\mathrm{f},0}}^2\,{k_\mathrm{m}}^2\,{x_2}^2\Big)^{-1} \\
&0.5968\,{A_\mathrm{m}}^2\,V_d\,{k_\mathrm{s}}^2\;(-1.0\,\gamma_{\mathrm{f,st}} + \gamma_\mathrm{f} - 1.0\,b_{\mathrm{f},1}\,\mathrm{pH_{st}} + b_{\mathrm{f},1}\,\mathrm{pH} + C_{\mathrm{f,st}}\,b_{\mathrm{f},0}) \\
&\Big(2.0\,M_\mathrm{m}\,b_{\mathrm{f},0}\,k_\mathrm{s} + \sigma_1\,\gamma_\mathrm{f}\,k_\mathrm{m} - 1.0\,\sigma_1\,\gamma_{\mathrm{f,st}}\,k_\mathrm{m} - 2.0\,M_\mathrm{m}\,b_{\mathrm{f},0}\,\Delta P\,k_\mathrm{m} - 1.0\,\sigma_1\,b_{\mathrm{f},0}\,k_\mathrm{m} \\
&\sqrt{2.0\,C_{\mathrm{f,st}}\,x_2 + {C_{\mathrm{f,st}}}^2 + {x_2}^2 + \frac{{\gamma_\mathrm{f}}^2}{{b_{\mathrm{f},0}}^2} + \frac{{\gamma_{\mathrm{f,st}}}^2}{{b_{\mathrm{f},0}}^2} + \frac{2.0\,\gamma_\mathrm{f}\,x_2}{b_{\mathrm{f},0}} - \frac{2.0\,\gamma_{\mathrm{f,st}}\,x_2}{b_{\mathrm{f},0}} + \frac{{b_{\mathrm{f},1}}^2\,\mathrm{pH}^2}{{b_{\mathrm{f},0}}^2} + \frac{{b_{\mathrm{f},1}}^2\,{\mathrm{pH_{st}}}^2}{{b_{\mathrm{f},0}}^2} + \frac{2.0\,C_{\mathrm{f,st}}\,\gamma_\mathrm{f}}{b_{\mathrm{f},0}} - \frac{2.0\,C_{\mathrm{f,st}}\,\gamma_{\mathrm{f,st}}}{b_{\mathrm{f},0}} - \frac{2.0\,\gamma_\mathrm{f}\,\gamma_{\mathrm{f,st}}}{{b_{\mathrm{f},0}}^2} + \frac{4.0\,{M_\mathrm{m}}^2\,\Delta P^2}{\sigma_1^2}} \\
&+ \frac{2.0\,C_{\mathrm{f,st}}\,b_{\mathrm{f},1}\,\mathrm{pH}}{b_{\mathrm{f},0}} - \frac{2.0\,C_{\mathrm{f,st}}\,b_{\mathrm{f},1}\,\mathrm{pH_{st}}}{b_{\mathrm{f},0}} + \frac{2.0\,b_{\mathrm{f},1}\,\gamma_\mathrm{f}\,\mathrm{pH}}{{b_{\mathrm{f},0}}^2} - \frac{2.0\,b_{\mathrm{f},1}\,\gamma_{\mathrm{f,st}}\,\mathrm{pH}}{{b_{\mathrm{f},0}}^2} - \frac{2.0\,b_{\mathrm{f},1}\,\gamma_\mathrm{f}\,\mathrm{pH_{st}}}{{b_{\mathrm{f},0}}^2} + \frac{2.0\,b_{\mathrm{f},1}\,\gamma_{\mathrm{f,st}}\,\mathrm{pH_{st}}}{{b_{\mathrm{f},0}}^2} + \frac{2.0\,b_{\mathrm{f},1}\,\mathrm{pH}\,x_2}{b_{\mathrm{f},0}} - \frac{2.0\,b_{\mathrm{f},1}\,\mathrm{pH_{st}}\,x_2}{b_{\mathrm{f},0}} - \frac{2.0\,{b_{\mathrm{f},1}}^2\,\mathrm{pH}\,\mathrm{pH_{st}}}{{b_{\mathrm{f},0}}^2} \\
&+ \frac{4.0\,{M_\mathrm{m}}^2\,{k_\mathrm{s}}^2}{\sigma_1^2\,{k_\mathrm{m}}^2} - \frac{4.0\,C_{\mathrm{f,st}}\,M_\mathrm{m}\,\Delta P}{\sigma_1} - \frac{4.0\,M_\mathrm{m}\,\Delta P\,x_2}{\sigma_1} + \frac{8.0\,{M_\mathrm{m}}^2\,\Delta P\,k_\mathrm{s}}{\sigma_1^2\,k_\mathrm{m}} + \frac{4.0\,C_{\mathrm{f,st}}\,M_\mathrm{m}\,k_\mathrm{s}}{\sigma_1\,k_\mathrm{m}} - \frac{4.0\,M_\mathrm{m}\,\Delta P\,\gamma_\mathrm{f}}{\sigma_1\,b_{\mathrm{f},0}} + \frac{4.0\,M_\mathrm{m}\,\Delta P\,\gamma_{\mathrm{f,st}}}{\sigma_1\,b_{\mathrm{f},0}} + \frac{4.0\,M_\mathrm{m}\,k_\mathrm{s}\,x_2}{\sigma_1\,k_\mathrm{m}} \\
&- \frac{4.0\,M_\mathrm{m}\,b_{\mathrm{f},1}\,\Delta P\,\mathrm{pH}}{\sigma_1\,b_{\mathrm{f},0}} + \frac{4.0\,M_\mathrm{m}\,b_{\mathrm{f},1}\,\Delta P\,\mathrm{pH_{st}}}{\sigma_1\,b_{\mathrm{f},0}} + \frac{4.0\,M_\mathrm{m}\,\gamma_\mathrm{f}\,k_\mathrm{s}}{\sigma_1\,b_{\mathrm{f},0}\,k_\mathrm{m}} - \frac{4.0\,M_\mathrm{m}\,\gamma_{\mathrm{f,st}}\,k_\mathrm{s}}{\sigma_1\,b_{\mathrm{f},0}\,k_\mathrm{m}} + \frac{4.0\,M_\mathrm{m}\,b_{\mathrm{f},1}\,k_\mathrm{s}\,\mathrm{pH}}{\sigma_1\,b_{\mathrm{f},0}\,k_\mathrm{m}} - \frac{4.0\,M_\mathrm{m}\,b_{\mathrm{f},1}\,k_\mathrm{s}\,\mathrm{pH_{st}}}{\sigma_1\,b_{\mathrm{f},0}\,k_\mathrm{m}} \\
&+ C_{\mathrm{f,st}}\,\sigma_1\,b_{\mathrm{f},0}\,k_\mathrm{m} + \sigma_1\,b_{\mathrm{f},1}\,k_\mathrm{m}\,\mathrm{pH} - 1.0\,\sigma_1\,b_{\mathrm{f},1}\,k_\mathrm{m}\,\mathrm{pH_{st}} + \sigma_1\,b_{\mathrm{f},0}\,k_\mathrm{m}\,x_2\Big)^2
\end{aligned}
\tag{A.2}
$$

$$
\sigma_1 = \mathcal{R}\,T \tag{A.3}
$$

B State-space Representation

B.1 Nonlinear State-space Representation

Nonlinear I/O relation of RO system (2.24-2.27):

$$
\begin{aligned}
\dddot{y} = \frac{1}{\sigma^{3/2}}\Bigg(& - 840\, y \left(\sigma\right)^{3/2} - 10.4\, \dot{y} \left(\sigma\right)^{3/2} - 6.8\, \ddot{y} \left(\sigma\right)^{3/2} - 7.6 \times 10^{-7} \left(\sigma\right)^{3/2} \\
& - A_{\mathrm{m}} \Big(6 \times 10^{65}\, y^2 \sqrt{\sigma} - 7.6 \times 10^{111}\, y^2\, \dot{y}^2 - 21.2 \times 10^{68}\, y^3 \sqrt{\sigma} + 4.4 \times 10^{63}\, \dot{y}^2 \sqrt{\sigma} + 4.4 \times 10^{71}\, \dot{y}^3 \sqrt{\sigma} + 34.8 \times 10^{106}\, y\, \dot{y} + 34.4 \times 10^{112}\, u\, y^3 \\
& + 20.8 \times 10^{109}\, u\, \dot{y}^3 - 31.6 \times 10^{-3}\, u \left(\sigma\right)^{3/2} - 27.2 \times 10^{114}\, y\, \dot{y}^2 - 5.2 \times 10^{116}\, y^2\, \dot{y} - 6 \times 10^{110}\, y\, \dot{y}^3 + 18.4 \times 10^{114}\, y^2\, \ddot{y} \\
& - 34.4 \times 10^{111}\, y^3\, \dot{y} - 22 \times 10^{110}\, y^3\, \ddot{y} + 13.2 \times 10^{112}\, \dot{y}^2\, \ddot{y} - 13.2 \times 10^{107}\, \dot{y}^3\, \ddot{y} + 22.4 \times 10^{-4}\, y \left(\sigma\right)^{3/2} + 14 \times 10^{-4}\, \dot{y} \left(\sigma\right)^{3/2} \\
& + 10 \times 10^{-5}\, \ddot{y} \left(\sigma\right)^{3/2} + 20.8 \times 10^{107}\, y^2 - 29.6 \times 10^{116}\, y^3 + 14.8 \times 10^{105}\, \dot{y}^2 - 24.4 \times 10^{111}\, y^4 - 25.2 \times 10^{112}\, \dot{y}^3 - 17.2 \times 10^{108}\, \ddot{y}^4 - 68 \left(\sigma\right)^{3/2} \\
& + 7.2 \times 10^{111}\, u\, y\, \dot{y}^2 + 8.8 \times 10^{112}\, u\, y^2\, \dot{y} - 4.8 \times 10^{109}\, y\, \dot{y}^2\, \ddot{y} - 5.6 \times 10^{110}\, y^2\, \dot{y}\, \ddot{y} + 10.4 \times 10^{64}\, y\, \dot{y} \sqrt{\sigma} + 10 \times 10^{72}\, y\, \dot{y}^2 \sqrt{\sigma} \\
& + 10 \times 10^{73}\, y^2\, \dot{y} \sqrt{\sigma} + 4.8 \times 10^{72}\, y^2\, \ddot{y} \sqrt{\sigma} + 35.6 \times 10^{69}\, \dot{y}^2\, \ddot{y} \sqrt{\sigma} + 30.8 \times 10^{113}\, y\, \dot{y}\, \ddot{y} + 8.4 \times 10^{71}\, y\, \dot{y}\, \ddot{y} \sqrt{\sigma} \Big) \\
& - A_{\mathrm{m}}^2 \Big(15.2 \times 10^{102}\, \ddot{y} - 14.4 \times 10^{105}\, \dot{y} - 17.2 \times 10^{106}\, y + 24.8 \times 10^{104}\, y^2\, \dot{y}^2 + 35.6 \times 10^{67}\, y^2 \sqrt{\sigma} + 11.6 \times 10^{69}\, y^3 \sqrt{\sigma} - 8 \times 10^{71}\, \dot{y}^2 \sqrt{\sigma} \\
& + 7.2 \times 10^{66}\, \dot{y}^3 \sqrt{\sigma} + 4.4 \times 10^{115}\, y\, \dot{y} - 15.2 \times 10^{113}\, y\, \ddot{y} - 12.8 \times 10^{112}\, \dot{y}\, \ddot{y} - 8.4 \times 10^{112}\, u\, y^2 - 6 \times 10^{110}\, u\, \dot{y}^2 + 12 \times 10^{110}\, y\, \dot{y}^2 \\
& + 8 \times 10^{111}\, y^2\, \dot{y} + 14 \times 10^{103}\, y\, \dot{y}^3 + 5.6 \times 10^{110}\, y^2\, \ddot{y} + 19.6 \times 10^{105}\, y^3\, \dot{y} + 38.8 \times 10^{107}\, \dot{y}^2\, \ddot{y} - 10 \times 10^{64}\, y \sqrt{\sigma} - 8.4 \times 10^{63}\, \dot{y} \sqrt{\sigma} \\
& - 24.4 \times 10^{-8}\, y \left(\sigma\right)^{3/2} - 20.8 \times 10^{-9}\, \dot{y} \left(\sigma\right)^{3/2} + 36.8 \times 10^{115}\, y^2 + 6 \times 10^{111}\, y^3 + 11.2 \times 10^{113}\, \dot{y}^2 + 5.6 \times 10^{106}\, y^4 + 4.8 \times 10^{109}\, \dot{y}^3 \\
& + 6.4 \times 10^{109}\, \ddot{y}^2 + 29.6 \times 10^{101}\, \dot{y}^4 - 12.4 \times 10^{-6} \left(\sigma\right)^{3/2} - 9.6 \times 10^{72}\, y\, \dot{y} \sqrt{\sigma} - 8 \times 10^{71}\, y\, \ddot{y} \sqrt{\sigma} - 6.8 \times 10^{70}\, \dot{y}\, \ddot{y} \sqrt{\sigma} + 25.2 \times 10^{67}\, y\, \dot{y}^2 \sqrt{\sigma} \\
& + 29.6 \times 10^{68}\, y^2\, \dot{y} \sqrt{\sigma} - 14.4 \times 10^{111}\, u\, y\, \dot{y} + 9.2 \times 10^{109}\, y\, \dot{y}\, \ddot{y} + 9.2 \times 10^{95} \Big) \\
& + A_{\mathrm{m}}^3 \Big(20.4 \times 10^{114}\, y + 12.4 \times 10^{113}\, \dot{y} - 4 \times 10^{112}\, \ddot{y} + 29.2 \times 10^{69}\, y^2 \sqrt{\sigma} + 20.8 \times 10^{66}\, \dot{y}^2 \sqrt{\sigma} - 7.2 \times 10^{111}\, u\, y - 6 \times 10^{110}\, u\, \dot{y} \\
& + 6 \times 10^{110}\, y\, \dot{y} + 4.4 \times 10^{109}\, y\, \ddot{y} + 38 \times 10^{107}\, \dot{y}\, \ddot{y} + 21.2 \times 10^{103}\, y\, \dot{y}^2 + 25.2 \times 10^{104}\, y^2\, \dot{y} \\
& + 15.6 \times 10^{66}\, y \sqrt{\sigma} - 4 \times 10^{71}\, \dot{y} \sqrt{\sigma} - 35.2 \times 10^{96}\, \ddot{y} \sqrt{\sigma} \\
& + 5.2 \times 10^{110}\, y^2 + 10 \times 10^{105}\, y^3 + 4.8 \times 10^{109}\, \dot{y}^2 + 6 \times 10^{102}\, \dot{y}^3 - 4.4 \times 10^{63} \sqrt{\sigma} - 19.6 \times 10^{-9} \left(\sigma\right)^{3/2} + 4.8 \times 10^{68}\, y\, \dot{y} \sqrt{\sigma} - 4.8 \times 10^{105} \Big) \\
& - A_{\mathrm{m}}^4 \Big(12.8 \times 10^{108}\, y - 19.6 \times 10^{109}\, u + 15.6 \times 10^{108}\, \dot{y} + 12.4 \times 10^{107}\, \ddot{y} + 20 \times 10^{103}\, y\, \dot{y} + 24.4 \times 10^{67}\, y \sqrt{\sigma} + 20.8 \times 10^{66}\, \dot{y} \sqrt{\sigma} \\
& + 12 \times 10^{104}\, y^2 + 8.4 \times 10^{102}\, \dot{y}^2 + 31.6 \times 10^{63} \sqrt{\sigma} + 4.4 \times 10^{113} \Big) \\
& + A_{\mathrm{m}}^5 \Big(12 \times 10^{103}\, y + 10.4 \times 10^{102}\, \dot{y} + 6.8 \times 10^{66} \sqrt{\sigma} - 7.6 \times 10^{106} \Big) \\
& - 4.8 \times 10^{102}\, A_{\mathrm{m}}^6 \\
& + 18 \times 10^{106}\, y\, \dot{y}^2 + 21.2 \times 10^{107}\, y^2\, \dot{y} - 30.4 \times 10^{113}\, y\, \dot{y}^3 - 21.6 \times 10^{116}\, y^3\, \dot{y} + 7.2 \times 10^{115}\, y^3\, \ddot{y} + 4.4 \times 10^{112}\, \dot{y}^3\, \ddot{y} + 8.4 \times 10^{108}\, y^3 \\
& - 8.8 \times 10^{117}\, y^4 + 5.2 \times 10^{105}\, \dot{y}^3 + 6.8 \times 10^{112}\, \dot{y}^4 + 16 \times 10^{113}\, y\, \dot{y}^2\, \ddot{y} + 18.8 \times 10^{114}\, y^2\, \dot{y}\, \ddot{y} - 16.4 \times 10^{115}\, y^2\, \dot{y}^2 \Bigg)
\end{aligned} \tag{B.1}
$$

$$
\sigma = 3.4 \times 10^{74}\, A_{\mathrm{m}}^2 - 6.8 \times 10^{74}\, A_{\mathrm{m}}\, \dot{y} + 14 \times 10^{74}\, \dot{y}^2 - 8.1 \times 10^{75}\, A_{\mathrm{m}}\, y + 8.3 \times 10^{75}\, y\, \dot{y} + 4.9 \times 10^{76}\, y^2 \tag{B.2}
$$

B.2 Linearized State-space Representation

Linearized I/O relation of RO system (2.31-2.34):

$$\begin{aligned}\dddot{y} =& 0.0099426\,A_\mathrm{m} - 5.5428\times10^{-22}\,{A_\mathrm{m}}^2 + 2.1407\times10^{-41}\,{A_\mathrm{m}}^3 + 0.062699\,A_\mathrm{m}\,u \\ & - 13.504\,\ddot{y} - 0.00040057\,A_\mathrm{m}\,\ddot{y} - 20.554\,\dot{y} - 0.0051405\,A_\mathrm{m}\,\dot{y} \\ & + 3.232\times10^{-41}\,{A_\mathrm{m}}^2\,\dot{y} - 8.0139\,y - 0.0047833\,A_\mathrm{m}\,y + 3.8212\times10^{-40}\,{A_\mathrm{m}}^2\,y \end{aligned} \quad \text{(B.3)}$$

B.3 Comparison of the Nonlinear and Linearized State-space Representation

For the following plots, the measured signals of the table 6.1 are taken:

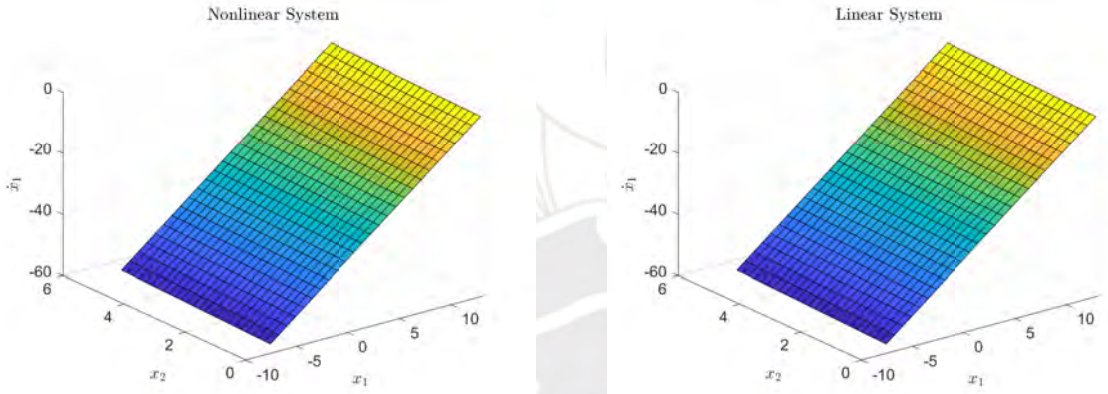

(a) (b)

Figure B.1: Evaluated $\dot{x}_1$

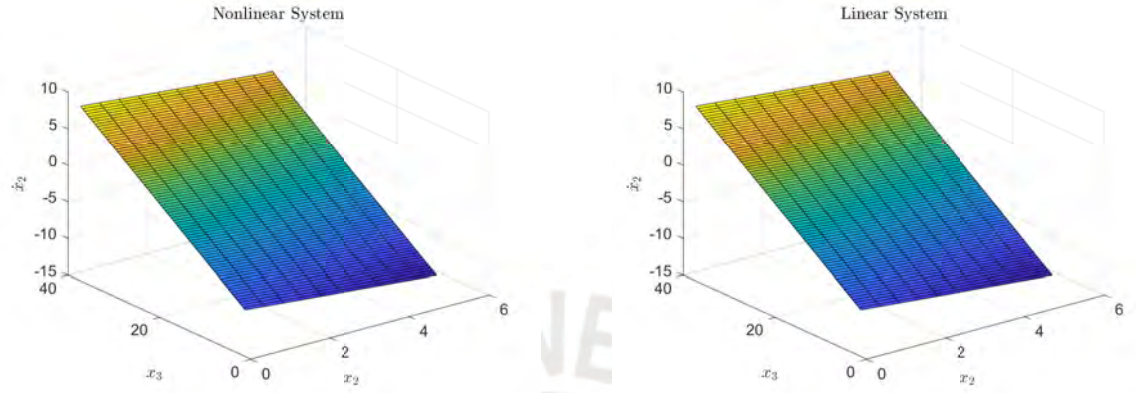

(a) (b)

Figure B.2: Evaluated $\dot{x}_2$

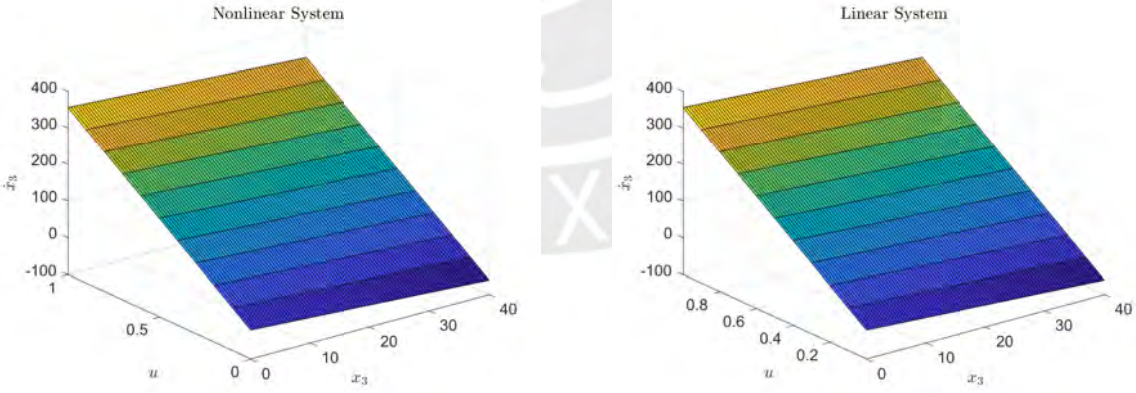

(a) (b)

Figure B.3: Evaluated $\dot{x}_3$

C Simulation Plots

C.1 Step Decrease

Parameter step at $t = 10\,\mathrm{s}$ from A_{m}^{*} to $A_m = 15\,\mathrm{m}^2$:

Operating Point Input

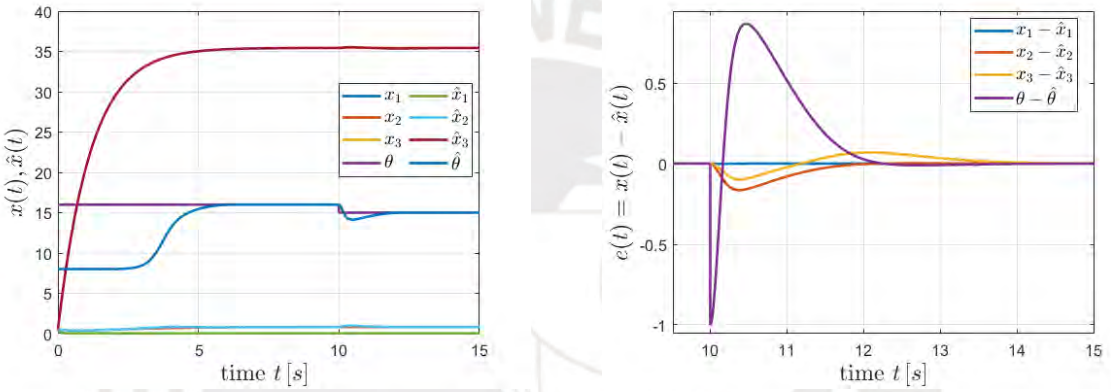

(a) State estimation (b) Zoom in the state estimation error

Figure C.1: State and parameter estimation by the coupled EKF with u_1, $\lambda_{\mathrm{EKF}} = 3.5$ and step decrease at $t = 10\,\mathrm{s}$

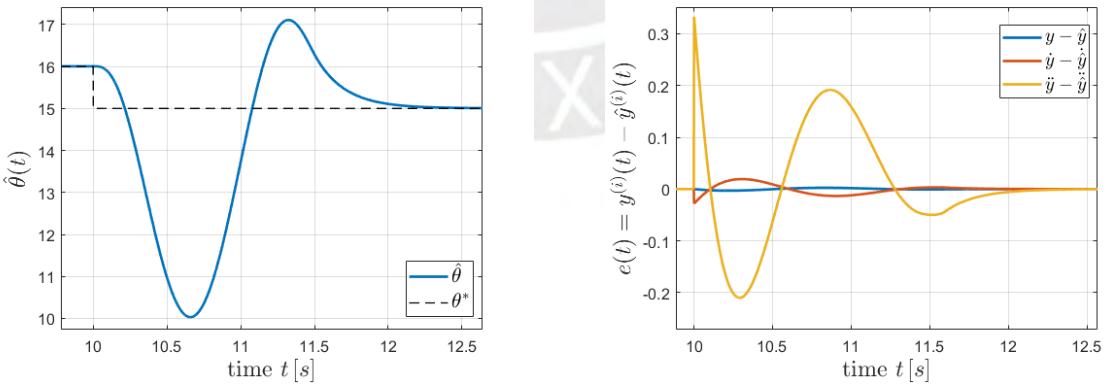

(a) Parameter estimation (b) Output error estimation

Figure C.2: Estimation results by the IEMF with u_1 and step decrease at $t = 10\,\mathrm{s}$

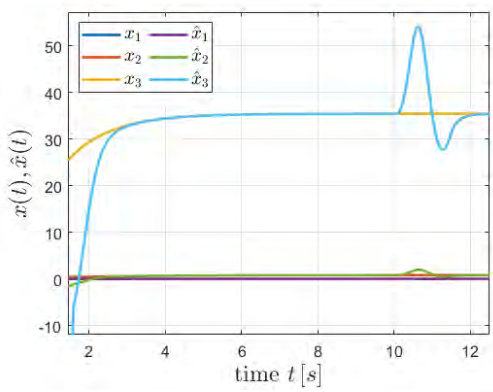

(a) Comparison of the real and estimated states by the IEMF

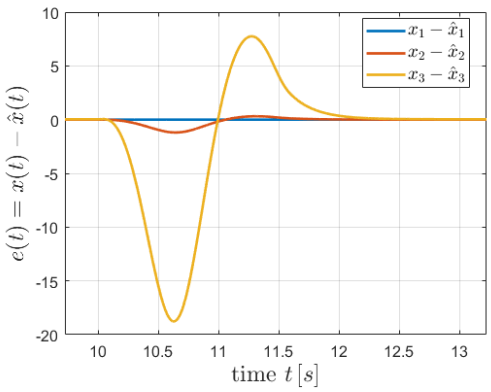

(b) Zoom in the state estimation error at the parameter step

Figure C.3: State estimation by the IEMF with u_1 and step decrease at $t = 10\,\mathrm{s}$

Excitation Mode Input

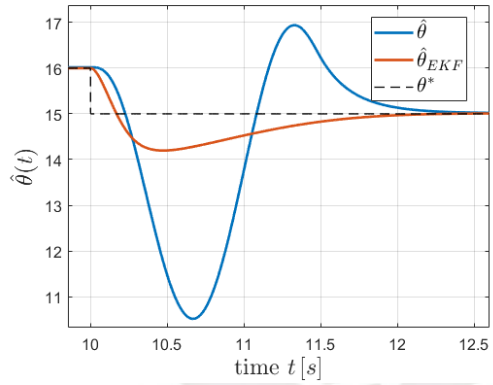

(a) Zoom of the parameter estimation

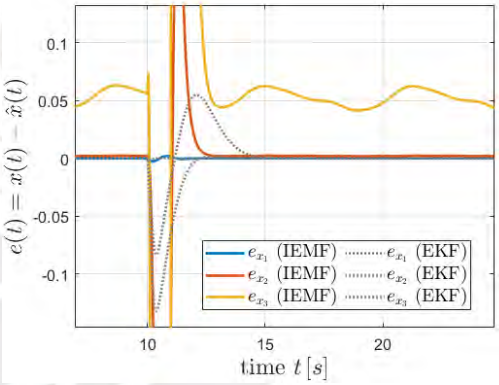

(b) Zoom of the state estimation error

Figure C.4: Comparison of the IEMF and the coupled EKF with u_2 and step decrease at $t = 10\,\mathrm{s}$

C.2 Noise Impact

Constant Parameter

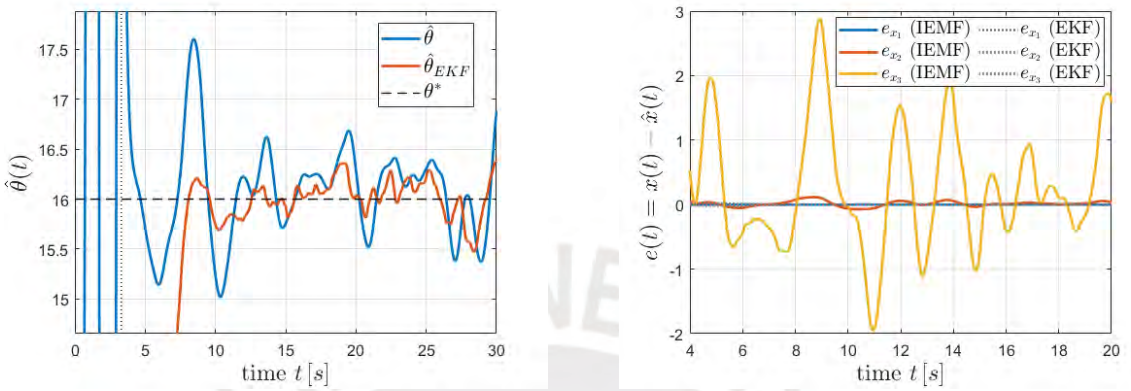

(a) Parameter estimation (b) State estimation error

Figure C.5: Comparison of the IEMF and the coupled EKF with u_2, $T_{\text{TMF}} = 3.3\,\text{s}$, $\lambda_{\text{EKF}} = 2$, constant parameter and noise impact

Gradual Decrease in Parameter

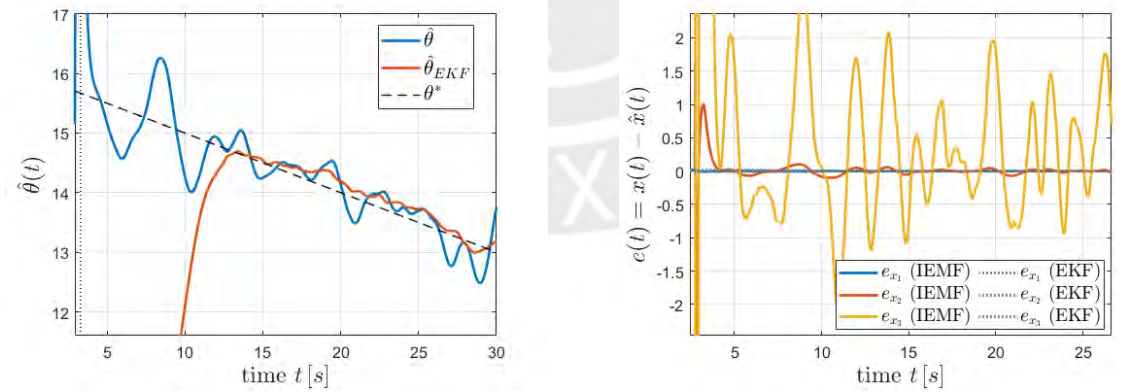

(a) Parameter estimation (b) State estimation error

Figure C.6: Comparison of the IEMF and the coupled EKF with u_1, $T_{\text{TMF}} = 3.3\,\text{s}$, gradually decreasing parameter and noise impact

Bibliography

[Bad+19] Mohammad Badruzzaman, Nikolay Voutchkov, Lauren Weinrich, and Joseph G. Jacangelo. "Selection of pretreatment technologies for seawater reverse osmosis plants: A review". In: *Desalination*. 449. Elsevier, 2019, pp. 78–91.

[Bak04] Richard W. Baker. *Membrane Technology and Applications*. 2. ed. Chichester: Wiley, 2004.

[Bes07a] Gildas Besançon. "Nonlinear Observers and Applications. Grenoble International Summer School on Control". In: ed. by Gildas Besançon. Lecture notes in control and information sciences 363. Chapter 1. Springer, 2007. Chap. An Overview on Observer Tools for Nonlinear Systems, pp. 1–33.

[Bes07b] Gildas Besançon. "Nonlinear Observers and Applications. Grenoble International Summer School on Control". In: ed. by Gildas Besançon. Lecture notes in control and information sciences 363. Chapter 7. Springer, 2007. Chap. Parameter/Fault Estimation in Nonlinear Systems and Adaptive Observers, pp. 218–229.

[BK20] Mohamed A. Bahloul and Taous-Meriem Laleg Kirati. "Finite-time joint estimation of the arterial blood flow and the arterial Windkessel parameters using modulating functions". In: *IFAC*. Vol. 53. 2. Elsevier, 2020, pp. 16286–16292.

[Bun17] Bundeszentrale für politische Bildung. *Wasser*. Accessed: 05.07.2021 -15:37. Sept. 2017. URL: `https://www.bpb.de/nachschlagen/zahlen-und-fakten/globalisierung/52730/wasserverbrauch`.

[CCE06] Tzahi Y. Cath, Amy E. Childress, and Menachem Elimelech. "Forward osmosis: Principles, applications, and recent developments". In: *Journal of Membrane Science 281*. 2006, pp. 70–87.

[CTR14] Oscar B. Cieza, Julio C. Tafur, and Johann Reger. "Frequency Domain Modulating Functions for Continuous-Time Identication of Linear and Nonlinear Systems". In: *16th Latinamerican Control Conference*. Oct. 2014, pp. 690–695.

[DU96] Sequare Daniel-Berhe and Heinz Unbehauen. “Parameter Estimation of Nonlinear Continuous-time Systems Using Hartley Modulating Functions”. In: *UKACC International Conference on Control*. 427. IEE, 1996, pp. 228–233.

[EE02] Hisham T. El-Dessouky and Hisham Mohamed Ettouney. *Fundamentals of Salt Water Desalination*. 1st ed. Includes bibliographical references and index. Elsevier, 2002.

[Foo17] Food and Agriculture Organization of the United Nations (FAO). *Water for Sustainable Food and Agriculture*. Rome, 2017.

[FRL17] V. Feliu-Batlle, R. Rivas-Perez, and A. Linares-Saez. “Fractional Order Robust Control of a Reverse Osmosis Seawater Desalination Plant”. In: *20th IFAC World Congress*. Vol. 50. 1. Elsevier, 2017, pp. 14545–14555.

[GB81] J. P. Gauthier and G. Bornard. “Observability for any u(t) of a class of nonlinear systems”. In: *Automatic Control*. Vol. 26. 4. IEEE, 1981, pp. 922–926.

[Gel+01] Arthur Gelb, Jr. Joseph F. Kasper, Jr. Raymond A. Nash, Charles F. Price, and Jr. Arthur A. Sutherland. *Applied Optimal Eestimation*. Ed. by Arthur Gelb. 16th ed. MIT Press, 2001.

[Gha+20] Lilia Ghaour, Matti Noack, Johann Reger, and Taous-Meriem Laleg-Kirati. “Non-asymptotic State Estimation of Linear Reaction Diffusion Equation using Modulating Functions”. In: *IFAC World Congress*. July 2020, pp. 4262–4267.

[GK01] Jean-Paul Gauthier and Ivan Kupka. *Deterministic Observation Theory and Applications*. Cambridge University Press, 2001.

[GKB07] A. Gambier, A. Krasnik, and E. Badreddin. “Dynamic Modeling of a Simple Reverse Osmosis Desalination Plant for Advanced Control Purposes”. In: *American Control Conference*. IEEE, July 2007, pp. 4854–4859.

[Göp21] Johannes Göpfert. “Model-Based Fault Diagnosis via Structural Analysis of a Reverse Osmosis Plant”. MA thesis. PUCP and TU Ilmenau, Feb. 2021.

[HK77] Robert Hermann and Arthur J. Krener. “Nonlinear controllability and observability”. In: *Automatic Control*. Vol. 22. 5. IEEE, 1977, pp. 728–740.

[IM11] Rolf Isermann and Marco Münchhof. *Identification of Dynamic Systems*. Springer, 2011.

[Ise06] Rolf Isermann. *Fault-Diagnosis Systems. An introduction from fault detection to fault tolerance*. Springer, 2006.

[JR15] Jerome Jouffroy and Johann Reger. "Finite-time simultaneous parameter and state estimation using modulating functions". In: *IEEE International Conference on Control Applications (CCA)*. Sept. 2015, pp. 394–399.

[JU04] Simon J. Julier and Jeffrey K. Uhlmann. "Unscented Filtering and Nonlinear Estimation". In: *Proceedings of the IEEE*. Vol. 92. 3. Mar. 2004.

[Kal60] Rudolph E. Kalman. "A New Approach to Linear Filtering and Prediction Problems". In: *Journal of Basic Engineering*. Vol. 82. D. ASME, 1960, pp. 35–45.

[KB61] Rudolph E. Kalman and R. S. Bucy. "New Results in Linear Filtering and Prediction Theory". In: *Journal of Basic Engineering*. ASME, Mar. 1961, pp. 95–108.

[Kha02] Hassan K. Khalil. *Nonlinear systems*. 3. ed. Upper Saddle River, NJ: Prentice Hall, 2002.

[Kim17] Albert S. Kim. "Review of Basics Reverse Osmosis Process Modeling: A New Combined Fouling Index Proposed". In: *Membrane Journal*. Vol. 27. 4. Aug. 2017, pp. 291–312.

[KR85] Arthur J. Krener and W. Respondek. "Nonlinear Observers with linear error dynamics". In: *SIAM J. Control and Optimization*. Vol. 23. 1985, pp. 197–216.

[Kre03] Arthur J. Krener. "Directions in mathematical systems theory and optimization". In: ed. by Anders Rantzer and Christopher I. Byrnes. Springer, 2003. Chap. The Convergence of the Extended Kalman Filter, pp. 174–182.

[Kuc15] Jane Kucera. *Reverse Osmosis - Design, Processes, and Applications for Engineers*. 2nd edition. Scrivener Publishing, 2015.

[Liu+14] D.Y. Liu, T.M. Laleg-Kirati, W. Perruquetti, and O. Gibaru. "Non-asymptotic state estimation for a class of linear time-varying systems with unknown inputs". In: *19th World Congress*. Vol. 47. 3. IFAC. Aug. 2014, pp. 3732–3738.

[Lju99] Lennart Ljung. *System Identification. Theory for the User*. Ed. by Thomas Kailath. 2. ed. Prentice Hall PTR, 1999.

[LL15] D.Y. Liu and T.M. Laleg-Kirati. "Robust fractional order differentiators using generalized modulating functions method". In: *Signal Processing*. Vol. 107. 2015, pp. 395–406.

[Lyc20] Prof. Tom Lyche. *Numerical Linear Algebra and Matrix Factorizations*. Springer International Publishing, 2020.

[Meh10] Angela C. Mehner. "Multimedia and Ultrafiltration for Reverse Osmosis Pretreatment Aboard Naval Vessels". In: *Inquiry: The University of Arkansas Undergraduate Research Journal*. Vol. 11. 14. 2010, pp. 79–87.

[MF72] A. V. Mathew and F. W. Fairman. "Indentification in the presence of initial conditions". In: *IEEE Transactions on Automatic Control*. Vol. 17. 6. 1972, pp. 394–396.

[Mor14] Jaime A. Moreno. *Nonlinear Observers*. XVI Congreso Latinoamericano de Control Automático - Workshop. Accessed: 23.07.2021 - 9:32. Oct. 2014. URL: `http://amca.mx/AMCA2/Texto/NonlinearObservers_CLCA_2014.pdf`.

[Noa+16a] Matti Noack, Juan G. Rueda-Escobedo, Johann Reger, and Jaime A. Moreno. "Fixed-Time Parameter Estimation in Polynomial Systems through Modulating Functions". In: *55th IEEE Conference on Decision and Control*. Dec. 2016, pp. 2067–2072.

[Noa+16b] Matti Noack, Kai Wulff, Johann Reger, and Marc-Hinrik Höper. "Observability Analysis and Nonlinear Observer Design for a Turbocharger in a Diesel Engine". In: *International Conference on Control Applications (CCA)*. IEEE, 2016, pp. 323–328.

[NW19] Bekele Debele Negewo and Christopher S. Ward. *The Role of Desalination in an Increasingly Water-Scarce World*. Tech. rep. The World Bank, Mar. 2019.

[Pér+20] Carlos Gustavo Pérez-Zuñiga, Raul Rivas-Perez, Javier Sotomayor-Moriano, and Victor Sánchez-Zurita. "Fault Detection and Isolation System Based on Structural Analysis of an Industrial Seawater Reverse Osmosis Desalination Plant". In: *Processes*. Vol. 8. 9: 1100. MDPI, Sept. 2020.

[Pér17] Carlos Gustavo Pérez-Zuñiga. "Structural analysis for the diagnosis of distributed systems". PhD thesis. INSA de Toulouse, 2017.

[PR93] H. A. Preisig and D.W.T. Rippin. "Theory and Application of the Modulating Function Method - I. Review and Theory of the Method and Theory of the Spline-Type Modulating Functions". In: *Computers and Chemical Engineering*. Vol. 17. 1. 1993, pp. 1–16.

[Riv+19] Raul Rivas-Perez, Javier Sotomayor-Moriano, Gustavo Pérez-Zuñiga, and Mario E. Soto-Angles. "Real-Time Implementation of an Expert Model Predictive Controller in a Pilot-Scale Reverse Osmosis Plant for Brackishand Seawater Desalination". In: *Applied Sciences*. Vol. 9. 14: 2932. MDPI, July 2019.

[RM15] Juan G. Rueda-Escobedo and Jaime A. Moreno. "Non-linear Gradient Algorithm for Parameter Estimation". In: *54th Annual Conference on Decision and Control (CDC)*. IEEE, Dec. 2015, pp. 4086–4091.

[RU06] G.P. Rao and H. Unbehauen. "Identification of continuous-time systems". In: *Control Theory and Applications*. Vol. 153. 2. IEE, Apr. 2006, pp. 185–220.

[Sab+01] S.S. Sablani, M.F.A. Goosen, R. Al-Belushi, and M. Wilf. "Concentration polarization in ultrafiltration and reverse osmosis: a critical review". In: *Desalination*. Vol. 141. 3. 2001, pp. 269–289.

[SB80] J. Stoer and R. Bulirsch. *Introduction to Numerical Analysis*. Springer, 1980.

[Shi54] Marvin Shinbrot. "On the analysis of linear and nonlinear dynamical systems from transient-response data". In: *National Advisory Commitee for Aeronautics NACA*. Technical Note 3288. 1954.

[SR14] Mahmoud Shatat and Saffa B. Riffat. "Water Desalination Technologies Utilizing Conventional and Renewable Energy Sources". In: *International Journal of Low-Carbon Technologies 9*. 1. 2014, pp. 1–19.

[Sta16] Christopher M. Stafford. "Scalable Manufacturing of Layer-by-Layer Membranes for Water Purification". In: *The Bridge*. Ed. by Ronald M. Latanision. Vol. 46. 4. National Academy of Sciences, 2016, pp. 32–35.

[Tia+19] Yang Tian, Yan-Qiao Wei, Da-Yan Liu, and Driss Boutat. "Fast and robust estimation for positions and velocities from noisy accelerations using generalized modulating functions method". In: *Mechanical Systems and Signal Processing*. Vol. 133. 106270. July 2019.

[TOR19] 'TORAY'. *TM700D*. Datasheet. Toray Membrane USA, Inc. 13435 Danielson St, Poway, CA 92064, USA, June 2019.

[Wan+11] Lawrence K. Wang, Jiaping Paul Chen, Yung-Tse Hung, and Nazih K. Shammas. *Membrane and Desalination Technologies*. Handbook of environmental engineering 13. Humana Press, 2011.

[Web17] Markus Weber. "Zustandsschätzung mittels Modulationsfunktionen auf Grundlage von Frequenzbereichsbetrachtungen". Bachelor thesis. TU Ilmenau, July 2017.

[WLB17] X. Wei, D.Y. Liu, and D. Boutat. "Non-asymptotic state estimation for a class of fractional order linear systems". In: *IEEE Transactions on Automatic Control*. Vol. 62. 3. 2017, pp. 1150–1164.

List of Figures

1.1 Structure of the thesis 3

2.1 Schematic representation of the RO [Göp21] 4
2.2 Process of reverse osmosis [EE02] 8
2.3 Hydraulic network with the electronic-hydraulic analogy [Göp21] 10
2.4 Schematic composition of a spiral wound membrane module [Kuc15] . . 14
2.5 Sensor configuration of the RO plant [Riv+19] 15
2.6 Comparison of the responses of the nonlinear (2.24-2.27) and the linearized system (2.31-2.34) 19

3.1 Determinant of the observability matrix evaluated with ΔP, x_2 and A_m 27

4.1 Structure of the EKF 33

5.1 Structure of the parameter estimator with $i \in \{0, 1, \cdots, n-1\}$ 41
5.2 Structure of the EMF with $i \in \{0, 1, \cdots, n-1\}$ 49
5.3 Error analysis of the EMF 50
5.4 Structure of the IEMF 52
5.5 Numerical implementation of the modulation operator 54
5.6 Structure of the adaptive observer 55

6.1 Transformation error by developing the nonlinear I/O relation (5.26) from the state-space representation (2.24-2.26) 57
6.2 Set of three GMFs for the state observation with the EMF and one TMF for parameter estimation with the DMR 58
6.3 Input signals for the operating point and the excitation mode scenarios 58
6.4 State and parameter estimation by the coupled EKF with u_1, $\lambda_\mathrm{EKF} = 3.5$ and constant parameter 60
6.5 Parameter estimation by the DMR with u_1 and constant parameter . . 60
6.6 State estimation by the EMF with u_1 and constant parameter 61
6.7 Estimation error of the output and its derivatives by the EMF and IEMF with u_1 and constant parameter 61
6.8 State and parameter estimation by the coupled EKF with u_2, $\lambda_\mathrm{EKF} = 3.5$ and constant parameter 62

6.9 Estimation of the output and its derivatives by the IEMF with u_2 and constant parameter 63
6.10 State estimation by the IEMF with u_2 and constant parameter 63
6.11 Comparison of the parameter estimation with u_1 and step decline of the parameter at $t = 10\,\mathrm{s}$ 64
6.12 Comparison of the IEMF and the coupled EKF with u_1 and step decline of the parameter at $t = 10\,\mathrm{s}$ 64
6.13 State and parameter estimation by the coupled EKF with u_1, $\lambda_{\mathrm{EKF}} = 1.2$ and gradually decreasing parameter 66
6.14 Parameter estimation and state error by the proposed adaptive observer with u_1, $T_{\mathrm{TMF}} = 1.5\,\mathrm{s}$ and gradually decreasing parameter 66
6.15 Comparison of the IEMF and the coupled EKF with u_1, $T_{\mathrm{TMF}} = 3.3\,\mathrm{s}$ and gradually decreasing parameter 67
6.16 State and parameter estimation by the coupled EKF with u_2, $\lambda_{\mathrm{EKF}} = 1.2$ and gradually decreasing parameter 67
6.17 Comparison of both observers with u_2, $T_{\mathrm{TMF}} = 3.3\,\mathrm{s}$ and gradually decreasing parameter 68
6.18 Comparison of parameter and output estimation with u_1, $T_{\mathrm{TMF}} = 3.3\,\mathrm{s}$, $\lambda_{\mathrm{EKF}} = 2$, constant parameter and noise impact 68
6.19 Comparison of the IEMF and the coupled EKF with u_1, $T_{\mathrm{TMF}} = 3.3\,\mathrm{s}$, $\lambda_{\mathrm{EKF}} = 2$, constant parameter and noise impact 69
6.20 Comparison of the parameter estimation by the IEMF and the coupled EKF with u_1, $T_{\mathrm{TMF}} = 3.3\,\mathrm{s}$, step decrease and noise impact 70
6.21 Comparison of the state estimation error by the IEMF and the coupled EKF wit u_1, $T_{\mathrm{TMF}} = 3.3\,\mathrm{s}$, step decrease and noise impact 70

B.1 Evaluated $\dot{x}_1$ 78
B.2 Evaluated $\dot{x}_2$ 79
B.3 Evaluated $\dot{x}_3$ 79

C.1 State and parameter estimation by the coupled EKF with u_1, $\lambda_{\mathrm{EKF}} = 3.5$ and step decrease at $t = 10\,\mathrm{s}$ 80
C.2 Estimation results by the IEMF with u_1 and step decrease at $t = 10\,\mathrm{s}$. 80
C.3 State estimation by the IEMF with u_1 and step decrease at $t = 10\,\mathrm{s}$ . . 81
C.4 Comparison of the IEMF and the coupled EKF with u_2 and step decrease at $t = 10\,\mathrm{s}$ 81

C.5 Comparison of the IEMF and the coupled EKF with u_2, $T_{\mathrm{TMF}} = 3.3\,\mathrm{s}$, $\lambda_{\mathrm{EKF}} = 2$, constant parameter and noise impact 82
C.6 Comparison of the IEMF and the coupled EKF with u_1, $T_{\mathrm{TMF}} = 3.3\,\mathrm{s}$, gradually decreasing parameter and noise impact 82

List of Tables

2.1 Parameter values taken for simulation 5

3.1 Simulation area for observability study 26

6.1 Measured signals for the simulation 56

Statutory Declaration

I declare that I have authored this thesis independently, that I have not used other than the declared resources, and that I have explicitly marked all material which has been quoted either literally or by content from the used sources.
This work has not been published and submitted, either in part or whole, for obtaining a degree at this or any other university.

Ilmenau, August 13, 2021

Kristina Korder